

Radar Sensing for Automotive Parking Distance Control Applications

UNIVERSITY OF TWENTE.

Tom van den Berg

Sensata Technologies

University of Twente

Report for

MSc. Computer Science

Version: 11:11, Thursday 2nd June, 2016

Abstract

This research is an investigation of the requirements for an automotive, frequency modulated constant wave radar based, Parking Distance Control (PDC) system. This thesis presents the results of experiments based on the specifications for automotive ultrasound systems. The processing of the recorded data from the experiments determines requirements for digitization, processing, and compares low complexity detection algorithms. The results show that it is possible to detect single objects using low complexity detection algorithms, such as CFAR. Additional experiments were conducted with more complex scenarios compromising of multiple objects and elongated objects. The results from this show that these scenarios pose problems for a radar based PDC system. The results from the thesis provide a basis on which a prototype system can be designed for further testing.

Preface

This research thesis was written as the final thesis for a title of Master of Science in the field of computer science. The research was done at the chair of Computer Architecture for Embedded Systems (CAES). The report is written as a follow up of literature research which is attached as ‘Research Topics’ and features the same introduction. For the thesis I would very much like to thank the guidance I received from Bert, André, Siebe and Paul. Furthermore I want to thank the support I received from my many friends in Enschede originating from AEGEE, NOES, CatchUp, Calslaan 18 and more. Without those friends I would not have such a great time in Enschede, allowing me to find the perfect balance between work and play. I also want to thank my parents for their unlimited support as they watched me leave the house and wander about on my own feet.

Contents

Preface	ii
Contents	iii
Nomenclature	viii
1 Introduction	1
1.1 FM-CW Radar	3
1.2 Scope	4
1.3 Goal	5
1.4 Research Question	5
1.5 Specifications	6
1.6 Metrics	6
1.7 Omnidirectional Chip	7
1.8 Acoustic Sensing	7
2 Theory	10
2.1 Block Diagram	10
2.2 Modulation	10
2.3 Transmitter	14
2.4 Radio Waves	15
2.5 Receiver	19
2.6 Digitization	22
2.7 Digital Signal Processing	24
2.8 Automatic Detection	26

3	Setup	29
3.1	Introduction	29
3.2	Experimental setup	29
3.3	Processing Toolchain	33
4	Experiments: surfaces	37
4.1	Method	37
4.2	Results	37
4.3	Conclusion and Discussion	41
5	Experiments: single Object	42
5.1	Method	42
5.2	Results	44
5.3	Conclusion and Discussion	66
6	Experiments - Two objects	68
6.1	Introduction	68
6.2	Method	68
6.3	Results	69
6.4	Conclusion and Discussion	70
7	Experiments - Elongated Objects	71
7.1	Introduction	71
7.2	Method	71
7.3	Results	71
7.4	Conclusion and Discussion	73
8	Conclusions	76
8.1	Discussion	76
8.2	Future Work	77
A	Research Topics Report	78
A.1	Introduction	83
A.2	Radar Introduction	85
A.3	Signal Processing	92

A.4	Architecture	100
A.5	Parking Sensor Norms and Standards	109
A.6	Conclusions	113
A.7	References	115
B	System Design	127
B.1	Introduction	127
B.2	Design Considerations	127
B.3	Recommended Design	132
C	MATLAB Code	134
	References	135

Nomenclature

ϵ	Electric permittivity
Γ	Reflection Ratio
λ	Wavelength of radio wave, in m
μ	Magnetic Permeability
ω	Angular Frequency
σ	Radio Cross Section in dB/m ²
σ_c	Electrical Conductivity
B	Bandwidth of radar system, in Hz
B_e	Effective Bandwidth
c	Speed of light: 299 792 458 m/s
E_L	Impedance of load
E_S	Impedance of source
f_b	Beat frequency returned by the mixer in the receiver of an FM-CW radar, in Hz
f_d	Doppler frequency or shift in frequency caused by Doppler effect, in Hz
G_{rx}	Gain of receiving antenna
G_{tx}	Gain of transmitting antenna

j	Complex number (square root of -1)
k	Boltzmann's Constant
P_{tx}	Gain of transmitting antenna
R	Range, distance from target to radar antenna, in m
T	Time or length of sweep in seconds
v	Speed, in m/s
ADC	Analog-to-Digital Converter
c	Speed of light
CFAR	Constant False Alarm Rate
Clutter	Reflections from objects that are not target and generally appear as 'noise'.
dBc	decibells relative to the Carrier
dBm	decibel Milliwatts
DDS	Direct Digital Synthesizer
DFT	Discrete Fourier Transform
DOA	Direction of Arrival
FFT	Fast Fourier Transform
FM-CW	Frequency modulated continuous wave
IF	Intermediate Frequency
PDC	Parking Distance Control
PLL	Phased-Locked Loop
PVC	Poly Vinyl Chloride
Range	Distance to target

RCS Radio Cross Section in dBm^2

SNR Signal-to-Noise Ratio

SPI Serial Peripheral Interface bus

SQNR Signal-to-Quantization-Noise Ratio in dB

Target Object to be detected

VCO Voltage Controlled Oscillator

Chapter 1

Introduction

Radar stands for radio detection and ranging. The development of radar started before World War II and continues until today with complex radar systems for many different applications [1]. In a basic radar system a pulse of radio waves is sent by a transmitter, reflected by an object and received by the receiver. The distance to this object can be calculated using the time it takes to travel to and from the object and the speed of the radio wave, which equals the speed of light, see Figure 1.1.

There are many kinds of different radar systems, the best known systems are: Moving Target Indication(MTI), Pulse Doppler Radar, Continuous-Wave (CW) and Frequency-Modulated Continuous-Wave (FM-CW) [1]. The last type, FM-CW, is of interest for our system because it is the best system allowing for detection

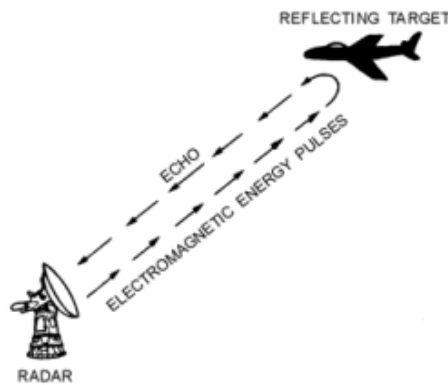


Figure 1.1: A radio wave reflecting off a target [2].

of short range static targets [3, 4].

1.1 FM-CW Radar

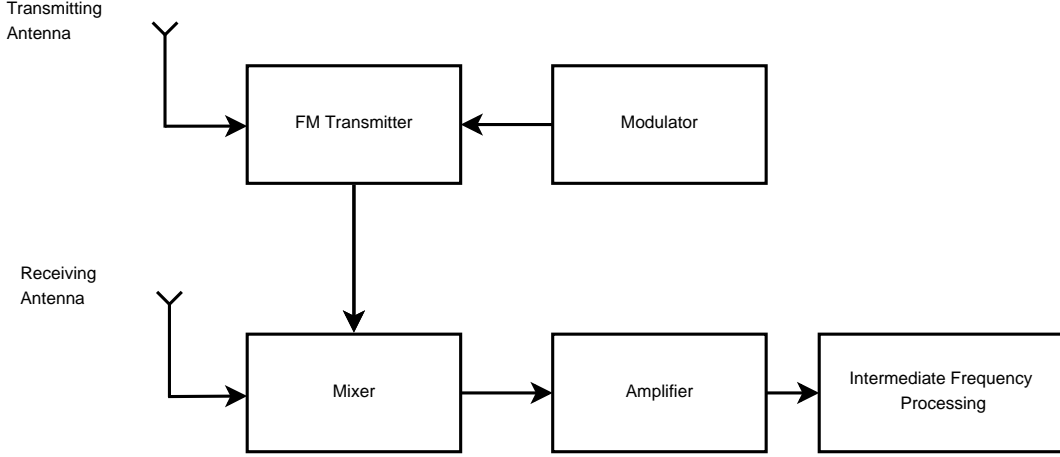


Figure 1.2: Block Diagram of FM-CW Radar.(Adapted from [3], page 83).

In Figure 1.2 the block diagram of an FM-CW radar is given, consisting of the frequency modulated (FM) transmitter, the modulator giving out the modulation of the signal, the mixer, amplifier and the intermediate frequency processing part. In FM-CW radar the transmitting frequency is modulated, in this example linearly with a triangle waveform as can be seen in Figure 1.3. When a reflected signal is received, the frequency of this reflected signal will differ from the current transmitting frequency since it will take a certain time (two times the distance to the object divided by the speed of light) before the signal returns. The mixing of the transmitted and received signals will cause a beat frequency to occur, being the difference between the transmitted and received frequency. This effect is illustrated in Figure 1.3. The analysis and extraction of targets from the intermediate frequency (IF) signal is done by an automatic detector. The range and beat frequency are related in Equation 1.1 [5]. In this equation f_b equals the beat frequency, B the bandwidth, R the target range, T is the period time of the modulation and c the speed of light. Figure 1.4 illustrates the effect of a moving target introducing a Doppler shift in the reflected signal, and the effect on the beat frequency from the intermediate frequency (IF) output of the mixer.

$$f_b = \frac{2BR}{cT} \quad (1.1)$$

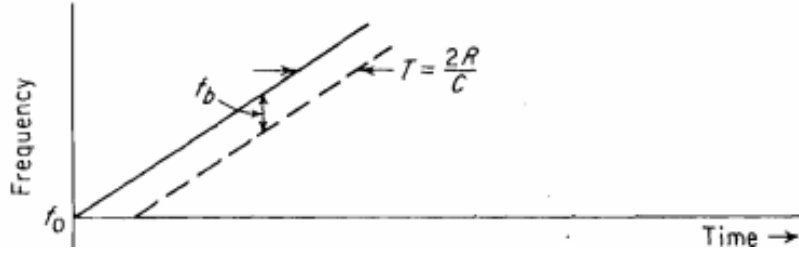


Figure 1.3: Illustration of Linear-Modulated CW transmitted and returned signal [3].

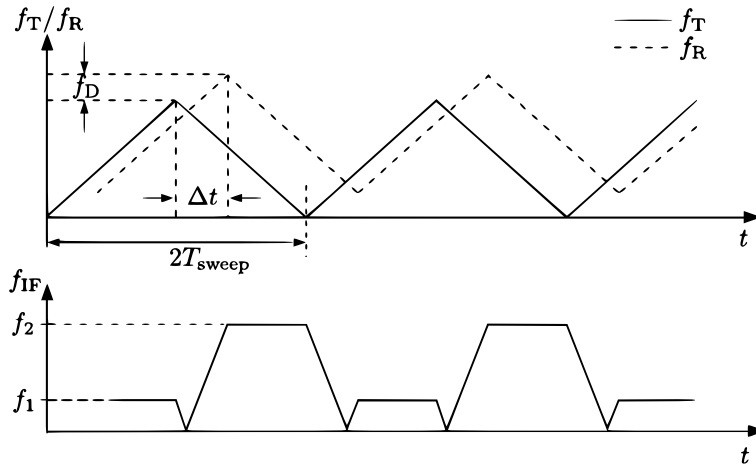


Figure 1.4: Triangularly modulated signal and the resulting beat frequency including Doppler shift from a moving target. f_1 and f_2 are the different resulting frequencies for the up and down going slope [6].

1.2 Scope

The scope of this research is to do an initial exploration of the technical feasibility of using radar technology as a means for parking distance control. This research however does not go into a prototype design. The experiments focus only on one sensor and static objects. Setups with multiple radar chips or moving platforms are out of scope.

1.3 Goal

The goal of this research is to determine the technical feasibility of a radar based FM-CW system. Sensata is also interested in determining the components and its specifications needed for this system to determine a price on which to base the business case.

1. Determine possibilities and limitations of FM-CW Radar based system for aiding the driver of a car with parking.
2. Test different modulation periods or sweep times.
3. Test detection methods.
4. Consider different architectures for the system.
5. Propose an architecture and system design for a radar based PDC system.

1.4 Research Question

The main research question is: How can a radar parking distance control system be implemented most cost effectively to match current ultrasound systems. To answer this question it is divided into several sub-questions:

1. What metrics are useful for comparing an ultrasound and radar PDC system?
2. Can the ultrasound specifications be met by radar?
3. How can these specifications be met?
 - (a) Which detector(s) meet(s) these specification?
 - (b) Which architecture is best fit for the detector(s)?

Question 1 is answered in [Appendix A: Research Topics Report](#), and the answer is repeated in [section 1.6: Metrics](#).

Table 1.1: Table showing objects and their ranges for different modes as defined in the Porsche specification.

Diameter (mm)	Mode	Range tart (cm)	Range end (cm)
75mm	PDC	10	450
50mm	PDC	10	200
30mm	PDC	10	150
75mm	Extended	20	700
50mm	Extended	20	600
30mm	Extended	20	500

1.5 Specifications

As discussed in [Research Topics Report](#) there are different ways to measure the performance for automotive PDC system. From the listed specifications Sensata chose the grid size and objects from the Porsche specifications. The size of the grid is 3.5 m wide and 7 m long. The specified objects are made from wood, metal or a hard plastic (like PVC) and have different diameters. Two different modes are specified with different specifications: PDC (regular Parking Distance Control) and extended mode, which is a special mode for long-range applications like finding parking spots. The objects and ranges are listed in [Table 1.1](#). The maximum vehicle speed is taken from the ISO 17386 norm which is a maximum of 0.6 m/s, which is the maximum speed of the vehicle during operation. The detection time is also taken from the ISO 17386 norm which specifies that the driver has be notified within 0.5 seconds of an object entering the specified area.

1.6 Metrics

The metrics for comparing processing and detection methods were investigated in [Appendix A: Research Topics Report](#). The metrics are listed below. From this list, metric 3 is not applicable for single sensor setups.

1. **Signal-to-noise ratio** is an important metric to select the right window type because it is connected with the probability of detection as shown in [Appendix A: Research Topics Report](#).

-
2. The **coverage ratio** as the ratio of grid cells in which a target is detected versus those where it is not, as specified by the ISO 17386 norm.
 3. The **largest blind spot**, as specified by the ISO 17386 norm.
 4. The **range accuracy** of the target, defined as the ratio between the error and the actual range.
 5. The **accuracy of the DOA estimator** as an error to the actual angle.
 6. The **complexity** of different detection, range and DOA estimators since higher complexity generally equals higher cost.

The complexity metric is discussed in [Appendix A](#).

1.7 Omniradar Chip

The Omniradar RIC60B is a programmable radar chip containing antennas, a PLL driven oscillator, a power amplifier, receivers with mixing capabilities, IF amplifiers and IQ demodulators [7]. All these items are programmable using a serial peripheral interface bus. All RF components are implemented on the chip. To use the chip as an FM-CW radar, a low frequency modulation signal is required to drive the PLL and the correct settings. After this the signals, containing the beat frequencies from the two receivers (rx1, and rx2) are available for processing as a pair of differential analog output signals. In [chapter 2](#) more specifications of the Omniradar chip are presented.

1.8 Acoustic Sensing

Acoustic sensing is done by sending out sound waves in the ultrasound region (30kHz+) and listening for their echo. In this sense it is similar to most radar systems that listen for the echo of radio waves. The waves themselves however differ. Sound waves are mechanical vibrations transmitted by a medium, air in most cases.

Radar uses electromagnetic waves that do not require a medium because, the exact explanation of its operation found in the field of quantum electrodynamics. Electromagnetic waves can travel through some materials easily like plastics, whereas sound waves will reflect off them. Sound waves however can be absorbed much easier by fabrics and other soft materials whereas with radio waves this is much harder to do. Another big difference between sound and electromagnetic waves is the speed. Sound travels at around 340 m/s whereas electromagnetic waves travel with the speed of light, $3.0 \cdot 10^8$ m/s.

1.8.1 Construction

Most acoustic sensors use a piezo transducer at the heart, as shown in Figure 1.5. The transducer can send sound waves and receive them. The properties of sound together with the construction of the transducer makes that they are generally very narrow beamed. The beamform of such a sensor is drawn in Figure 1.6.

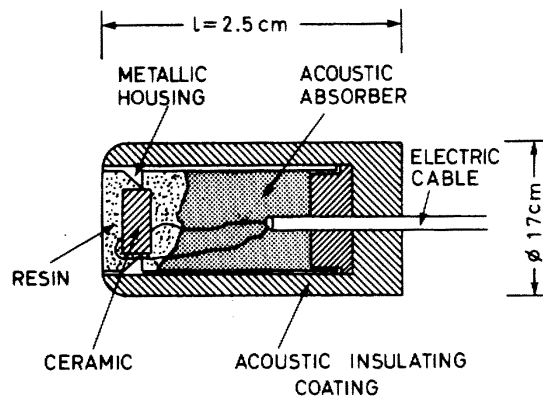


Figure 1.5: The construction of an ultrasonic sensor [8].

1.8.2 Operation

A receiver system determines the time between transmitting and reception of signals, and using the speed of sound a distance to the reflecting object can be computed. In cars the front and rear bumpers are equipped with multiple sensors, the signals of which are fed into a central computer that feeds the data back to

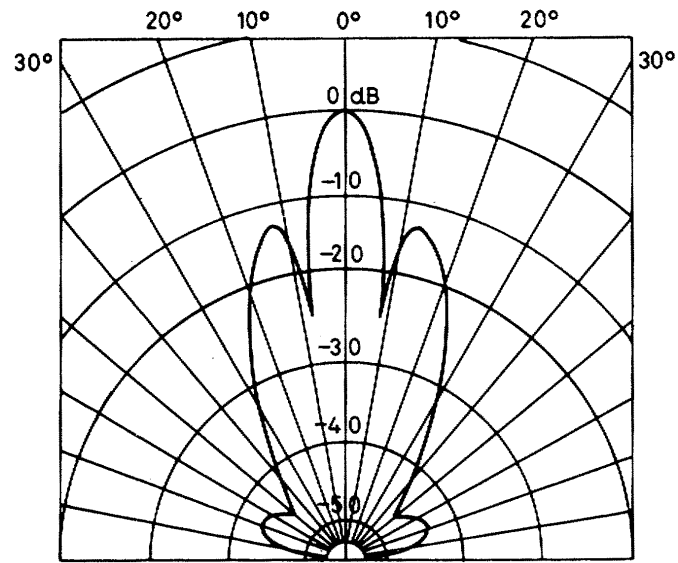


Figure 1.6: The sound radiation power of an ultrasonic sensor [8].

the driver and possibly safety features in the vehicle or auto-mobility functions like self-parking.

Chapter 2

Theory

This chapter discusses how a radar system with the Omniradar RIC60B radar chip works. The first sections shows the theoretical block diagram. The second section discusses the modulation. The transmitter and receiver are discussed in section four and six and automatic detection in section nine. The other sections discuss the intermediate components or effects like propagation.

2.1 Block Diagram

[Figure 2.1](#) shows a theoretical block diagram of the Omniradar chip, modulation, propagation and object, analog to digital converter (ADC) and the detector. The Omniradar chips contains the transmitter and receiver blocks. The blocks are elaborated on in the following sections.

2.2 Modulation

2.2.1 Bandwidth

The bandwidth B determines the (theoretical) range resolution, the relation is shown in [Equation 2.1](#) with c being the speed of light.

$$Sr = \frac{c}{2B} \quad (2.1)$$

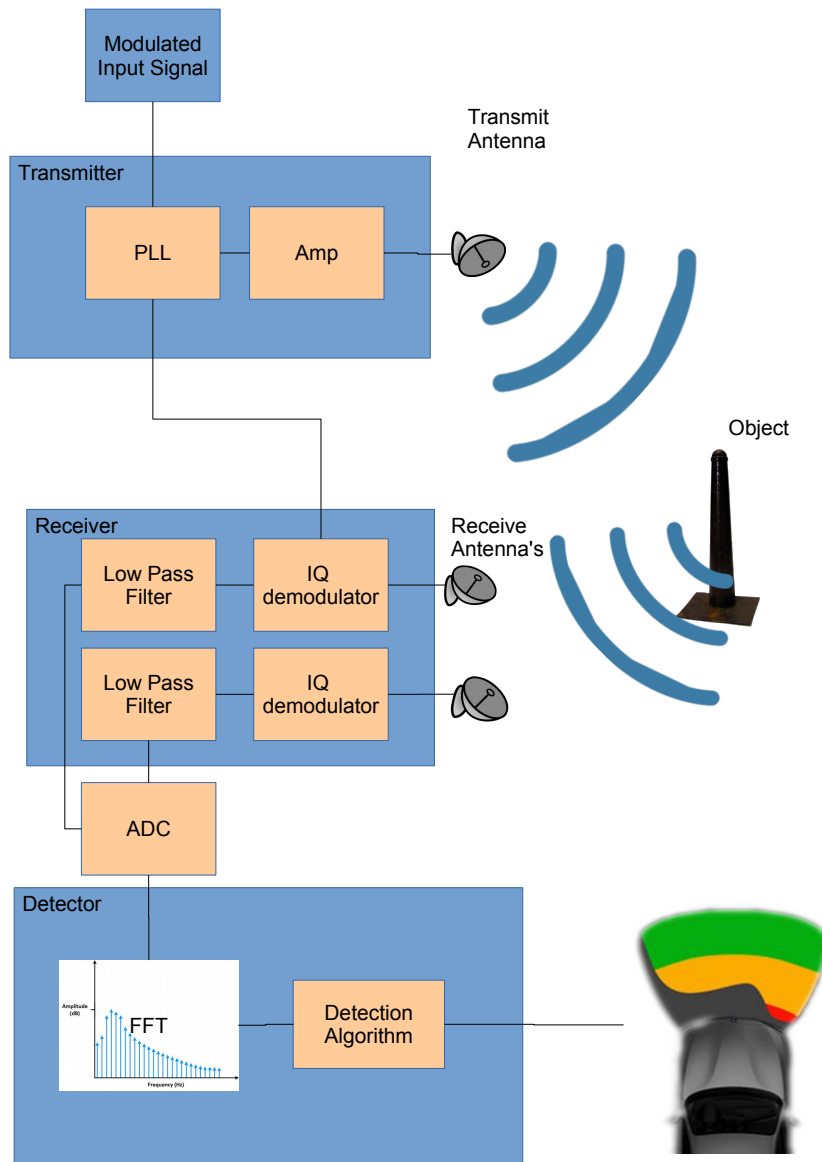


Figure 2.1: Schematic illustration of double antenna FM-CW radar system based on RIC60B

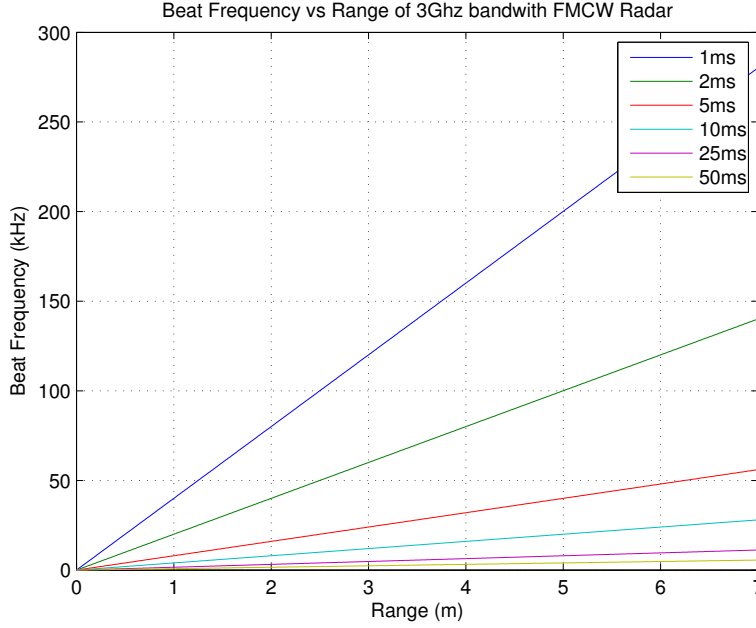


Figure 2.2: Beat frequency versus range plotted for different sweep times.

The bandwidth used for the parking assist application is 3 GHz since this is the maximum bandwidth that can be used for automotive applications by the International Telecommunication Union (ITU). With this 3 GHz the maximum theoretical range resolution becomes 5 cm.

2.2.2 Sweep Time

The beat frequency (f_b) of a target at range R after the received signal is mixed with the transmitted signal can be described in terms of its bandwidth B and the time duration of the frequency sweep T :

$$f_b = \frac{2BR}{cT} \quad (2.2)$$

The different lengths of the linear frequency sweep, or sweep times, available for our system are limited to a minimum of 1 ms by the Omnicar chips internals and a maximum 50 ms by the time constraints of detection. In Figure 2.2 the beat frequencies of the target range (0-7 m) are plotted for different sweep times. In general the shorter the sweep time, the higher the beat frequency. The speed of the

target versus the receiver is not accounted for in these formulas. The difference in frequency f_d is independent of the sweep time following Equation 2.3. The relative small effect of the 3 GHz of modulation and thus change in the wavelength is neglected.

$$f_d = \frac{v}{\lambda} \quad (2.3)$$

This Doppler frequency induces a shift in the beat frequency causing a range to be calculated reversing Equation 2.2 to differ from the actual range. The ratio of this difference is equal to the ratio of the Doppler frequency versus the beat frequency. Since the Doppler frequency remains constant with a constant speed, but the beat frequency differs with the sweep time, the sweep time will affect this ratio. The effect is plotted in Figure 2.3 for a target at 7 m for different speeds. From this plot one would assume shorter sweep times are better since they feature minimal effect of the Doppler speed. However increasing the sweep time has a positive effect on the maximum range that can be achieved, which in the case of FM-CW radar improves the signal-to-noise ratio (SNR). This effect can be seen when observing the radar equation in Equation 2.4 [1].

$$R^4 = \frac{P_{tx} G_{tx} G_{rx} \lambda^2 \sigma}{(4\pi)^3 k B_e \text{SNR}} \quad (2.4)$$

The variable of interest here is B_e which is the effective bandwidth defined in Equation 2.5 where α is a constant determined by features from signal processing like windowing and digitisation.

$$B_e = \frac{1}{\alpha T} \quad \text{where } \alpha \geq 1 \quad (2.5)$$

From these two equations it can be seen that the maximum range is proportional to the sweep time in theory. This assumption holds for uncorrelated noise effects, correlated noise such as clutter will not be reduced by increasing the effective bandwidth.

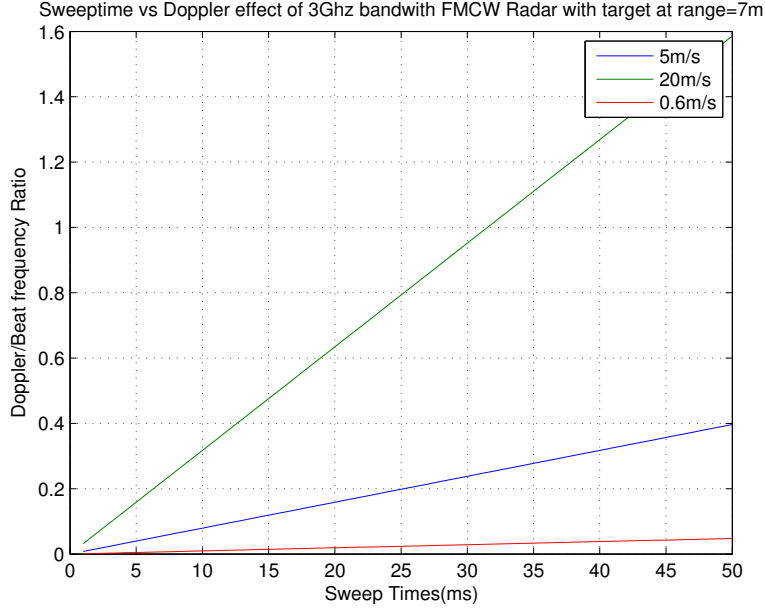


Figure 2.3: Doppler- and Beat-frequency ratio for target at a range of 7 m for different vehicle speeds.

2.3 Transmitter

The transmitter in the RIC60B consists of a voltage controlled oscillator (VCO) and a phase-locked loop (PLL). The PLL is fed by a linear frequency modulated input signal of approximately 25 MHz. The PLL tunes the VCO to the base frequency of 60 GHz. The signal is then passed to the amplifier which can generate a signal with 8 dBm of power. This transmitter features a phase noise of -75 dBc/Hz and spurious components of -40 dBc [7].

2.3.1 Antennas

The antennas on the Omniradar chip RIC60B consist of three rows of eight small patches totalling a length of 8mm. A picture of the antennas surrounded by radar absorbing materials is shown in [Figure 2.4](#).

Two rows contain the receiving antennas and the third the transmitting antennas. The radiating pattern and reception pattern of the antenna arrays are given in [Figure 2.5](#) and [Figure 2.6](#). These radiation patterns are measured using

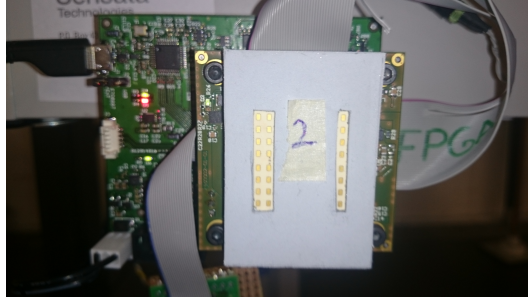


Figure 2.4: The front of the RIC60B chip on the sensor and evaluation board featuring the patch antennas.

a reference target at different angles of the module.

These gain values are a combination of the transmitted and receiving gain, given in Equation 2.4 by $G_{tx} \cdot G_{rx}$.

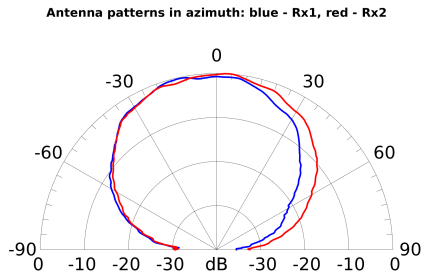


Figure 2.5: The antenna array pattern for different azimuth as supplied by Omniradar.

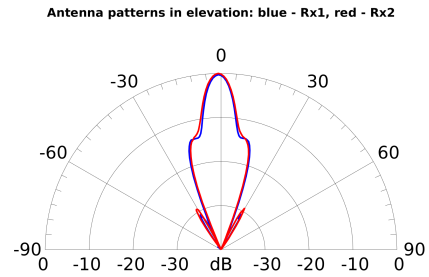


Figure 2.6: The antenna array pattern for different elevation as supplied by Omniradar.

2.4 Radio Waves

The radar system hinges on the fact that the target object will reflect the transmitted radio waves back to the receiving antennas. For this the radio waves have to propagate to the target and back again. Apart from reflecting, targets (and also clutter) can also refract and scatter radio waves. The combination of all of these signals returned and received is called the Radar Cross Section (RCS). In

the next subsections the propagation and the reflections are discussed further, as well as the exact definition of the RCS and its estimation.

2.4.1 Propagation

In the theoretical model of an isotropic antenna, radio waves radiate equally in all directions. Because of this the power is spread over an area defined by the area of a sphere with radius R given by $4\pi R^2$. In radar systems this propagation loss is often given as $4\pi R^4$ because of atmospheric losses [1]. The factor R^4 can also be seen in Equation 2.4. These atmospheric losses are caused by the absorption of the radio waves by oxygen and water vapour in the atmosphere. From Figure 2.7 it can be seen that the attenuation at 60 GHz is 16 dB per km. At a maximum range of 7 m this is 0.1 dB which is low compared to other losses. Other sources

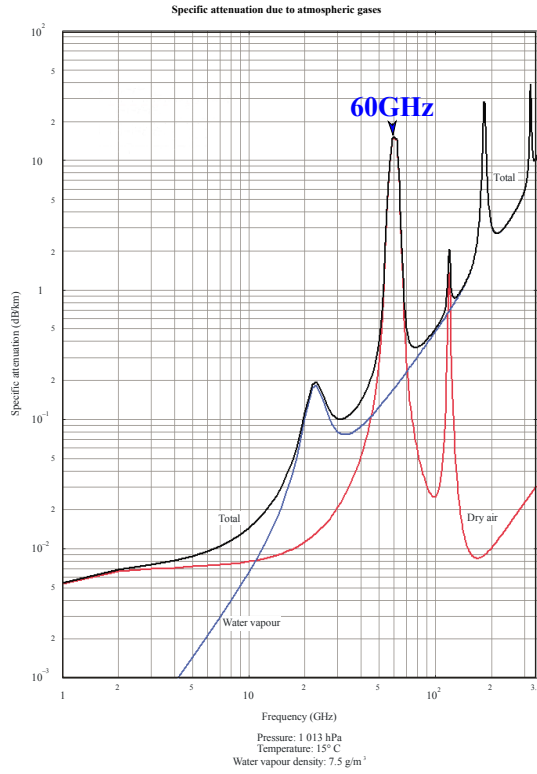


Figure 2.7: Attenuation by atmospheric gasses from [9].

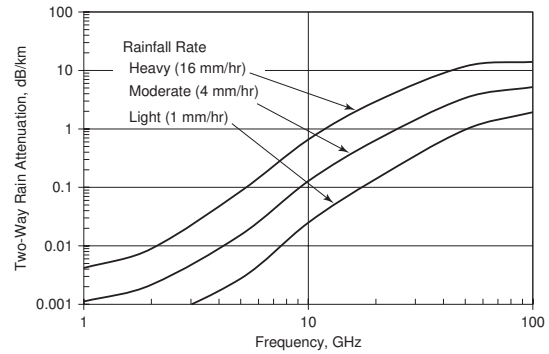


Figure 2.8: Attenuation by rain for different frequencies from [10].

of attenuation are rain, hail, fog and snow. From Figure 2.8, rain attenuation

equals that of the atmospheric losses. At the 60GHz frequency however rain will be more likely to reflected than only disperse or absorb the rain waves. Hail is said to attenuate only by a hundredth of that of rain [11] and is therefore negligible. Fog attenuation is even lower and therefore can be neglected [1].

2.4.2 Reflection

The amount of radio waves reflected is given by the reflection coefficient between two mediums which is determined by the differences in impedance of the materials (see Equation 2.6 from [12]). In this equation Γ is the reflection ratio and Z_S and Z_L stand for respectively the impedance of the source material versus (in this case: air) and the load (the material of the target).

$$\Gamma = \frac{E^-}{E^+} = \frac{Z_L - Z_S}{Z_L + Z_S} \quad (2.6)$$

The impedance of a material is defined by Equation 2.7 where j is the imaginary unit, μ the magnetic permeability, ω the angular frequency, σ the electrical conductivity and ϵ the electric permittivity.

$$Z = \sqrt{\frac{j\omega\mu}{\sigma_c + j\omega\epsilon}} \quad (2.7)$$

Metallic objects have a very high electric conductivity (σ_c), causing the impedance to be very low (close to 0 Ω). Given that the impedance of air is high compared to this (367 Ω) the reflection ratio reaches close to -1, implying full reflection. The negative sign indicates that the waveform is inverted on reflection. For non-metallic objects, having no conduction, the formula for impedance reduces to Equation 2.8.

$$Z = \sqrt{\frac{\mu}{\epsilon}} \quad (2.8)$$

Air, wood and plastic have very similar magnetic permeability (μ) of $1.3 \cdot 10^{-6}$. Therefore the main difference in impedance, and hence the reflection ratio must be caused by difference in electric permittivity. For wood the dielectric constant (or electric permittivity relative that of free space) is between 1.2 and 2.1. PVC has

a relative permittivity of 3 [13]. The reflection ratios of wood is therefore between 0.045 and 0.18 and the reflection ratio of PVC 0.26. This means that wood will reflect the least of these materials and will therefore be the hardest to detect.

2.4.3 Radar Cross Section

The total amount of radio waves reflected does not only depend on the material and propagation. The main factor is the actual size of the object in the radiated area of the transmitted signal. The Radar Cross Section is measured in dB/m². It is normalized to the reflection of a fully radiated perfectly conducting sphere with a cross-sectional area of 1m² [14]. The RCS is used as a comparison of the amount of reflected energy independent of different objects. The ratio of the wavelength and the diameter of objects gives different scattering and reflection of the radio waves and therefore affect the RCS. Figure 2.9 shows the effect of the size of an object on the RCS for 60 GHz. One can see from this graph that for objects 10 mm and larger the effect reaches zero. The objects of interest, specified earlier in section 1.5: Specifications, are not smaller than 10 mm and therefore this effect can be neglected.

2.4.4 RCS Estimation for simple objects

RCS estimation for simple objects can be done using simple formulas, whereas complex objects like cars, planes and other are much harder to estimate. The specifications define cylindrical objects, and the formula for determining the RCS is given in Equation 2.9 from [14]. In this formula σ is the RCS, r the diameter of the cylinder and l the length of the cylinder that is within the antenna pattern.

$$\sigma = \frac{2\pi r l^2}{\lambda} \quad (2.9)$$

For the smallest object from section 1.5: Specifications, a 12 mm wooden cylinder, the maximum RCS is 1.34 dB/m² when fully conducting and positioned at the angle of full specular reflection. However, at a slight offset the RCS is much less, as shown in Figure 2.10. The practical RCS therefore is -34 dB/m², calculated as the average over 88 to 92 degrees. Since the reflection ratio of wood is only

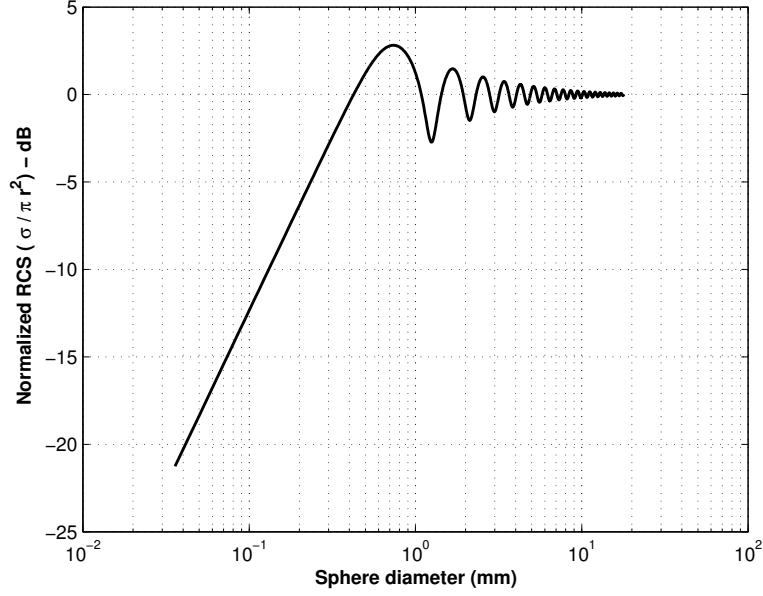


Figure 2.9: Radar Cross section of a conducting round sphere normalized to πa^2 versus diameter in mm, adapted from [1].

between 0.046 and 0.18, the actual RCS is between -65 dB/m^2 and -51 dB/m^2 .

2.4.5 Complex Targets

Not all targets feature such simple geometry. Complex geometries like aeroplanes have an RCS that varies heavily with the angle of inclination with moving parts causing variations over time. Generally the variations in angle also become variations over time since the incident angle varies over time. These targets are classified as Swerling targets [15] and are much harder to detect due to their varying nature. In this thesis however, these targets are out of the scope of this thesis.

2.5 Receiver

After the radio waves reflect off the target, they arrive at the antennas of the receiver. In the receiver, the returned signal is mixed with the transmitted signal using a multiplication. This process is also known as heterodyning.

The mixing results in two different signals being the difference between the

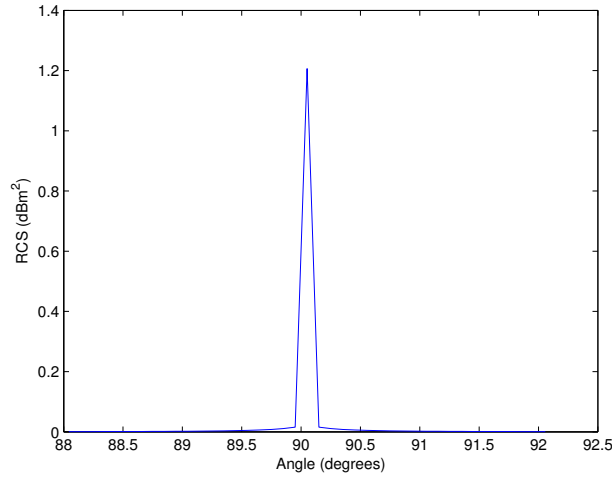


Figure 2.10: RCS of a wooden cylinder with a diameter of 12 mm with 0.4 m ‘illuminated’ length versus angle.

frequencies of the two signals and the sum of the frequencies of the two signals. The sum is very high (two times 60 GHz) and this signal is filtered out, which leaves the difference signal. This difference signal, also called the beat frequency, is related to the range since the frequency of the base signal is modulated over time, see [section 2.2: Modulation](#).

2.5.1 Direction Of Arrival

There are different methods for determining the incident angle, see the research topics report Section 3.3: Direction Of Arrival. The antenna pattern of the Om-niradar chip is very usable for phase comparison determination of the direction of arrival, a typical radio pattern for this is shown in [Figure 2.11](#). Using the difference in phase because of slightly larger path length between the two antennas, the angle of the incoming radio wave can be determined. The antenna patterns from the Omniradar chip are suitable for the phase comparison sum and difference method. Omniradar has tested the sum and difference method using an object with a reference RCS of $1\text{dB}/\text{m}^2$ at 1 meter distance. The results are shown in [Figure 2.12](#).

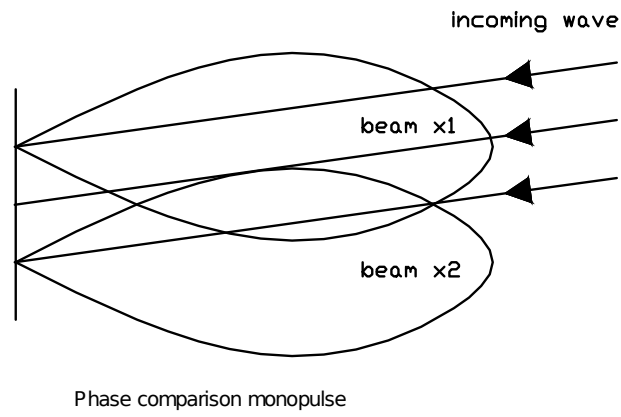


Figure 2.11: Antenna Pattern for Phase Comparison [16].

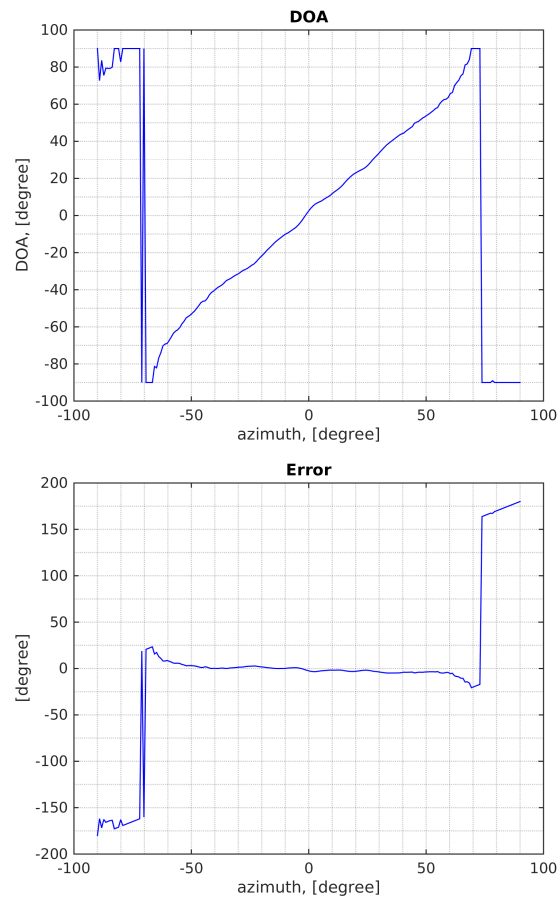


Figure 2.12: DOA measurements by Omniradar.

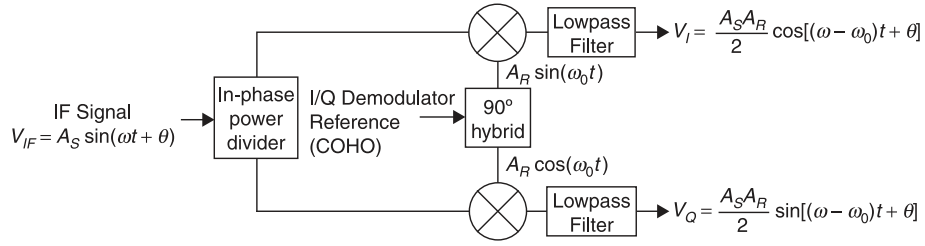


Figure 2.13: Block diagram of an IQ demodulator [1].

2.5.2 Demodulator

To be able to determine the exact phase of the signals, an in-phase and quadrature (IQ) demodulator is used, shown in Figure 2.13. An IQ demodulator allows for better performance after digitization. This is because when using mixing, when the the two mixed signals are zero, the output power of the signal will be zero. This makes it impossible to find the signal power at that point in time, therefore another mixer is used where a phase shift of 90 degrees is introduced.

2.5.3 Amplifier and Low Pass Filter

The demodulator is followed by an amplifier and a low pass filter. The noise figure of the I and Q demodulator, amplifier and low pass filter is given in Figure 2.14. The noise figure is the degradation of the SNR caused by the amplifier and low pass filter components. The main component of the noise in the receiver is so called 1/f noise, or pink noise. This noise tends to decrease with frequency. The low pass filter is needed to filter out the frequencies that cause aliasing and other unwanted effects at the digitization stage.

2.6 Digitization

To allow the analog signals to be processed by a digital architecture, they have to be converted to a digital (binary) representation. This is done by devices called Analog-to-Digital converters, also known as A/D converters or ADCs. Analog to digital converters are characterized by two main features: Sample Rate and (stated) Resolution.

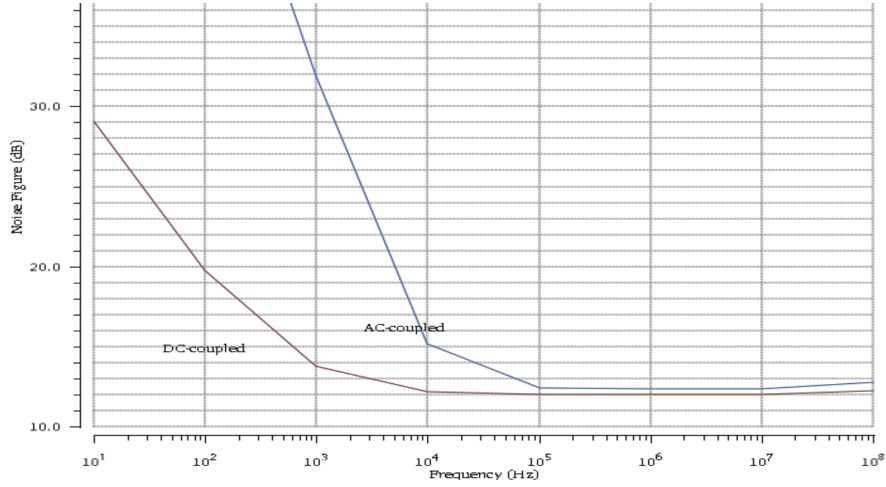


Figure 2.14: Noise figure for receiver of Omniradar RIC60B chip [7].

2.6.1 Sample rate

The sample rate is the number of samples, of the analog signal, taken by the A/D converter per second, often given in Hz. With a sample rate of f_s the maximum frequency that can be detected without aliasing is $f_s/2$, also known as the Nyquist frequency. Typically however the sample rate is much higher than this to reduce quantization noise [1].

2.6.2 Resolution

The resolution of an A/D-converter is generally characterized by the number of bits used for quantifying the analog signal. The number of different values for an A/D-converter with a resolution of N bits is 2^N . This resolution affects the (digital) signal-to-noise ratio. For an ideal A/D converter this so-called signal-to-quantization-noise ratio (SQNR) is given in Equation 2.10.

$$\text{SQNR} = 6.02N + 1.76 \quad (2.10)$$

This equation only holds if the signal is sufficiently large relative to the quantization size and noise sources are uncorrelated to the A/D converter, meaning, for example, that the sample and hold circuitry in the A/D-converter should not affect the signal [1].

2.7 Digital Signal Processing

After digitization the digital signal is processed by a computer architecture to be able to detect objects (targets) that later might damage the vehicle. In FM-CW, signal processing determining the frequency components of the returned signals is the way to detect targets since targets at different ranges induce different beat frequencies. The most common way to determine the frequency components of a digital signal is to use a Fast Fourier Transform (FFT).

2.7.1 FFT

To compute the discrete Fourier transform(DFT) of a digital signal a fast Fourier algorithm is used because calculating a DFT is computationally much harder [17]. FFT algorithms come in various shape and sizes with the most well known the Cooley-Tukey algorithm [18]. The speed of the calculation depends on the ‘size’ of the FFT, meaning the amount of samples used to compute the FFT from, generally denoted as N . The complexity of FFT calculations is $O(N\log_2(N))$. The time to calculate an FFT depends not only on the size and the precision (floating point for instance) but also on the computer architecture. Together with the speed of the processing unit and memory speed, the architecture determines the time it takes to calculate an N point FFT [19]. Since FFTs are very computationally heavy they are even used as a benchmark to compare performance [20] between CPU’s.

A complex FFT of a sample of N elements will yield a resulting set of points of size N containing the amplitude coefficients per frequency component. A non-complex FFT will result in $N/2$ points. The frequency components are referred to as (frequency) bins and each contain a frequency band with width f_n/N , where f_n is the Nyquist frequency. The amount of bins in an FFT that feature the range of interest is a constant over sweep time for a given sampling rate because the maximum frequency for the range of interest and the amount of samples during the modulation cancel each other out. For sampling frequency of 1 MHz and a maximum range of interest of 7 m there will be 140 bins that feature the range of interest for different sweep times. This set of bins for the range of interest is also known as the range-FFT. Figure 2.15 shows an example of a range FFT from the

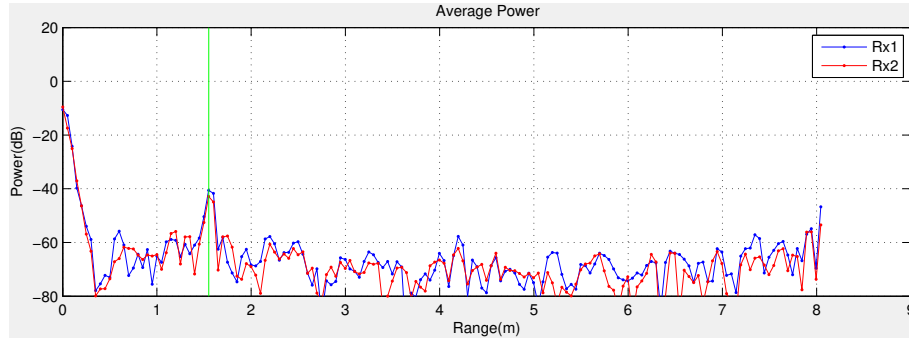


Figure 2.15: An example range FFT from the experimental setup showing a 12 mm thick Wooden pole at a range of 1.5 m. Rx1 and Rx2 are the signals from the two receivers of the Omiradar RIC60B.

experimental setup.

Noise

Noise is also apparent in an FFT. White noise is a special case of this, since it features all frequencies at equal power. The power of white noise is spread over all the bins of the FFT, and since the total noise power is constant the white noise component in every range bin decreases when the amount of bins increases.

Spectral leakage and Windowing

To avoid energy to leak into adjacent frequency bins in an FFT, a phenomenon known as spectral leakage, windowing is used [21]. Figure 2.16 shows how windowing is done in the time domain. It shows an unwindowed signal, the window function, and the result of multiplying the latter two. In Figure 2.17 the FFTs of the un-windowed and windowed signals are shown. Spectral leakage causes some of the power from one peak to leak into nearby bins, causing the peak to be lower and the surrounding range bins to feature ‘tails’ or ‘side-lobes’. Windowing is used to counter-act this effect. In [chapter 5: Experiments: single Object](#) the raw data after digitization is gathered, which allows to test different windowing functions. [22] lists a set of popular windows and their main characteristics.

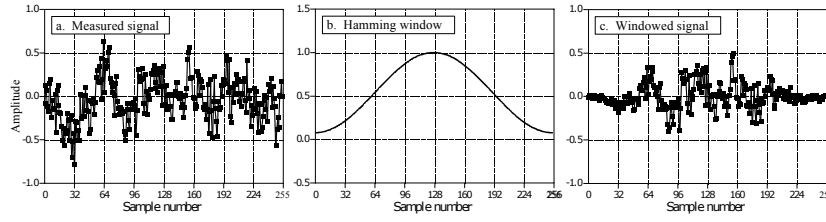


Figure 2.16: Graphs showing the effect of windowing in the time domain [23].

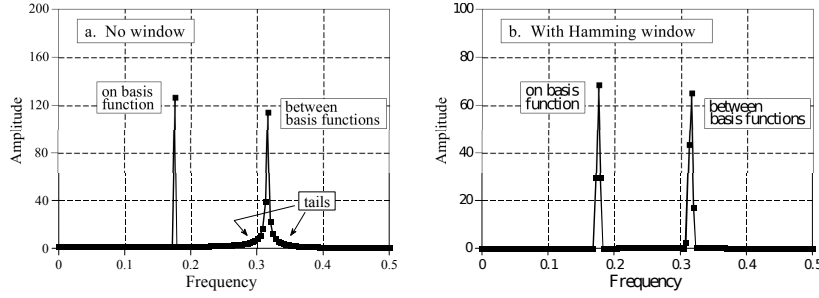


Figure 2.17: Graphs showing FFT of signals with and without a window [23]. Notice the difference in amplitude and scale.

2.8 Automatic Detection

In [Research Topics Report](#) the theory of different methods for automatic detection are given. In this research two different methods will be explored, they are fixed threshold and CFAR as the other methods were deemed to complex for cost effective implementation.

2.8.1 Fixed Threshold

A fixed threshold is the simplest way of detecting objects from the range FFT. [Figure 2.18](#) shows an example range FFT from the experimental setup with a fixed threshold line. A fixed threshold works well if the noise level is constant over the range and the difference between signal and noise is quite large. In the range FFT, a problem is apparent at short range, where the parasitic coupling of the transmitting and two receiving antennas show high power levels at short range. This problem is easily averted by finding the second place where the signal crosses the threshold instead of the first place. This means that it is not possible to find targets at close range.

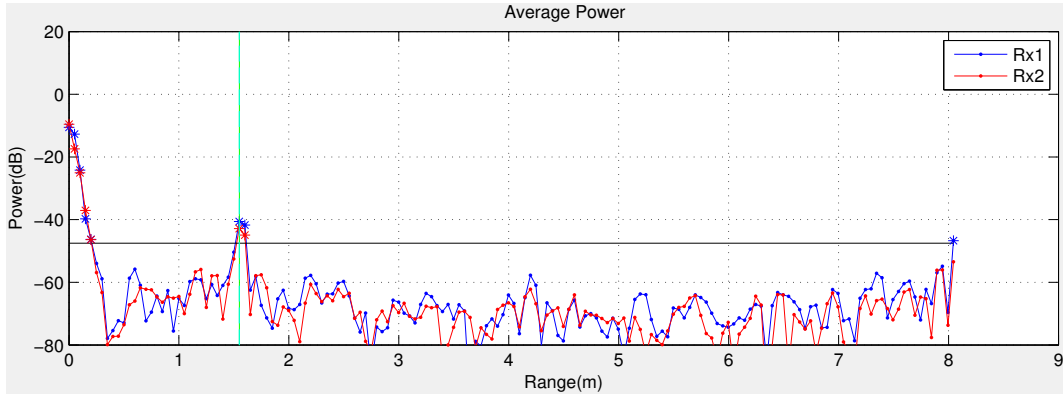


Figure 2.18: An experimental range FFT with a target at 1.5 m which is detected by the fixed threshold line (black).

Table 2.1: Table containing CFAR methods and their advantages and disadvantages.

Name	Method	Advantage(s)	Disadvantage(s)
CFAR-CA	Cell Averaging	Simple Implementation	Can cause false detection at clutter edges. Suppresses multiple targets.
SOCA CFAR	Smallest of cell averaging	Combats multiple targets problem of CFAR	High probability of detection at clutter edges.
GOCA CFAR	Greater of cell averaging	Combats false detection of clutter edges	Higher suppression for multiple targets.
S-CFAR	Switching between SOCA, GOCA and CA	Combats both problems	Only combats one problem at a time. Has higher implementation costs.
OS-CFAR ^[25]	Order Statistic	Combats both problems simultaneously	Sorting required of test cells gives higher complexity ^[26] .
And-CFAR Or-CFAR ^[27]	Combines OS and CA	Better SNR performance	Twice as much processing.

2.8.2 CFAR

Because the noise level is not constant and identifying objects at close range is desired, a different method for detection was developed [24]. This method is called constant false alarm rate (CFAR) and is well described in [Research Topics Report](#) with all the different variants. Table 3.1 from this appendix contains the different CFAR methods is reproduced here in [Table 2.1](#) for easy reference. Using CFAR Ordered Statistic (OS) on the experimental range FFT results in [Figure 2.19](#). The problem with the fixed threshold where detection at low range suffered because of the coupling of the two antennas is still present. This problem can be averted by padding the range FFT with the first power value (the value from the first FFT bin) to the ‘negative’ range as shown in [Figure 2.20](#). Due to their nature, only CFAR OS and CFAR GOCA have behaviour that can be used to avert the sharp rise in power at low range. The other CFAR procedures cannot be tweaked to show this behaviour and are therefore not investigated in the experiments.

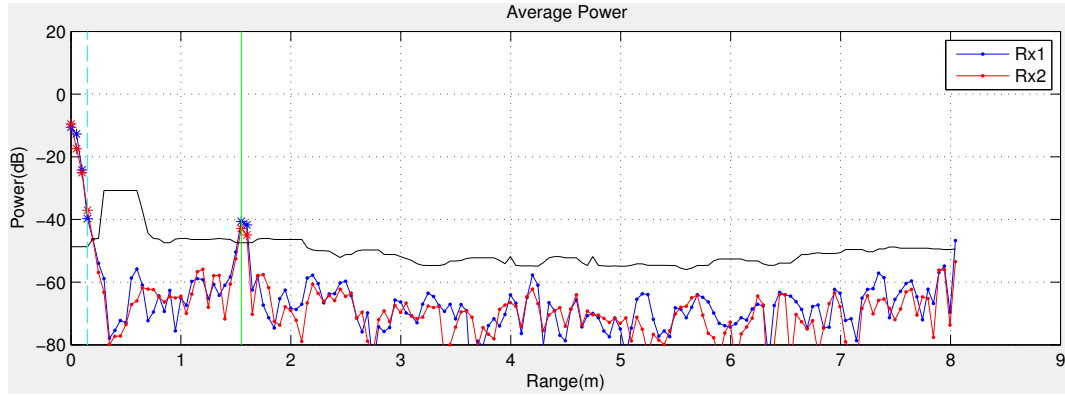


Figure 2.19: An experimental range FFT with a target at 1.5 m and the CFAR OS threshold line shown.

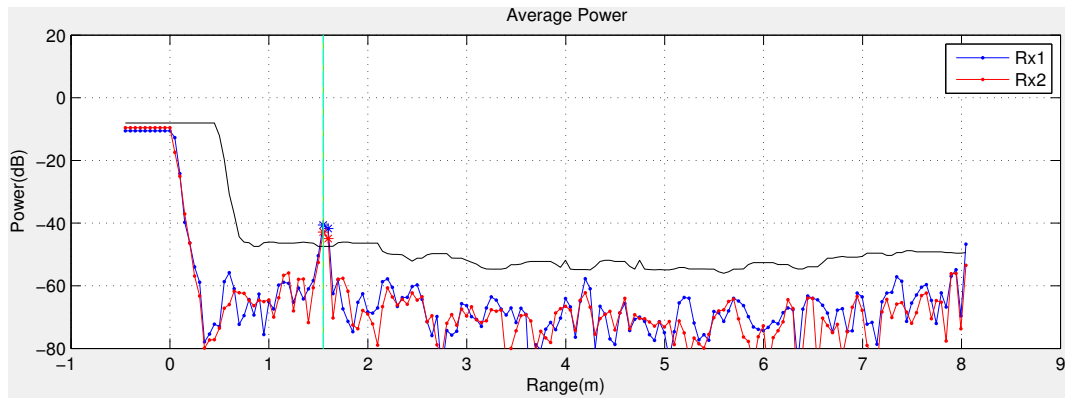


Figure 2.20: [Figure 2.19](#) with additional padding.

Chapter 3

Setup

3.1 Introduction

The experimental setup is created to store the raw (digitized) I and Q signals for later processing. These signals can then be processed to test different windows and different detection methods to determine how to design the full system later on. The experiments are divided into four chapters. In the first chapter outdoor and indoor measurements are done to determine outdoor noise levels. The second chapter is to determine optimum processing settings and methods using a grid that is compliant with the Porsche specifications from [section 1.5: Specifications](#). The third and fourth experiments look at scenarios that are more realistic than just a single object in an otherwise empty area.

3.2 Experimental setup

The experimental setup is built around the Omnicar RIC60B. The RIC60B has an internal voltage controlled oscillator (VCO) which can be used for the sawtooth modulation. The first version of the chip available however has a non-linear VCO making it unsuitable for the measurements. Instead the PLL of the RIC60B is fed directly from a direct digital synthesizer (DDS). The DDS is a chip from Analog Devices, the AD9913 mounted on an evaluation board EVAL-AD9913 [\[28\]](#). The AD9913 is controlled using an Arduino [\[29\]](#) so the modulation can be controlled

using Matlab [30].

To be able to feed the single-ended signal from the evaluation board to a differential signal that mimics the behaviour of a crystal a differential amplifier is added. The RIC60B can also be controlled by MATLAB modifying the settings listed in the datasheet [7]. The analog differential I and Q signals from both receivers and the synchronization signal from the Arduino is recorded using a National Instrument Digital Acquisition device (NI-DAQ). The NI-DAQ 6366 allows for the sampling of the signals at 1MHz and 16 bits of resolution [31]. The raw data is recorded using MATLAB and stored as files, see [section 3.3: Processing Toolchain](#). A picture of the setup is shown in [Figure 3.2](#) and a closeup without a lid on the box in [Figure 3.3](#).

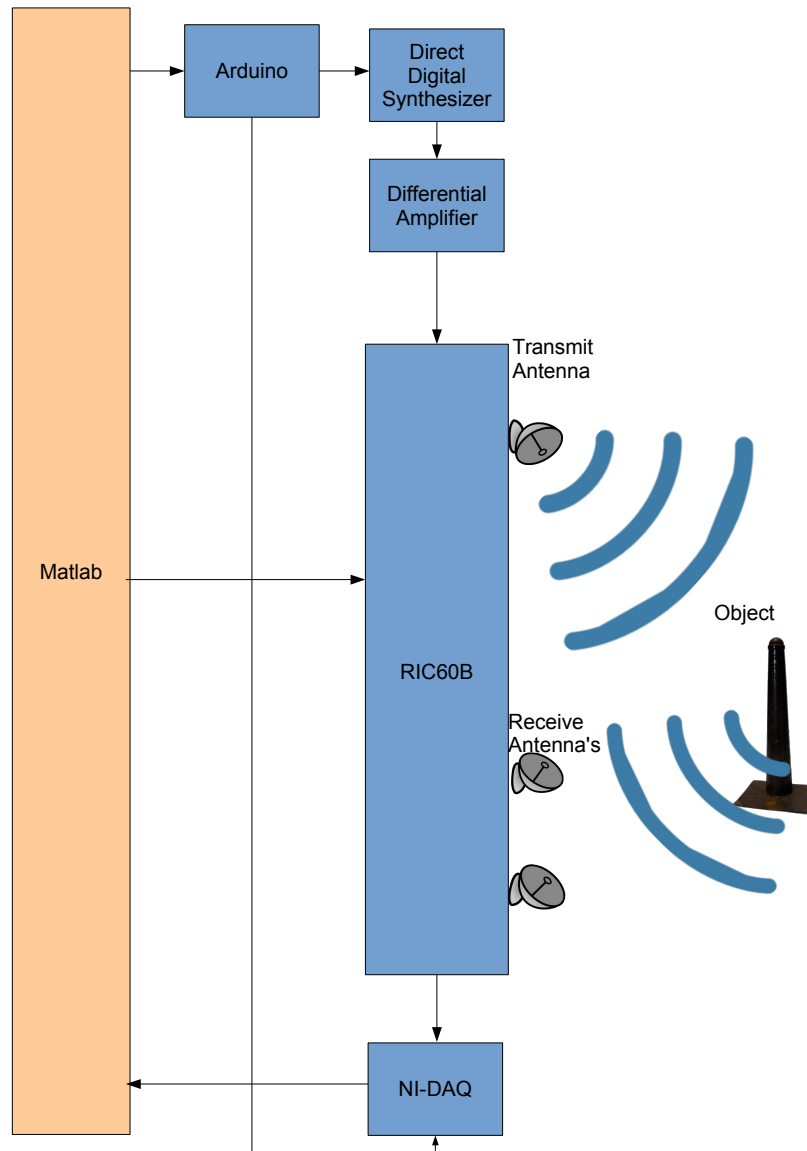


Figure 3.1: Block diagram of experimental setup, showing the RIC60B, NI-DAQ, DDS, Arduino and amplifier and their signal connections.



Figure 3.2: Experimental setup inside.



Figure 3.3: A closeup of the setup with an open box.

3.3 Processing Toolchain

The processing toolchain consists of three parts: recording and replaying raw data, processing raw data, and plotting the results of the processed data. All the MATLAB files that the toolchain consists of are found in [MATLAB Code](#) and contain more than 5000 lines of code.

3.3.1 Record and Replay

The first step in the toolchain is to record the digital I and Q signals. In [Figure 3.5](#) the interface created using MATLAB is shown in replay mode. The interface shows a measuring grid on the left, which allows to record and replay at different positions. The MATLAB files for this part are *record.m*, *replay.m*, *makegrid.m*, *startplots.m*, *updateplots.m*, *get_IQcombined_profile_sawtooth.m*, *dds_arduino.m*, *get_received_dataNI.mat*, *getSplitData.m*, *radarkit.m*, *slider.m* and *updatemeasurements.m*.

Record Mode

The interface for record mode is shown in [Figure 3.4](#). It contains buttons for all locations of the grid, with the selection marked with X. The action of pressing a button in the grid on the left starts the recording of digital raw I and Q signals. The graphs on the right show information from the running setup to confirm that it is working properly before starting recording. The recording is done in multiple steps for different sweep times of 1, 2, 5, 10, 25 and 50 ms. The different sweep times are recorded in order.

When the button is pressed, a signal is sent to the Arduino to set the DDS to the sweep time. The Arduino also produces the trigger signal that starts a sweep on the DDS. The time between the triggers on this signal is slightly longer than the sweep time, allowing the DDS and the RIC60B to step back from 66 GHz to 63 GHz. The trigger signal is also recorded to allow for the splitting of the sweeps (one sweep being one sawtooth modulation) later on. After the correct settings are set in the DDS and Arduino, the recording of the NI-DAQ is started, which is triggered by the same trigger signal. After the first trigger, the NI-DAQ records

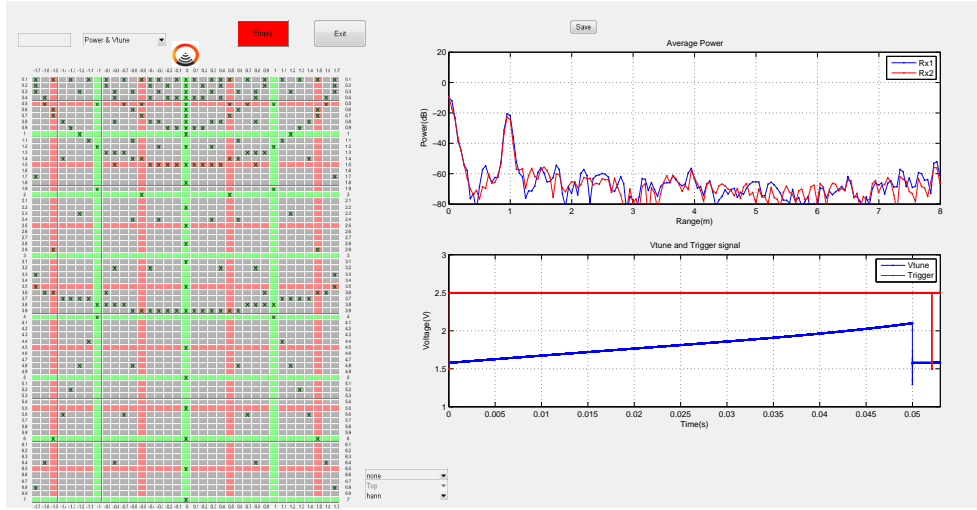


Figure 3.4: The interface used for recording data.

for the time it takes to acquire at least 40 samples. This raw data is then stored in a .mat file in the format of *x-y-sweeptime.mat* where x is the horizontal position on the grid (-1.7-1.7 m) and y the vertical position (0.1-7 m).

Replay Mode

In replay mode, the interface is similar to record mode. The recorded data can be plotted in different graphs (raw I and Q signals, with or without windows, Range Power plots, Range RCS plots and more). When started in replay mode, the interface only activates the button in the grid that have measurements for them in the file system. When such a button is clicked the file is loaded and the data is split into individual sweeps using the synchronization signal. Using this data, different methods for processing the data can be tested, including averaging, direction of arrival (DOA), detection and different windows. This replay mode was extensively used to test different settings for detection and processing on single measurements, before running these settings over all data since this was much more time consuming.



Figure 3.5: The interface used for replaying data.

3.3.2 Process Data

To process the entire set of measurements, the `processdata` function was used (`processdata.m`). It takes as input the path towards the measurements to test, and parameters related to processing, combining measurements and detection. For every single measurement it calculates SNR, range accuracy, DOA accuracy, detection and other metrics.

3.3.3 Plot Processed

To visualize the results of processing the data, `plotProcessed.m` is used. The interface for this MATLAB script is shown in Figure 3.6. In this interface the different results from the processing of the data can be plotted for different parameters, for instance signal-to-noise ratio for different objects. The plots can be made over range using the objects placed at zero degrees azimuth, or over angle, using objects placed in a semi-circle at a range of 1.7 m.

Chapter 4

Experiments: surfaces

In this section the results from indoor en outdoor measurements are presented to determine clutter power for different surfaces. The measurements are conducted by recording the radar signals with no targets within the 7 m range. The surfaces chosen outside are wet grass seen in [Figure 4.1](#) and paved street shown in [Figure 4.2](#). Indoors, the experiment is conducted on PVC tiles shown in [Figure 3.2](#).

4.1 Method

The measurements were done with a sweep time of 100 ms. This long sweep time causes any noise from the electrical system to spread out in the frequency domain, therefore the noise seen in the range FFT is caused by the reflections, diffraction and scattering of the surface and surrounding. This noise is also known as clutter.

4.2 Results

Per surface, the I and Q signals from 50 different sweeps are averaged, and the range FFT is calculated using a Hanning window. Rx1 and Rx2 are the two different receivers. The choice for the window is discussed in [chapter 5: Experiments: single Object](#). The range FFTs are shown in [Figure 4.3](#). Outside, on wet grass, the average power is -62.8 dB and on the paved street section the average power

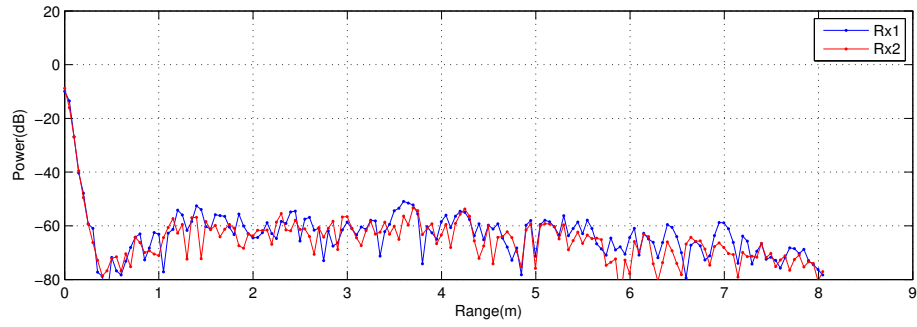


Figure 4.1: The measurement setup outside on wet grass.

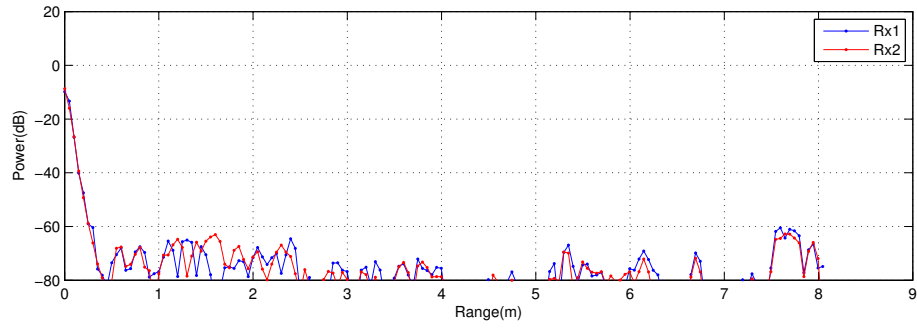


Figure 4.2: The measurement setup outside on a paved street section.

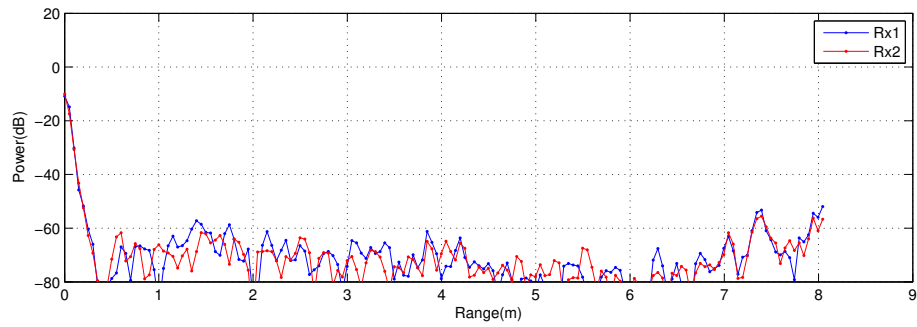
is -76.7 dB. Inside, the average power is -72.2 dB.



(a) Wet grass (outside).



(b) Paved street (outside).



(c) PVC tiles (inside).

Figure 4.3: Range FFT's for different surfaces

4.3 Conclusion and Discussion

From the results it can be deducted that wet grass features the highest amount of clutter power of -62.8 dB. This is as expected since grass is a very uneven surface that will cause scattering, reflection and diffraction. The paved street section is significantly lower with -76.7 dB. This is also as expected since the paved street is much smoother, leaving a lot less room for scattering, reflection or diffraction. Inside, on PVC tiles the clutter power is -72.2 dB. This clutter power is in between that of wet grass and paved street outside. However, the PVC tiles are flat, therefore observed clutter power is higher than expected. This can be explained however because indoors features a ceiling that has contains sharp and metallic objects causing a higher clutter power. Based on these conclusions for the more elaborate experiments indoors is chosen. This because the average clutter power inside is between the two outside surfaces, and with the added benefits for control of temperature, humidity and other weather factors like rain that influence measurements this location is chosen for further measurements.

Chapter 5

Experiments: single Object

The indoor, single object measurements are based on the specifications of Porsche described earlier in [section 1.5: Specifications](#). The goal of the indoor measurements is to determine the digitization requirements, appropriate sweep time, window and detection method.

5.1 Method

The measurements are performed on a grid with a width of 3.5 m and a length of 7 m. The grid points are separated 10 cm apart. Targets are placed on the points in the grid and a measurement is taken as described in [section 3.3.1: Record Mode](#).

Not all the points on the grid are used since this is too time-consuming. A selection of points is chosen using a combination of radial lines radiating outward from the radar sensor and arcs at constant distances from the sensor. This way tests can be done for range and angle in high resolution, but only for a limited amount of angles and ranges respectively. The grid and points are shown in [Figure 5.1](#). Due to time constraints a subset of these points is used in some measurements. A selection of three objects of different diameters and materials is used. They are a 12 mm wooden pole and a 32 mm steel tube of 1 m in height each. The third object is a radar corner reflector with a reference RCS of 1 dB/m² mounted at the same height as the radarchip (34 cm above the ground). The objects are shown in [Figure 5.2](#).

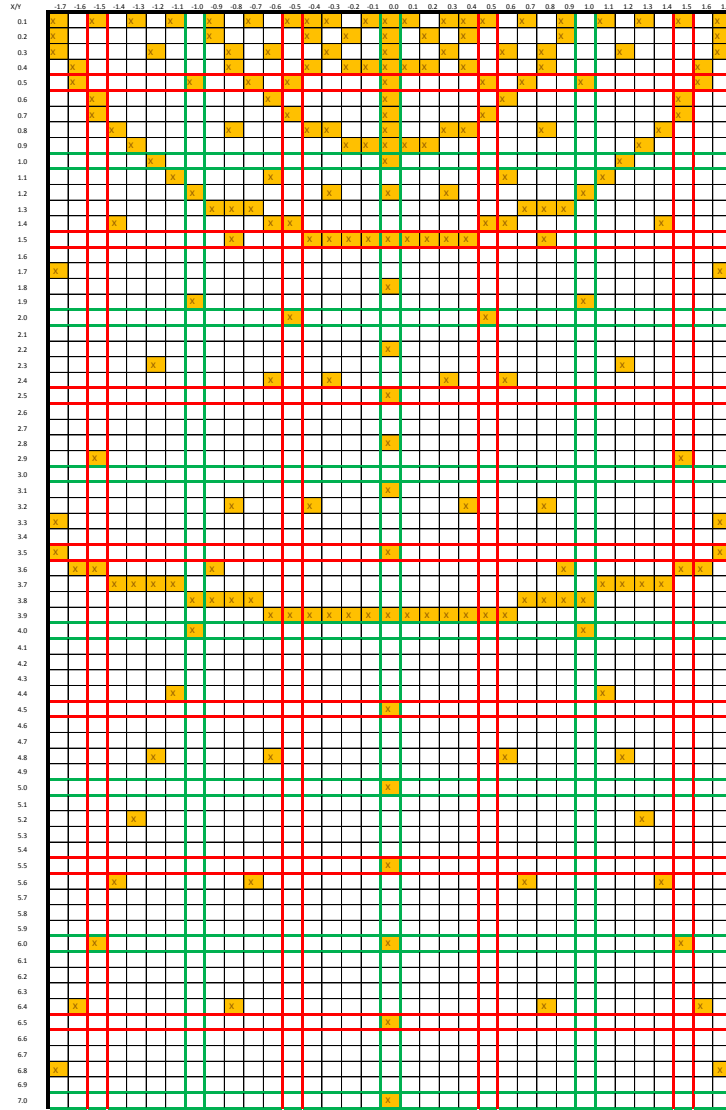


Figure 5.1: The measurement grid and selection points denoted by x. Red and green lines are for easy reference.



Figure 5.2: The objects used for testing.

5.2 Results

5.2.1 Sample rate

To determine how to shape the digitization in the architecture, knowing the effect of different sample rates is important. The sample rate also affects the cost, since ADC's with higher sample rate are more expensive. The recorded measurements are sampled at 1 MHz.

In [Figure 5.3](#) the mean squared error between the original FFT, calculated with a Hanning window and data sampled at 1 MHz, and the FFT at the different sample rates. The plot was made by down-sampling of the original signal in MATLAB. The plot shows that the error approaches zero after 100 kHz. This frequency is higher than the Nyquist frequency of 5.6 kHz at a range of 7 m. Based on these results a minimum sample rate of 100 kHz is needed.

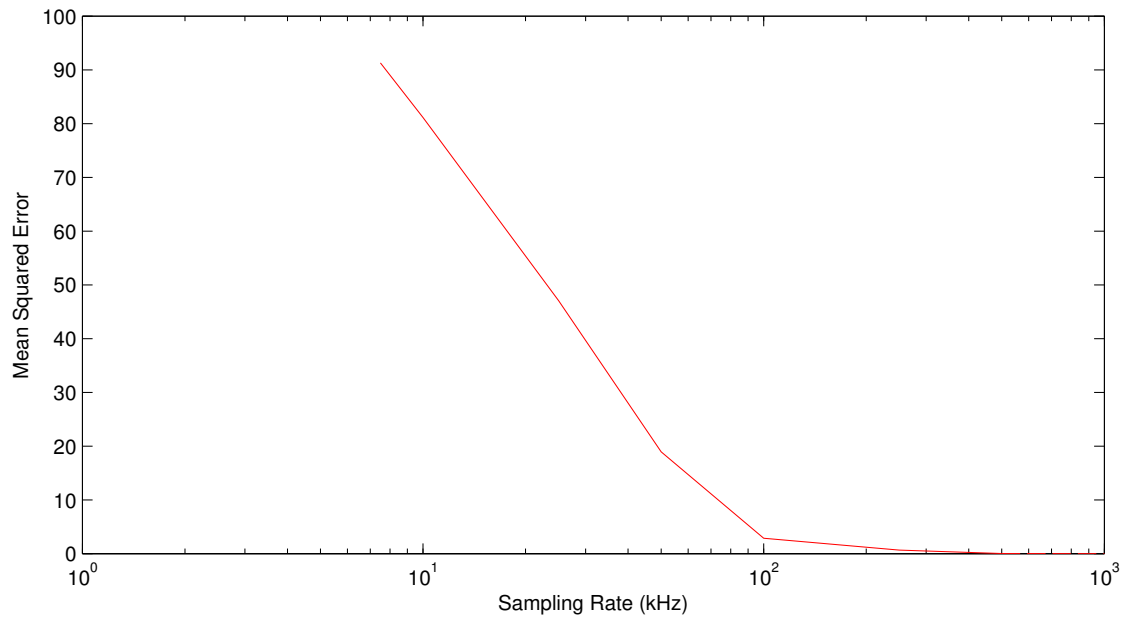


Figure 5.3: Mean squared error of an empty 50 ms measurement versus sampling rate.

5.2.2 Precision

The NI-DAQ 6366 has a precision of 16 bits. This section determines the minimum precision needed for the system by reducing the precision digitally. This is to determine the minimum precision needed because higher-precision ADC's are more expensive

In [Figure 5.4](#) the same sweep as in the previous section is plotted for different numbers of bit for the digital representation. In this case the error approaches zero at 10 bits. Using the formula from [subsection 2.6.2: Resolution](#), this gives an SQNR of 62 dB. Based on the results from [subsection 5.2.5: Objects](#), this SQNR of 62 dB meets the average SNR of the objects at short range. Based on these results a minimum precision of 10 bits is needed.

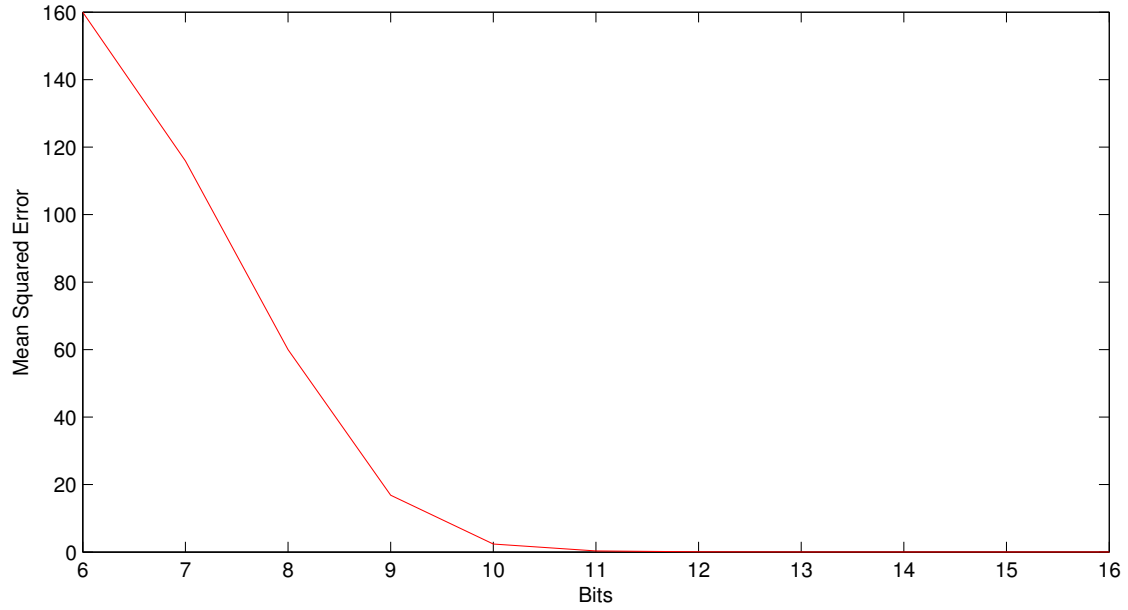


Figure 5.4: Mean squared error of an empty 50ms measurement over precision.

5.2.3 Window functions

The window function has an effect on the SNR since it determines the suppression of the side lobes and the amount of spectral leakage. The SNR is calculated from the FFT's using the power in decibels at the range of the object minus the average power of the other bins within the range of interest (0 to 7 m). To avoid taking the slope of the peaks of the average, bins that are less than 15 cm away from the peak are also removed before calculating the average power. The definition of SNR is illustrated in [Figure 5.5](#), an equation is given in [Equation 5.1](#).

$$\text{SNR} = P_{N(\text{target range})} - \frac{\sum_{N(\text{range}=0\text{m})}^{N(\text{range}=\text{target range}-0.15\text{m})} P_N + \sum_{N(\text{range}=\text{target range}+0.15\text{m})}^{N(\text{range}=7\text{m})} P_N}{N - 7} \quad (5.1)$$

In [Figure 5.6](#) the SNR for a 12 mm wooden pole at different ranges from the sensor at an angle of zero degrees is drawn. The SNR reduces with an increase of range for all windows as expected caused by the propagation of the radio waves discussed earlier in [subsection 2.4.1: Propagation](#). In [Figure 5.7](#) the SNR at a range of 1.7 m is shown versus azimuth. It shows that the SNR of an object also reduces over azimuth. This is caused by the gain at these angles being lower, as

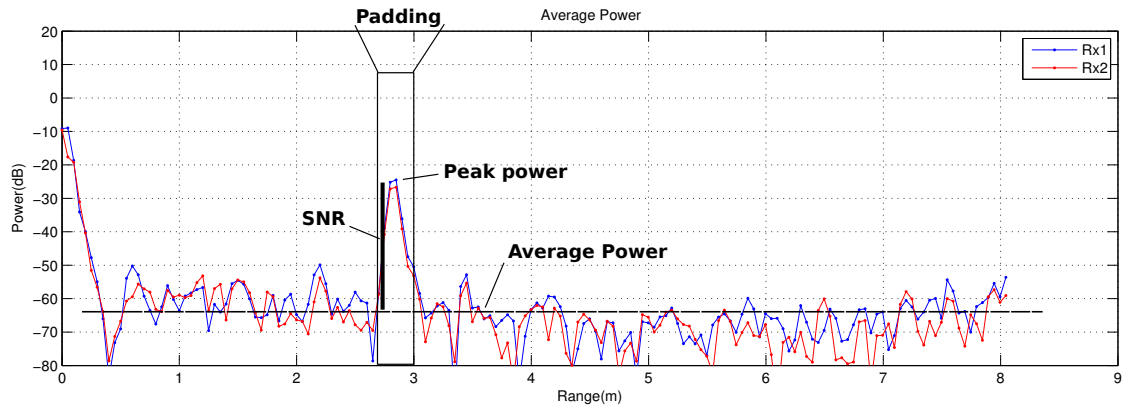


Figure 5.5: A visualization of the SNR definition used.

can be seen in [subsection 2.3.1: Antennas](#).

Both plots show that for the SNR definition used Hanning, Blackman and BlackmanHarris have similar SNR values, differing no more than 1 dB. Hamming and Kaiser have a lower SNR, with Hamming being up to 5 dB lower and Kaiser 10 dB lower than Hanning. The exception here is that at angles over 60 degrees of azimuth, the Hamming window outperforms the other windows with approximately 2 dB.

For the similar performance of the Hanning, Blackman and BlackmanHarris windows a possible explanation can be given by comparing the performance characteristics from Harris [22]. Kaiser and Hamming windows have the same falloff rate of -6 dB per octave. Hanning and Blackman have a falloff rate of -18 dB per octave, which can explain their higher resulting SNR.

BlackmanHarris however has a falloff rate of -6 dB similar to Kaiser and Hamming. The difference between Blackman-Harris, Kaiser and Hamming however is that the side-lobe level of the first side-lobe is much lower for BlackmanHarris (-92 dB) than for Kaiser(-46 dB) and Hamming(-43 dB). This can explain the better performance of Blackman-Harris versus Kaiser and Hamming. The definition of SNR can also be the cause of the difference in performance, but the investigation in the exact causes of the difference in performance are out of scope. Since at all other points and ranges the SNR of the Hanning window is highest, the Hanning window is used to produce the rest of the results.

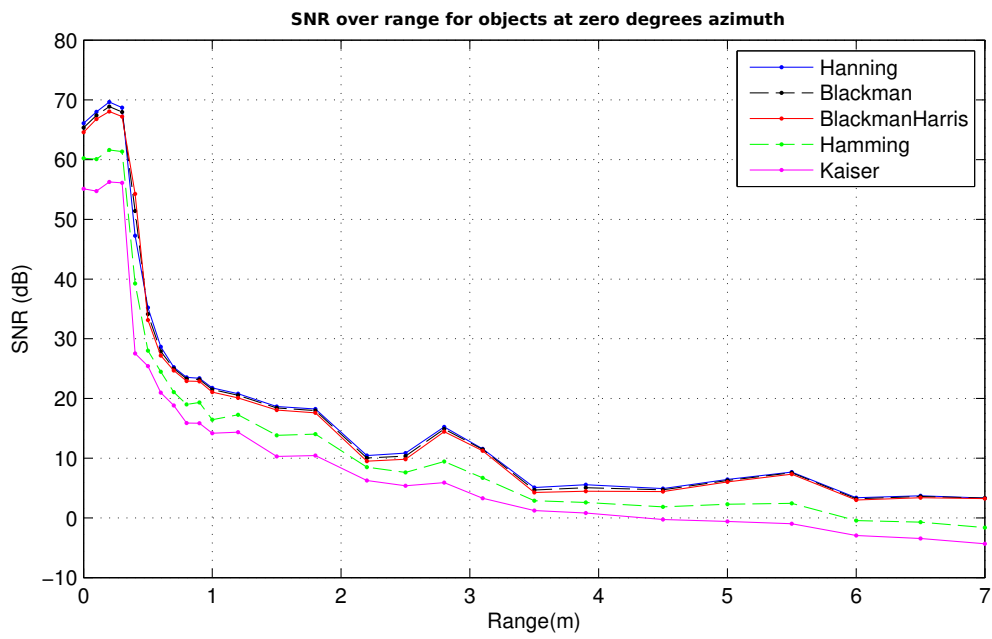


Figure 5.6: SNR over range for a 12 mm wooden pole for different windowing functions.

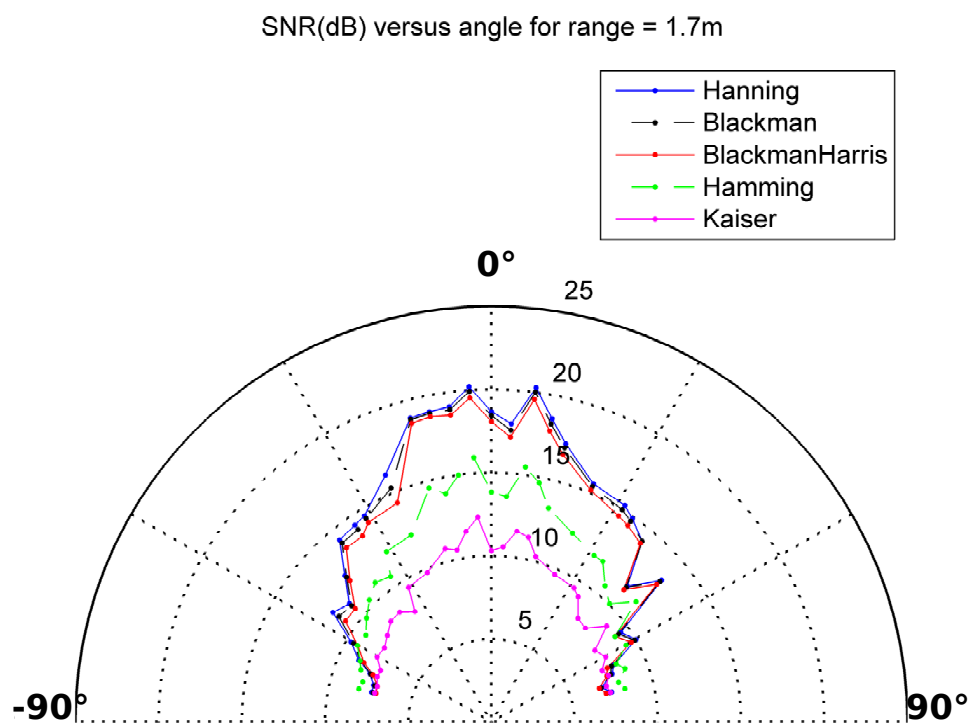


Figure 5.7: SNR over angle for a 12 mm wooden pole for different windowing functions using a 25 ms sweep.

5.2.4 Sweep time and Averaging

For the architecture it is important to determine the needed sweep time and the desired amount of averaging (in the time domain) to achieve the highest SNR. This is done by computing the SNR for various sweep times and averaging numbers using the 32 mm steel object at a range of 3.5 m. The results are shown in a three-dimensional logarithmic plot in [Figure 5.8](#).

This plot indicates an increase in SNR with longer sweep times and also with more averaging. The increase in SNR due to averaging manifest stronger when the sweep time is higher than when a longer sweep time is used. This increase in SNR is also stronger when looking at the difference between two short sweep times and two long sweep times. The SNR seems to have a maximum plateau.

From the theory, it would be expected that doubling the sweep time would lead to an increase of 3 dB every time, but it does not. This is can be caused by the fact that the noise not only consists of the electrical noise of the components, but also of the clutter as seen in the previous surface experiments. This means that the maximum SNR achievable is limited by the clutter power.

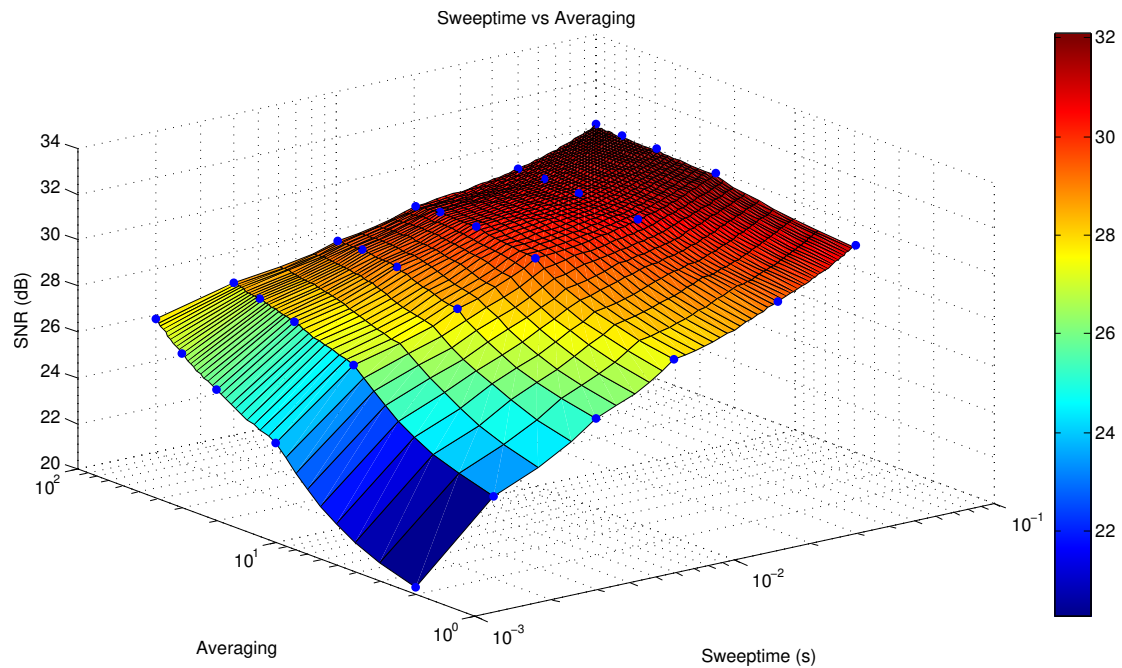


Figure 5.8: SNR for different sweep times and averaging numbers.

5.2.5 Objects

As discussed in theory, different objects have different reflectiveness caused by variations in material, size and shape. In this experiment, the three objects are compared by SNR. Figure 5.9 shows the SNR for the objects placed at different ranges at zero degrees. This difference is not apparent within the first 0.3 meters of range. This has to do with the parasitic antenna coupling between the receiving and transmitting antennas causing the SNR calculations to be flawed in the first range.

The SNR of all objects reduces over range, this is expected due to the fact that radio waves lose power per surface area, therefore the further away the object the lower absolute strength of the electric field and the lower the electric field from the reflection back at the radar sensor. The SNR for the wood and steel object do not drop consistently though, there is a dip in SNR at 2.25 and 5 meters respectively. It is unclear what is the cause of this non-uniformity. A possible explanation is interference from other radio devices at time of measurement

Taking the reference RCS of 1 dB/m^2 , the 32 mm steel pole has an SNR 15 dB

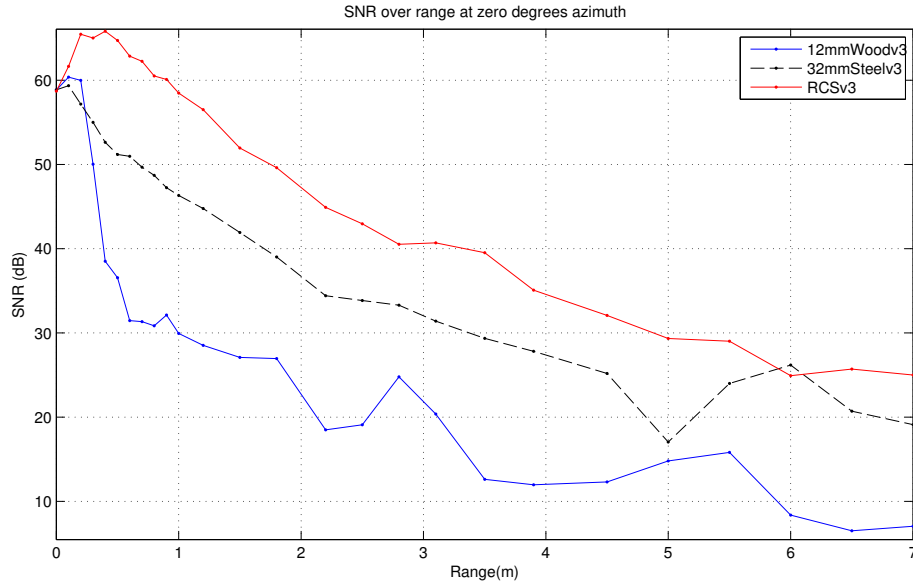


Figure 5.9: SNR over range for different objects.

lower than the RCS until a range of 5 m. The 12 mm wooden pole has an SNR approximately 30 dB lower which is expected due to the smaller size and lower reflection because the object is non-conductive.

Using the reference RCS the RCS of the 12 mm wooden pole is calculated to be -30 dB/m^2 . This is much higher than expected from [subsection 2.4.4: RCS Estimation for simple objects](#) where the RCS calculated was between -65 dB/m^2 and -51 dB/m^2 . Possible explanations are that the reflection is higher due to the smoothed surface, or the specular reflection is stronger. Despite this expected difference, the wooden pole is the object with the lowest SNR and in line with the theory the object hardest to detect.

5.2.6 Direction of Arrival

For calculating the direction of arrival (DOA), a modified sum and difference method is used based on the phase of the two incoming signals, see also the section on DOA in [Research Topics Report](#). [Figure 5.10](#) shows the calculated and real DOA with a blue reference line and [Figure 5.11](#) for different objects. These plots show that the DOA has a slight error factor, it is linear however so it can be compensated for with ease. The plots also show that between -60 and 60 degrees

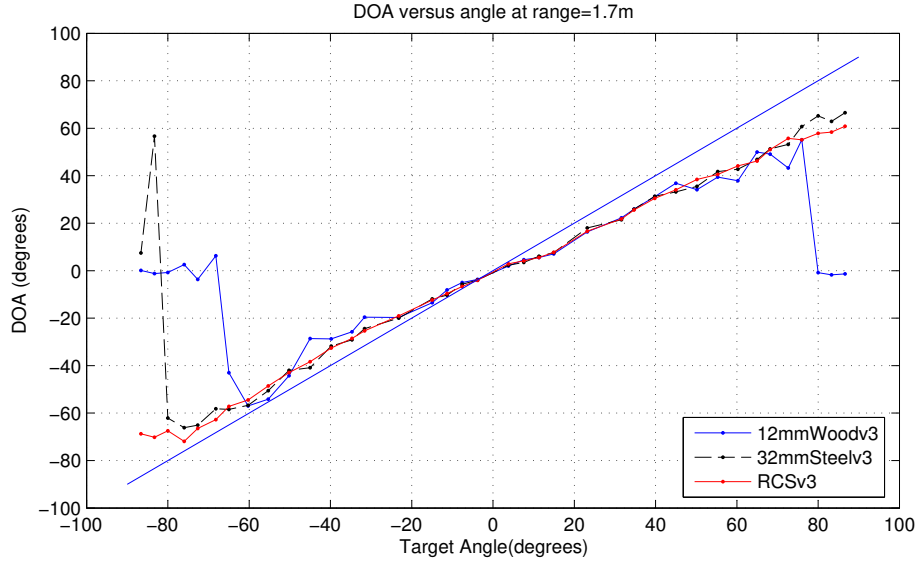


Figure 5.10: The observed direction of arrival versus the actual angle of the target object for different objects. The blue line is the ideal response.

the DOA of all three objects can be determined between with a relative low error. Outside these bounds however, the 12 mm wooden pole features large errors DOA calculations, whereas the other two objects show a relative low error 20 degrees more outwards. The results here match the theory and the results from Omni-radar. The large error at large angles corresponds to the low SNR at these angles as seen earlier. Figure 5.10 also show a different slope between the actual DOA and the calculated DOA. This slope is caused by different lengths in cabling and length difference in the paths of the HF signal inside the Omniradar chip causing slight differences in phase and thus an error in the DOA. Using a linear fit the error in the DOA can be reduced to less than eight degrees, from -60 to 60 degrees. The fitted DOA and the error are plotted in Figure 5.12.

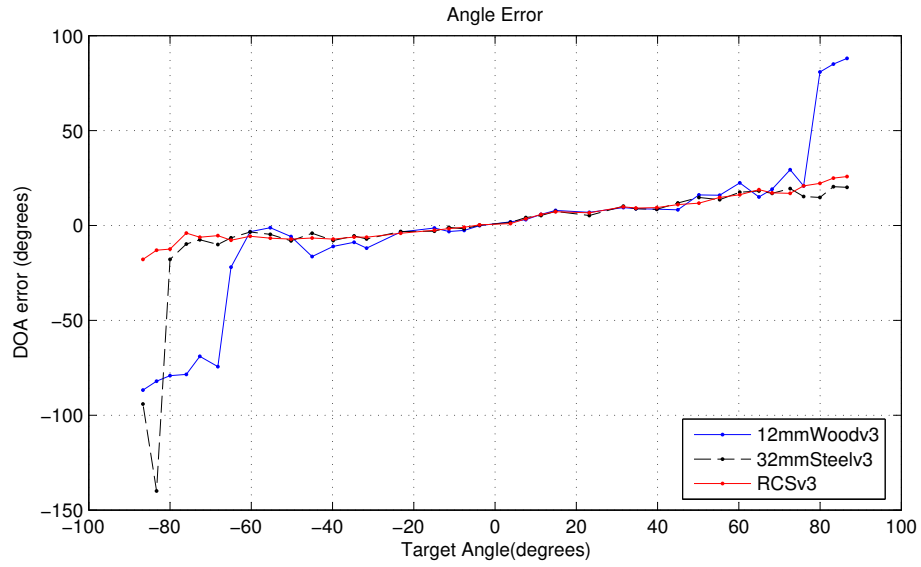


Figure 5.11: The error in angle between real and observed DOA for different objects.

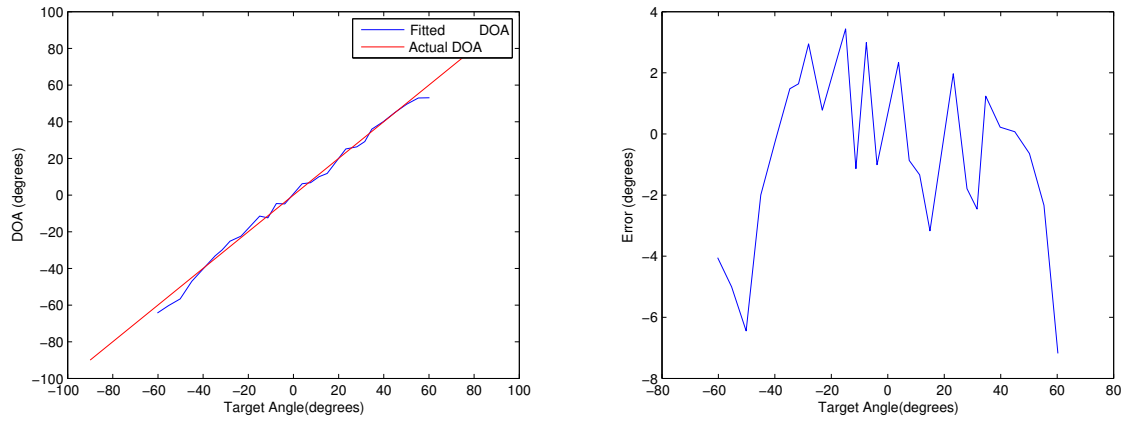


Figure 5.12: Fitted DOA and the error.

5.2.7 Detection

The challenge in detection is to distinguish between noise and clutter power and an object, or target. Using [Replay Mode](#), [Process Data](#) and [Plot Processed](#) fixed threshold and CFAR were tested and compared. To optimize the parameters, first [Replay Mode](#) is used to find working settings by eye. Next, to find a local optimum, [Process Data](#) was used to calculate detection rates for a set of parameters surrounding the working set of parameters.

A correct detection of a measurement is defined as a measurement of which the detected range is within 20 cm of the actual target range. The detection rate is defined as the percentage of correct detections in the set of measurements. The next two subsections will discuss the results of using a fixed threshold and CFAR for detection. The other detection methods discussed in [Appendix A: Research Topics Report](#) are too complex and therefore out of scope of this research.

Fixed Threshold

Using [Process Data](#) threshold levels between -44 dB and -56 dB were processed. Then [Plot Processed](#) is used to plot the detection rate for different thresholds (percentage of correct detections) for a 12 mm wooden pole placed at different ranges at zero degrees azimuth. The plot is shown in [Figure 5.13](#) and shows that -52 dB gives a 100% detection rate until 3.1 meters. The plot also shows that using a fixed threshold, detection fails at short range, which is expected due to the power increase at short range. The detection shows an increase in detection rate between 4.5 and 6 meters. When comparing this with the SNR results from [Figure 5.9](#), the figure shows an increase in SNR around the same range. Combining the information from these two figures, using a fixed threshold the minimum SNR needed for a detection rate of 100% is 15 dB.

To get a better insight in the covered area, a two-dimensional plot in [Figure 5.14](#) shows the correct and incorrect detections by colour for the same wooden pole, with red indicating no correct detection at that position and green fully correct detection at that position. In [Figure 5.15](#) the same plot is made for the 32 mm steel pole, it shows that the detection area for the steel pole is larger than the wooden pole. This is expected since the SNR for the steel object is larger than

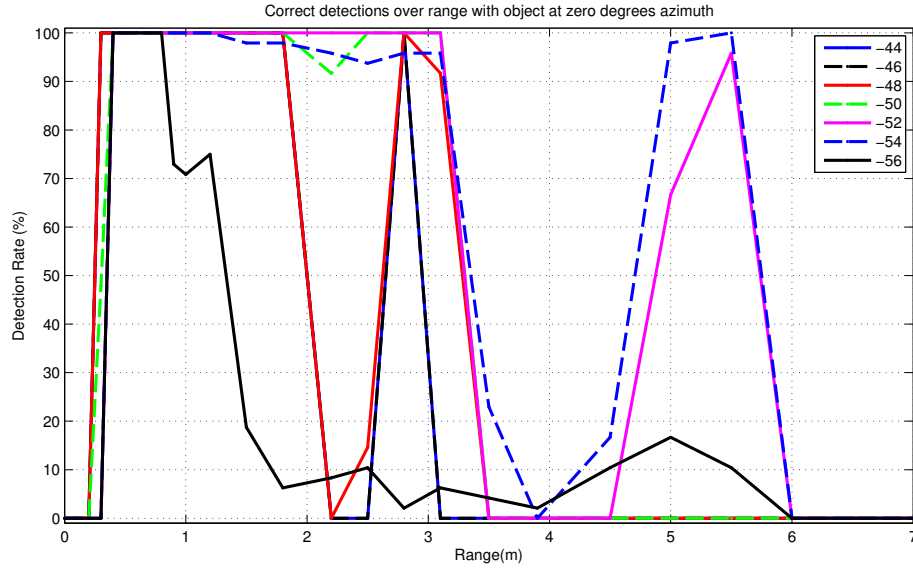


Figure 5.13: Detection rate over range for different threshold levels using an average of two 25 ms sweeps.

that off the wooden pole.

When using a fixed threshold, the threshold does not move with the noise level. On wet grass for instance, noise can be falsely identified as an object with this threshold level (in dB) as shown in Figure 5.16. Furthermore, the threshold level used here is optimal for the set of measurements chosen, that is 25 ms sweep time and an average of 2 sweeps. When using a different sweep time, averaging or other processing options the optimum fixed threshold level will change. To illustrate this, Figure 5.17 shows the same threshold levels for a sweep time of 50 ms. In this case, it shows that a threshold level of -56 dB has a higher detection rate than -52 dB. The exact value for the fixed threshold does not significantly impact the total system complexity and cost.

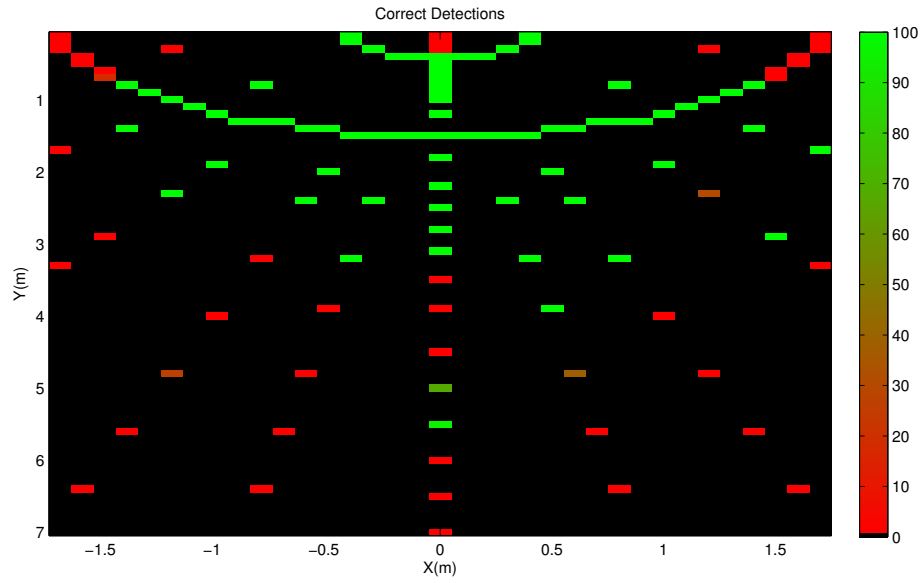


Figure 5.14: Two-dimensional plot showing the tested positions and their detection for the wooden pole.

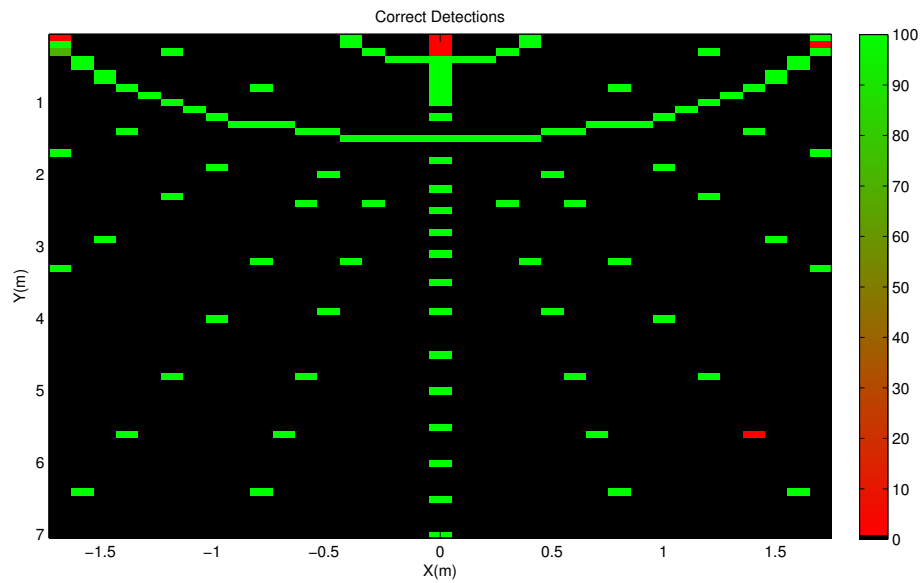


Figure 5.15: Two-dimensional plot showing the tested positions and their detection for the 32 mm steel pole.

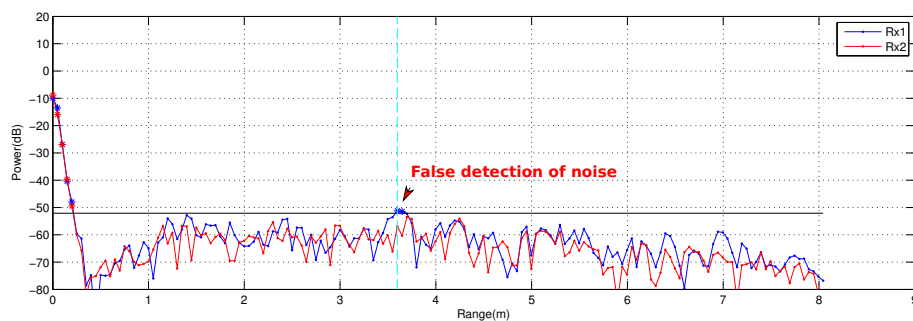


Figure 5.16: The range FFT of a measurement with no targets within range on wet grass, note the false detection of noise at 3.6 meters with the optimum threshold level found on PVC tiles.

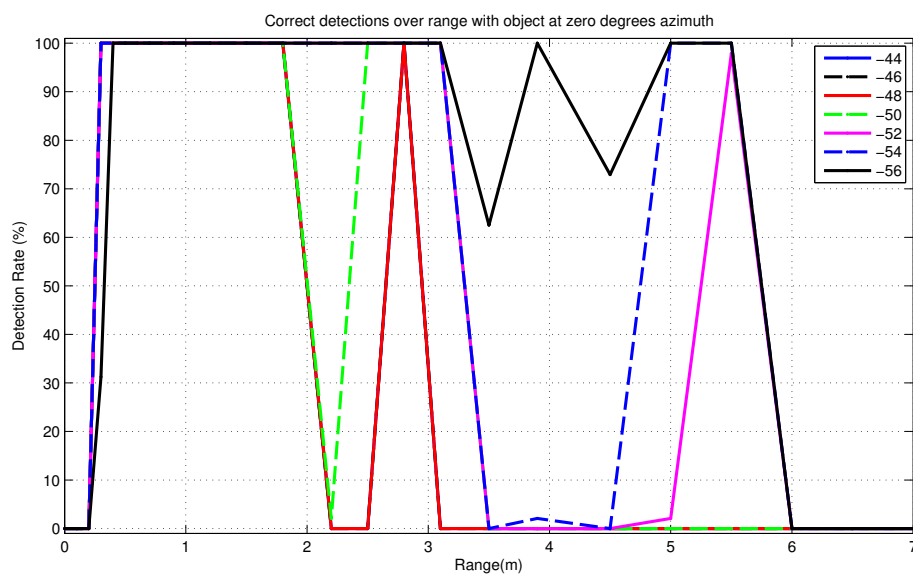


Figure 5.17: Detection rate over range for different threshold levels (in dB) using an average of two 50 ms sweeps.

CFAR

To have an optimum detection for CFAR, the challenge is similar to that of a fixed threshold. With CFAR however, the threshold is not fixed but differs over range according to the range cells around that range. The challenge is to find the correct settings for the amount of training cells, guard cells, threshold cells and in the case of OS CFAR also rank. The optimum settings for CFAR are found in a similar fashion as the fixed threshold detection. But because of time constraints, this research focuses, in the case of OS CFAR, on two parameters: training cells and rank. The effect of threshold factor is not investigated. By testing the detection rate over range for different training cells and rank, a local optimum of CFAR OS is found. In [Figure 5.18](#) an example of a part of this process is shown for different ranks of CFAR OS with 24 training cells. [Figure 5.18](#) shows that the detection rate is 100% with 24 training cells and a rank of 12 from 0.1 meters until 3.1 meters. Between 3.1 and 5 meters the detection rate drops, only to increase again after 5 meter to 100%. This sudden rise matches the rise in SNR of the wooden object shown in [subsection 5.2.5: Objects](#). After 5.5 meters the detection rate drops to 0%.

To determine the optimum number of training cells, the training cells are varied together with the ranks. For each number of training cells, the start and the end of the first streak of 100% detection rate as shown in [Figure 5.18](#) is determined. [Figure 5.19](#) shows these lengths, and based on this using any value between 20 and 32 training cells gives the largest range area. Based on these results the choice is made to use 24 training cells and a rank of 12. In [Figure 5.20](#) the two-dimensional plot of the correct detection using CFAR OS with these settings is plotted for the 12 mm wooden pole. It shows that more area is covered than when using a fixed threshold. In fact, using CFAR, the average detection rate for all points is 72% for wood, whereas for the fixed threshold the average is 64%. When comparing steel, the difference is smaller, using CFAR OS the average detection rate is 95%, only 1% more than when using fixed threshold which is at 94%.

This is shown in [Figure 5.22](#), where there is no false detection of clutter, which does happens with threshold as seen before in [Figure 5.16](#). In [Figure 5.21](#) the correct detections for the 32 mm steel pole are given. As expected the detection

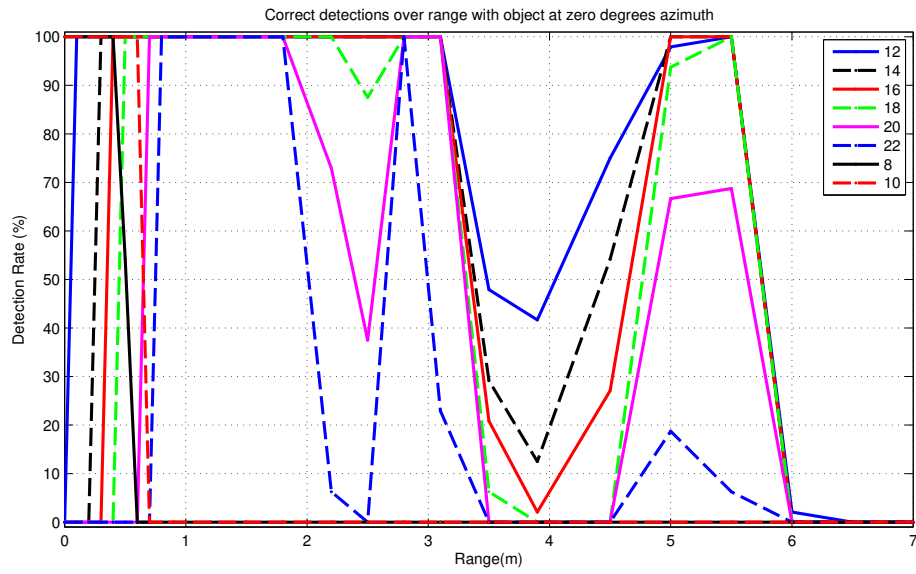


Figure 5.18: Correct detections using CFAR OS with different ranks with 24 training cells over range.

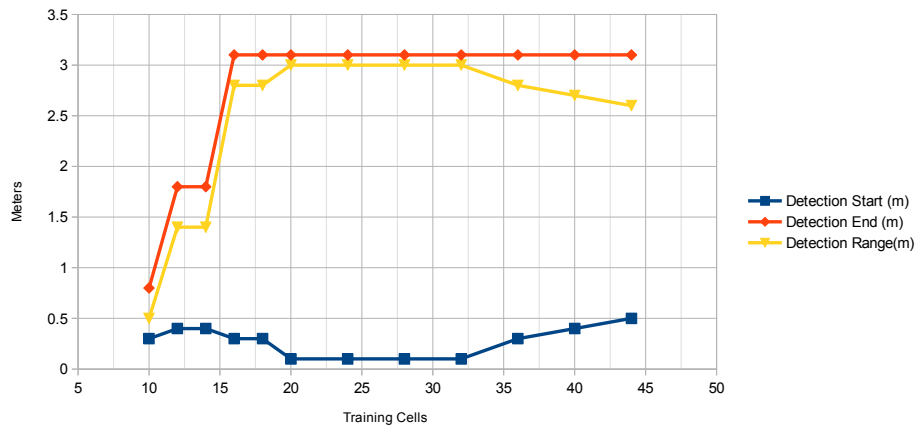


Figure 5.19: The start, end and detection range for different number of training cells.

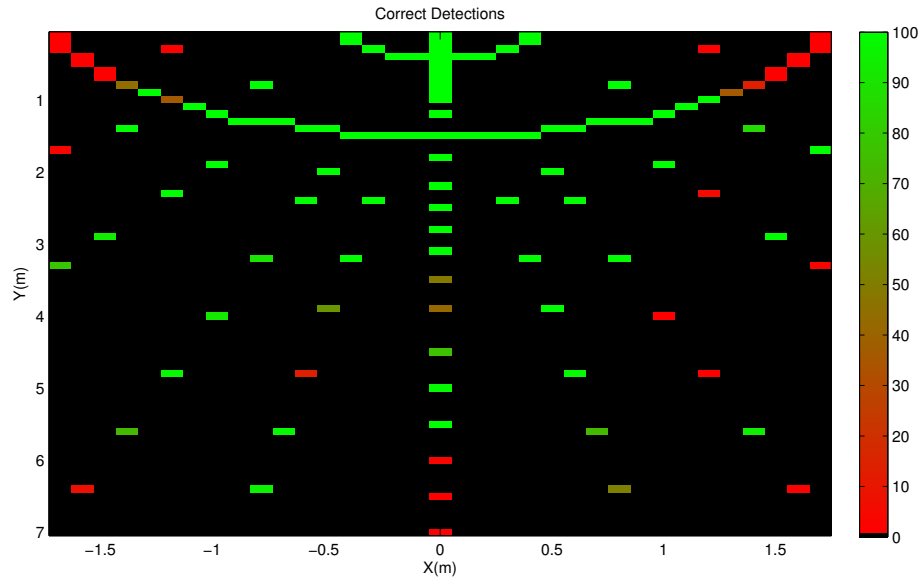


Figure 5.20: Correct detections for the 12 mm wooden pole using CFAR OS with 24 training cells and a rank of 12.

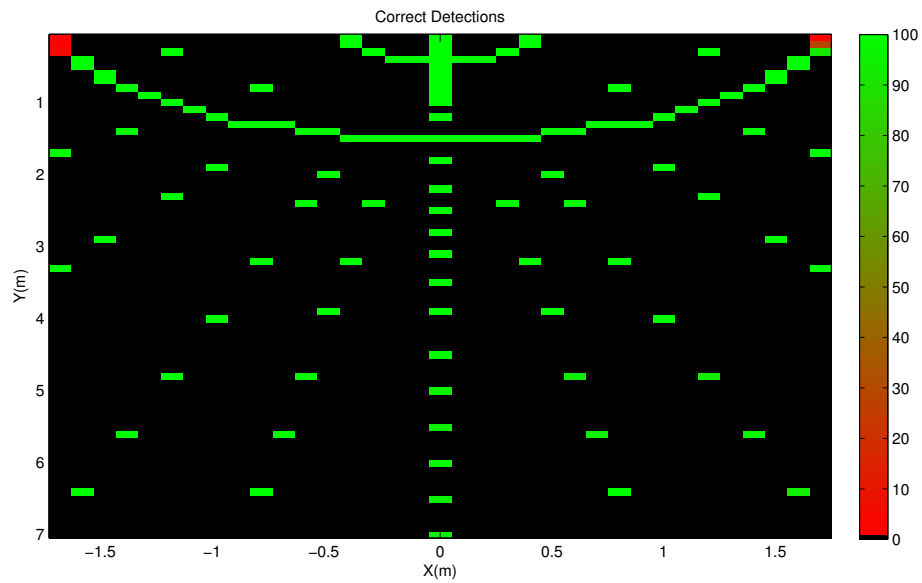


Figure 5.21: Correct detections for the 32 mm steel pole using CFAR OS with 24 training cells and a rank of 12.

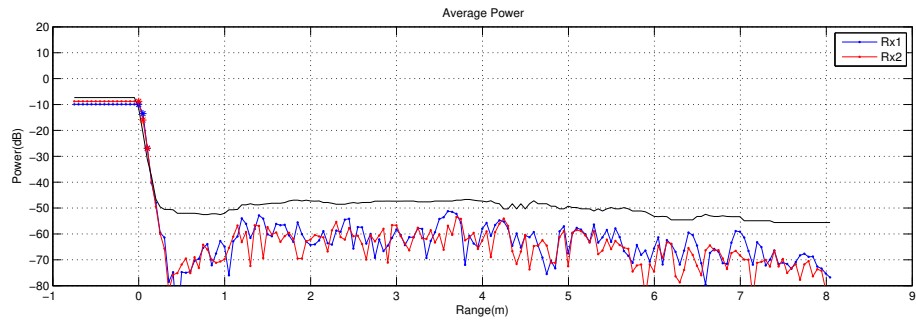


Figure 5.22: Empty outdoor measurement on wet grass with the CFAR OS threshold shown in black.

here is better than that of the wooden object, due to the higher SNR.

CFAR GOCA is also tested. Using the same system as for fixed threshold and CFAR OS the optimum was found to be with 18 training cells, no guard cells and a threshold factor of 0.86. In [Figure 5.23](#) and [Figure 5.24](#) the same detection as [Figure 5.20](#) and [Figure 5.21](#) plots are made with these optimum settings for the wooden and steel object respectively.

The results show that the coverage area using GOCA for steel as well as the wooden pole is smaller than when using CFAR OS. This matches the theory and the literature [\[25\]](#) stating that CFAR OS has better performance than other CFAR methods.

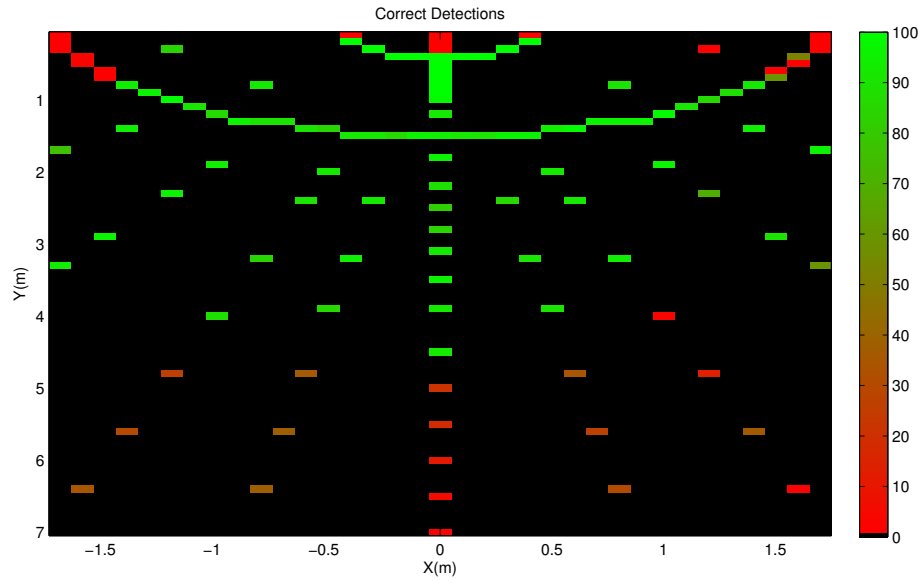


Figure 5.23: Correct detections using CFAR GOCA with 18 training cells and object 12 mm wooden pole.

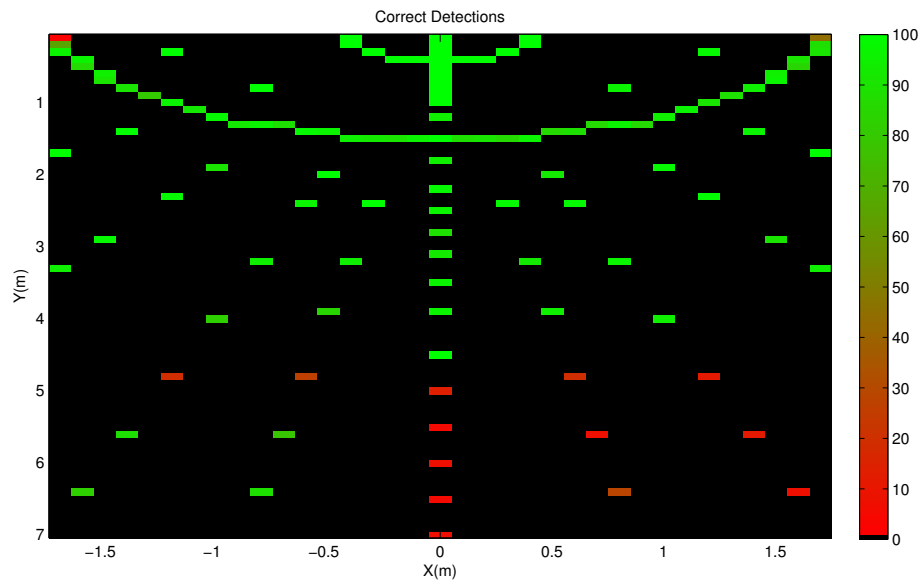


Figure 5.24: Correct detections using CFAR GOCA with 18 training cells and object 32 mm steel pole.

5.2.8 Range Error

Another metric from [section 1.6: Metrics](#) is the range accuracy. Using the best detection method (CFAR OS) with optimum settings, and the wooden object, the range error is measured as the absolute difference between the measured and actual range. This range error is plotted in [Figure 5.25](#). The maximum range error here is approximately 6.3 cm which is 1.3 cm over the theoretical resolution of 5 cm. The slightly higher error than the resolution is likely caused by the actual range between the sensor and the object varying due to inaccuracies in object placement during measurements since the objects are placed manually.

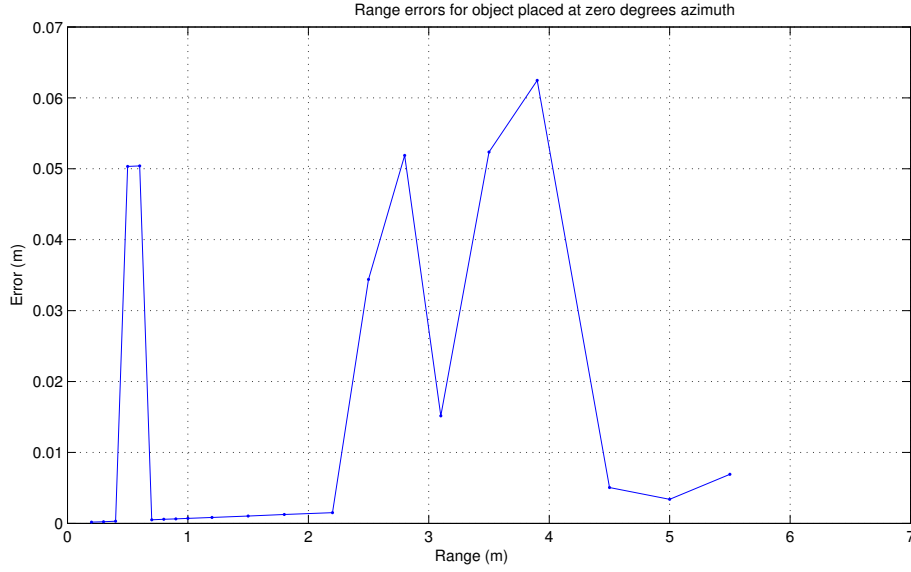


Figure 5.25: Range error for correct detections using CFAR OS and the wooden object.

5.3 Conclusion and Discussion

The experiments conducted in this chapter give good insight into the requirements on the processing chain for an FM-CW radar PDC system. The results from testing different sample rates are unexpected, it is possible that due to aliasing or other problems the sampling rate determined here is higher than actually necessary. Furthermore, the difference in performance from the different windowing functions is hard to explain, and is likely to be very dependent of the SNR definition that was used here. As expected, CFAR OS performed better than a fixed threshold, especially in different clutter scenarios. The fixed threshold however showed similar performance at zero degrees azimuth, but a lower average detection rate than when using CFAR OS. This is unexpected, and needs further investigation to explain, for the processing requirements however CFAR OS seems a suitable method for detection. The settings found here as optimum however, are local optimum since due to time constraints it was not possible to test all different settings, we expect a near optimum, at least locally has been found though. The DOA accuracy using the method proposed by Omniradar turned out to have a lower error than documented by Omniradar. The maximum range error is slightly over the

theoretical resolution, which can be explained by the fact that the objects were placed manually without millimetre perfect alignment. All the settings used here are valid for single objects in an otherwise empty area. In realistic PDC scenarios however, multiple objects and elongated objects are very common. Therefore, in the next two chapters the detection performance for these two scenarios is tested.

Chapter 6

Experiments - Two objects

6.1 Introduction

A PDC will not only be used for situations where there is only one object to avoid. More realistic scenarios for use include multiple objects. To determine the minimum separation needed between objects to allow a PDC system, with the processing used in the previous chapter, to distinguish between two objects

6.2 Method

In this experiment two different objects are placed at different positions, these are the objects:

- (a) **Set 1:** Two objects with a low RCS (the 12mm wooden pole (object 1) and a 60mm wooden pole (object 2) with similar RCS).
- (b) **Set 2:** Two objects with a high RCS (the 32mm steel pole (object 1) and the $1db/m^2$ reference RCS).
- (c) **Set 3:** An object with a low RCS (the wooden pole, object 1) and a high RCS (the 32mm steel pole, object 2).
- (d) **Set 4:** An object with a high RCS (the 32mm steel pole, object 1) and a low RCS (the wooden pole, object 2).

Table 6.1: The different positions to determine the detection rate for multiple objects at different azimuth angles.

Obj 1 azimuth (degrees)	Object 1 range (m)	Object 2 azimuth (degrees)	Object 2 range (m)
-60	1.7	60	1
-60	1.7	45	1
-60	1.7	20	1
-60	1.7	0	1
-45	1.7	45	1
-45	1.7	20	1
-45	1.7	0	1
-20	1.7	20	1
-20	1.7	0	1

As for the locations of the objects, the separation in azimuth and in range are tested. For the separation in azimuth, for each set of objects, the objects are placed at different azimuth angles listed in [Table 6.1](#).

To test the separation in range, the first object is placed at a range of 0.5 and 3 meters at zero degrees azimuth. The second object is placed at intervals of 0.1 meters starting at 0.6 and 3.1 meters respectively until 1 and 3.5 meters respectively. For every situation the detection is determined using CFAR OS with the settings from [chapter 5: Experiments: single Object](#). The measurements were conducted on the PVC tiles as [chapter 5: Experiments: single Object](#).

6.3 Results

The results from the measurements are shown in [Table 6.2](#). A detection of zero (marked in red) means that this object has not been detected, a detection of one (marked in green) means that the object has been detected. In all but one case the object closest in range was detected. The detection of the second object varied with the different situations. The results show that in the case of a separation of 0.1 meters both objects were never detected. The minimum detection separation over range is 0.1 meters when the objects were situated behind each other. In cases where the separation is 0.2 meters or more, object set 2 with two objects with low RCS had the most scenarios in which the detection of the second object failed. This is likely caused by the first object blocking the radio waves from the second object.

Table 6.2: Results from the experiment showing whether detection was 1 (100%) or 0 (0%) for different situations.

Object 1		Object 2		Set 1			Set 2			Set 3			Set 4		
Azimuth	Range	Azimuth	Range	Object 1	Object 2	Both	Object 1	Object 2	Both	Object 1	Object 2	Both	Object 1	Object 2	Both
0	0.5	0	0.6	1	0	0	1	0	0	1	0	0	1	0	0
0	0.5	0	0.7	1	0	0	1	0	0	1	1	1	1	1	1
0	0.5	0	0.8	1	0	0	1	1	1	1	1	1	1	1	1
0	0.5	0	0.9	1	0	0	1	0	0	1	1	1	1	1	1
0	0.5	0	1	1	1	1	1	0	0	1	1	1	1	1	1
0	3	0	3.1	1	0	0	1	0	0	1	0	0	1	0	0
0	3	0	3.2	1	0	0	1	0	0	1	0	0	1	1	1
0	3	0	3.3	1	1	1	1	0	0	1	1	1	1	1	1
0	3	0	3.4	1	1	1	1	1	1	1	0	0	1	1	1
0	3	0	3.5	1	1	1	1	1	1	1	0	0	1	1	1
-60	1.7	60	1	1	1	1	1	0	0	0	1	0	1	0	0
-60	1.7	45	1	1	1	1	1	0	0	1	1	1	1	0	0
-60	1.7	20	1	1	1	1	1	0	0	1	1	1	1	0	0
-60	1.7	0	1	1	1	1	1	0	0	1	1	1	1	0	0
-45	1.7	45	1	1	1	1	1	1	1	1	1	1	1	1	1
-45	1.7	20	1	1	1	1	1	1	1	1	1	1	1	1	1
-45	1.7	0	1	1	1	1	1	1	1	1	1	1	1	1	1
-20	1.7	20	1	1	0	0	1	1	1	1	1	1	1	1	1
-20	1.7	0	1	1	0	0	1	1	1	1	1	1	1	1	1

In the case of separation over angle set 3 has only one scenario in which not both objects were correctly detected, in the other scenarios both objects were detected correctly. This detection over angle does fail for two strong objects when the angle by which they were separated was 20 degrees, this supports the possibility that radio waves can be blocked by strong objects. When one or both objects have a low RCS and the azimuth of both objects is between -45 and 45 degrees, both objects are detected.

6.4 Conclusion and Discussion

The experiment conducted here shows that objects with a high RCS can cause an object behind it (from the view of the sensor) to remain undetected. This is important since, depending on the angle of which one mounts the radar sensor on a bumper, objects that are not closer in range to the radar sensor, but closer to the bumper can go undetected. It also shows that the low RCS at higher azimuth angles, as shown in [chapter 5: Experiments: single Object](#), causes objects to become undetected. The experiment, however, does not give insight in exact values of the minimum separation in angle and range that is needed for detection of both objects. This is because the detection for multiple objects appears to depend heavily on the objects used.

Chapter 7

Experiments - Elongated Objects

7.1 Introduction

Another situation that can occur in PDC systems is where there are elongated objects to avoid. In this experiment, we explore the effects of elongated objects on the detection.

7.2 Method

For the experiment, an elongated reflector was created using two light reflectors from fluorescent light tube housings. The reflectors are mounted on poles and placed in the same line to form one metallic reflective object with a length of two meters. The reflectors are shown in [Figure 7.1](#), together with the radar sensor of which a small part can be seen at the bottom. Measurements are taken with the objects at different positions and different angles relative to the sensor.

7.3 Results

The resulting FFT from the measurement displayed in [Figure 7.1](#) is shown in [Figure 7.2](#). Using CFAR OS, the elongated object is detected at approximately 1.3 m. The actual object however starts at 0.7 m. The CFAR OS threshold line is higher than the power at that range, even though the power shows a sharp increase.

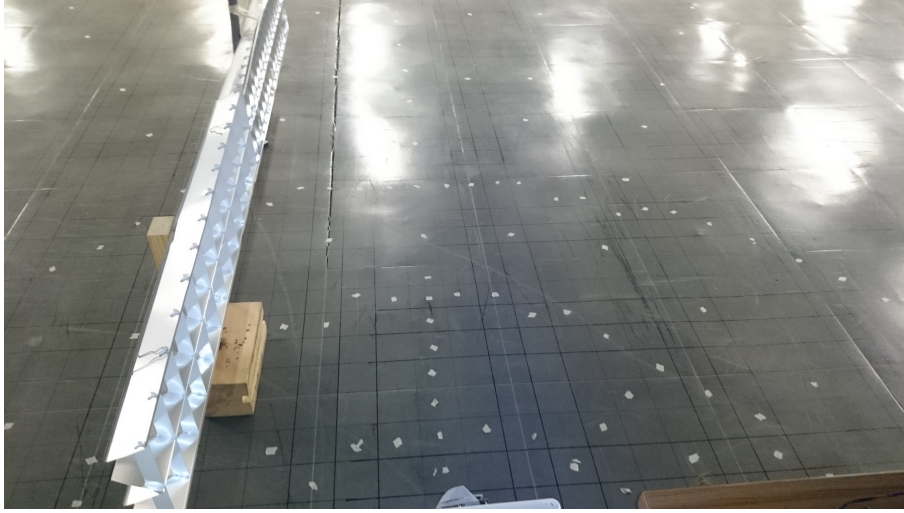


Figure 7.1: Two light reflectors forming an elongated object at close range. The sensor is visible at the middle of the bottom.

This is caused by the nature of CFAR that estimates the noise level by looking at the surrounding bins. In this case, these surrounding bins do not contain the noise level, but reflections from the same object. This is falsely identified as the noise level, and since the power at the bin that is tested is as high, it is identified as noise as well. A solution for this could be to use a combination of a fixed threshold and CFAR OS to clamp the threshold line that CFAR OS determines by the surrounding cells.

To test this hypothesis, the detection rate of the elongated object at five differ-

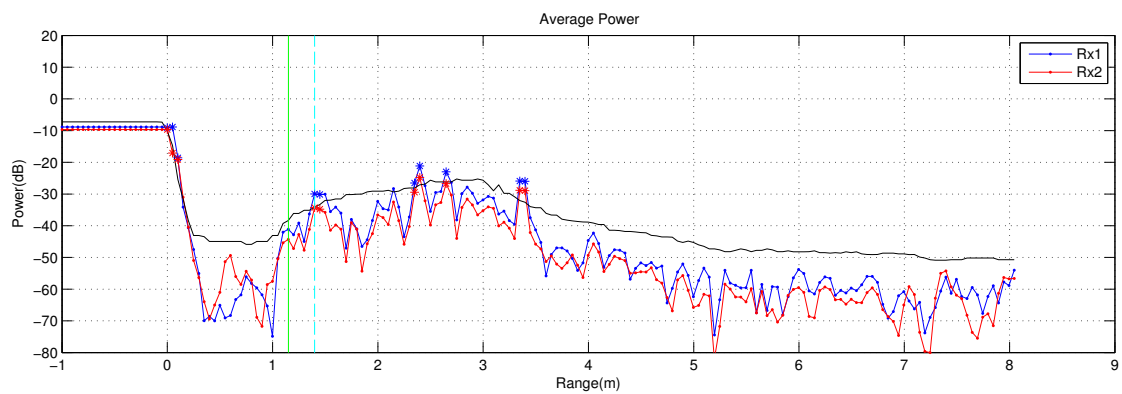


Figure 7.2: The resulting FFT using an elongated object.

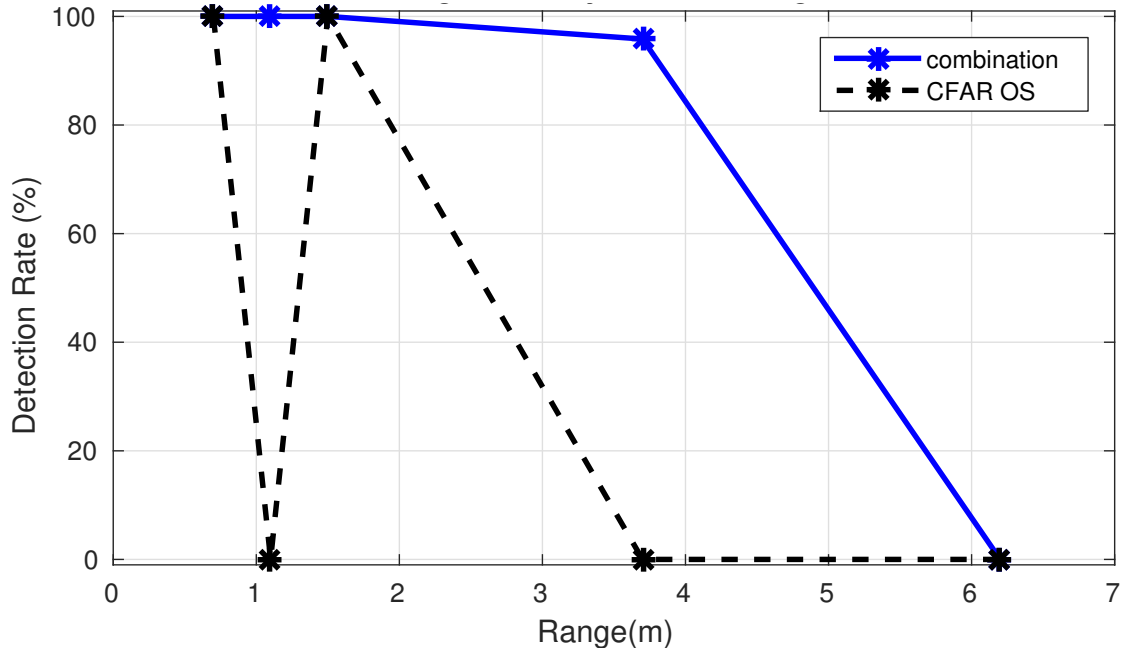


Figure 7.3: The detection rates of elongated objects placed at different ranges using CFAR OS and the combination with fixed threshold.

ent ranges is measured for the used CFAR OS settings, and the combination with a fixed threshold is determined. The results from this test are shown in [Figure 7.3](#). The clamped threshold value used here is -45 dB, which is well above the maximum clutter noise seen in [chapter 4: Experiments: surfaces](#) to avoid false detections in these high clutter situations. The results show that at certain ranges the detection using the combinations improves on the detection of CFAR OS. The combination method was also tested on the grid experiments, and the three objects did not show any degradation in average detection rate, as shown in [Figure 7.4](#) where the detection rate is equal to that of using only CFAR OS.

7.4 Conclusion and Discussion

CFAR OS has a problem with elongated objects due to its noise estimating nature. This problem can be mitigated by using a maximum threshold level of CFAR that is just above the maximum expected noise level. In this experiments the elongated objects used had a high reflection. However, elongated objects with a low RCS will

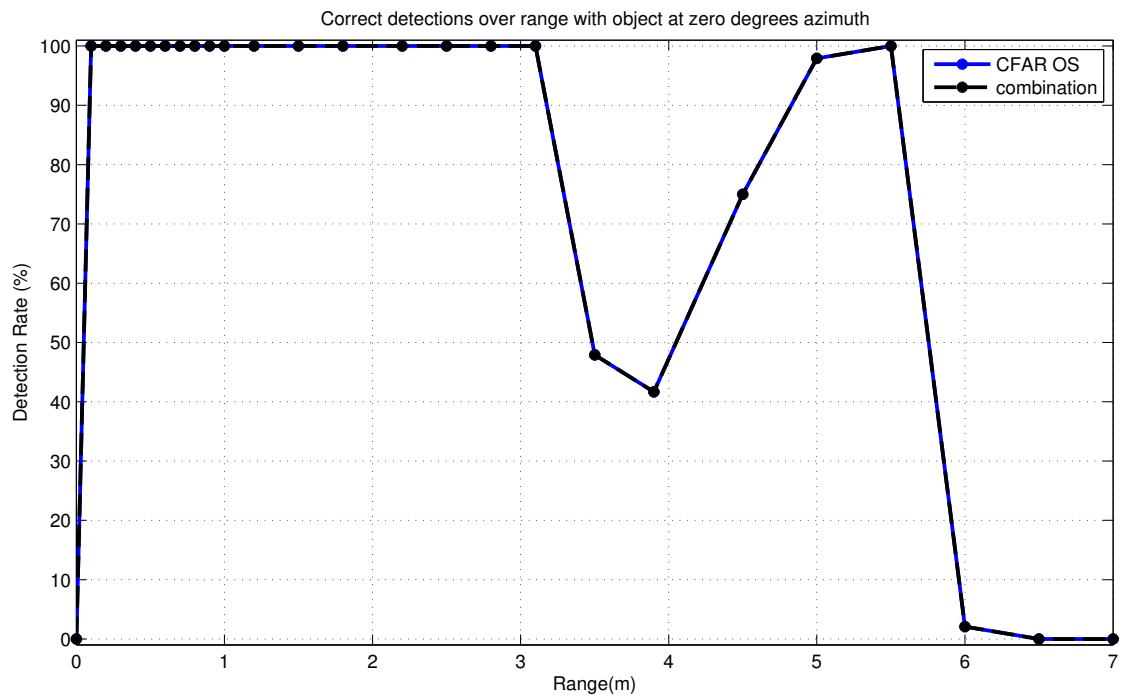


Figure 7.4: The detection over range for the combination of fixed threshold and CFAR OS for the 12 mm wooden pole.

have a lower reflection and therefore might go undetected, even when using the combination of the two detection methods. This however still needs to be tested.

Chapter 8

Conclusions

This thesis is intended to answer the research question ‘How can a parking distance control system be implemented most cost effectively to match current ultrasound systems. From the results from [chapter 5: Experiments: single Object](#) the processing requirements and a suitable detection algorithm were determined. Furthermore, in [chapter 6: Experiments - Two objects](#) and [chapter 7: Experiments - Elongated Objects](#) more realistic scenarios were tested that gave insight into the performance in more real-world scenarios. The results show a large detection area in the case of single objects, and using CFAR OS good resistance to noise and clutter. These results give a good basis on which to design a prototype system. The experiments resulted in the right information needed to discuss different architecture options and detection methods. The experiments also show that a radar PDC suffers from problems caused by fundamental physics in some scenarios.

8.1 Discussion

Unfortunately due to time constraint it was not possible to test actual ultrasound PDC systems and compare the performance based on our measurements of the radar PDC system. Furthermore, some results like the high sampling rate needed and the cause of the difference in window performance could not be fully explained. Also, the experiments conducted were limited mostly to indoors environment, without any weather influence that would apply to realistic scenarios in which the PDC system would be used. Furthermore, the optimum detection pa-

rameters shown here are specific to the system used, the results do not prove that these settings are optimal in other systems, they even point towards the opposite in the case of fixed threshold detection.

8.2 Future Work

The future work to be done in line to a product delivered to market is to create multiple prototype sensors and with processing and detection based on the recommended design. Using these sensors, research can be done into the placement of sensors around the car to cover the full area on either side of a car. Then these prototypes can be used to determine the performance of an actual PDC system, and compare this to an ultrasound PDC system. The tests should involve a wider range of weather conditions and object scenarios than used in this initial research.

Appendix A

Research Topics Report

Radar Sensing for Automotive Applications — FMCW Radar Processing Architecture

UNIVERSITY OF TWENTE.

Tom van den Berg

Sensata Technologies

University of Twente

Report for

Research Topics 192199508

Version: 14:39, Monday 7th March, 2016

Contents

Contents	i
Nomenclature	iii
1 Introduction	1
1.1 Structure	1
1.2 Goals	1
2 Radar Introduction	3
2.1 Introduction	3
2.2 FM-CW Radar	4
2.2.1 Modulation	5
2.3 Radar Reflection	7
2.4 Automotive FM-CW Radar	8
3 Signal Processing	10
3.1 Discrete Time Signals for Radar	10
3.1.1 Matched Filter	10
3.2 Automatic Detection	12
3.2.1 Criteria	12
3.2.2 Integrators	13
3.2.2.1 Moving Window Integrator	13
3.2.2.2 Batch Integrator	13
3.2.2.3 Binary Integrator	15
3.2.3 Detectors	15

3.2.3.1	Threshold	15
3.2.3.2	CFAR	15
3.2.3.3	Image Processing Technique	18
3.2.3.4	Other	18
3.2.3.5	Overview	19
3.3	Direction of Arrival	19
4	Architecture	22
4.1	Digital Architecture	22
4.1.1	Microprocessor	22
4.1.1.1	General Purpose Microprocessor	24
4.1.1.2	Microcontroller	24
4.1.1.3	Digital Signal Processor	24
4.1.1.4	FFT Processors	25
4.1.2	Field-programmable Gate Array	26
4.1.3	Other	28
4.1.4	Overview	28
4.2	Radar Chips Comparison	28
5	Parking Sensor Norms and Standards	31
5.1	Target Speed	34
5.2	Detection Time	34
6	Conclusions	35
6.1	Research Questions	35
6.2	Research Method	35
6.2.1	Metrics for comparison	36
	References	37

Nomenclature

c	Speed of light
CFAR	Constant False Alarm Rate
Chirp	Pulse or period of modulated waveform
DOA	Direction of Arrival
DSP	Digital Signal Processor
DSP	Fast Fourier Transform
FM-CW	Frequency modulated continuous wave
FPGA	Field-programmable Gate Array
IF	Intermediate Frequency
MCU	Microcontroller
PDC	Park Distance Control
PSD	Power Spectral Density
RAM	Random Access Memory
Range	Distance to target
RCS	Radar Cross Section
SNR	Signal-to-Noise Ratio
Target	Object to be detected

Chapter 1

Introduction

Sensors to help drivers park their vehicle by indicating the distance between their vehicle and surrounding obstacles are said to be invented already in 1970's [1]. Radar development has started in the early 1900's [2] mostly for military purposes. The use of radar in automotive has been mostly restricted to adaptive cruise control [3]. Sensata Technnologies BV has set out to develop a radar park distance control system as a way to enter the market with an alternative to ultrasound parking sensors.

1.1 Structure

This report discusses relevant literature in the perspective of the goals stated. The report consists of the following four chapters: radar basics, digital signal processing for radar, digital architecture and automotive norms and standards for parking applications. The report ends with a conclusion containing the research questions for further research and proposes a research method to answer these questions.

1.2 Goals

The goals of this research are the following:

- Find and discuss relevant literature on this automotive radar subject.

-
- Formulate research questions to achieve the goal of Sensata Technologies.
 - Propose a research method to answer these questions.

Chapter 2

Radar Introduction

2.1 Introduction

Radar stands for radio detection and ranging. The development of radar started before world war II and continues until today with very complex radar systems for many different applications [2]. In a basic radar system a pulse of radio waves is sent by a transmitter, reflected by an object and received by the receiver. Distance to this object can be calculated using the time it takes to travel to and from the object and the speed of the radio wave (speed of light), see [Figure 2.1](#).

There are many kinds of different radar systems, the best known systems are: Moving Target Indication(MTI), Pulse Doppler Radar, Continuous Wave (CW)

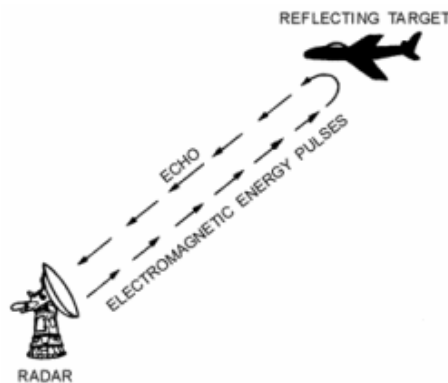


Figure 2.1: A radio wave reflecting of a target [4].

and Frequency Modulated Continuous Wave (FM-CW) [2]. The last type, FM-CW, is of interest for our system because it is the best system allowing for detection of short range static targets [5, 6].

2.2 FM-CW Radar

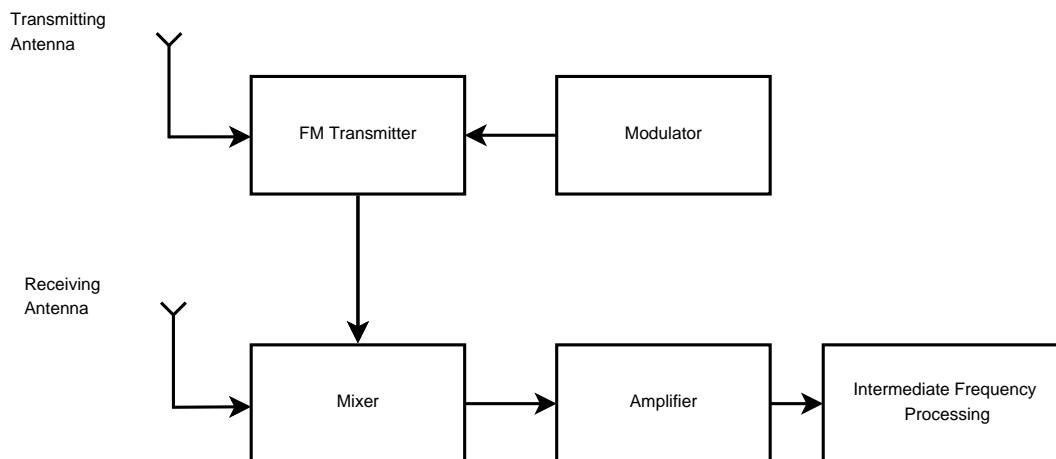


Figure 2.2: Block Diagram of FM-CW Radar.(Adapted from [5], page 83).

In [Figure 2.2](#) the block diagram of an FM-CW radar is given consisting of the frequency modulated (FM) transmitter, the modulator giving out the modulation of the signal, see also [subsection 2.2.1: Modulation](#), the mixer, amplifier and the intermediate frequency processing part. In FM-CW radar the transmitting frequency is modulated, in this example in a linear fashion. When a reflected signal is received, the frequency of this reflected signal will differ from the current transmitting frequency since it will take some time (two times the distance of the object divided by the speed of light) before the signal returns. The mixing of the transmitted and received signals will cause a beat frequency to occur, being the difference between the transmitted and received frequency. This effect is illustrated in [Figure 2.3](#). The analysis and extraction of targets from the intermediate frequency (IF) signal is done by an automatic detector, see [chapter 3: Signal Processing](#). The range and beat frequency are related in [Equation 2.1](#) [7]. In this equation f_b equals the beat frequency, Δf the bandwidth, R the range, T_d is the

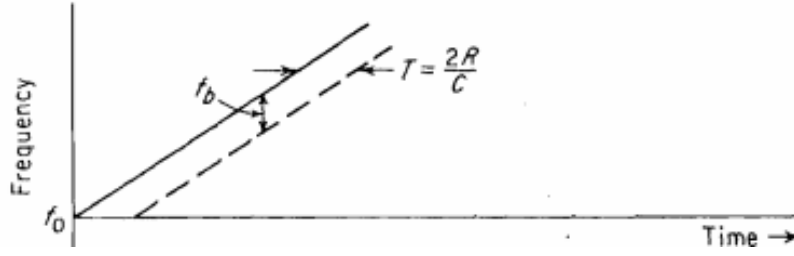


Figure 2.3: Illustration of Linear modulated CW transmit and return signal [5].

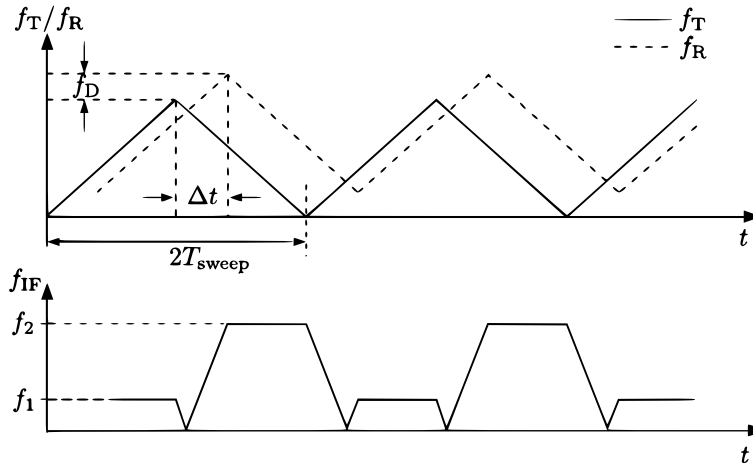


Figure 2.4: Triangularly modulated signal and the resulting beat frequency including Doppler shift from a moving target. f_1 and f_2 are the different resulting frequencies for the up and down going slope [8].

period time of the modulation and c the speed of light. Figure 2.4 illustrates the effect of a moving target introducing a doppler shift in the reflected signal, and the effect to the beat frequency from the intermediate frequency (IF) output of the mixer.

$$f_b = \frac{\Delta f}{T_d} \frac{2R}{c} \quad (2.1)$$

2.2.1 Modulation

One can choose to use linear (sawtooth or triangle) or non-linear (sinusoidal) modulation for FM-CW radar [9]. Linear modulation is very commonly used since

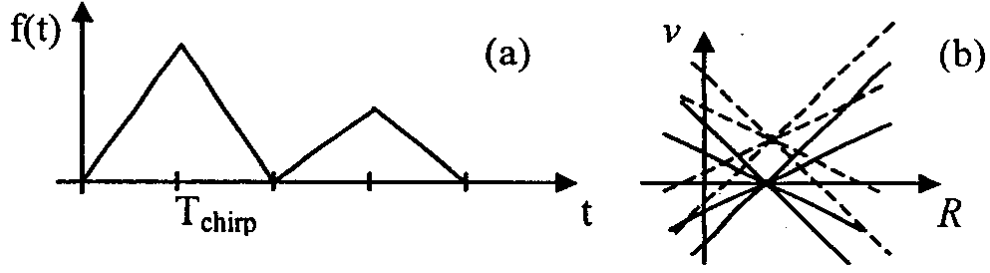


Figure 2.5: Proposed waveform and corresponding range-velocity (R-v) diagram for a two target situation [10].

the beat frequency stays constant over the length of a linear slope (given constant range). With a non-linear slope, the beat frequency of a target is spread out over a large spectrum making it much more harder to do the processing and detection. When using a repeating triangle wave, the Doppler shift can cause ghost targets to occur or incorrect range measurements. A single period or pulse of the modulated waveform is often referred to as a chirp.

A paper from 2001 by Rohling [10] proposes a modulation where two triangle chirps of the same length but different slopes are used, see Figure 2.5. Drawing all possible range and doppler combinations as lines, at the intersection targets with their respective range and speed are found. This technique however does not use the full available bandwidth in the second chirp.

A later paper by Hyun [11] proposes a waveform where two different length

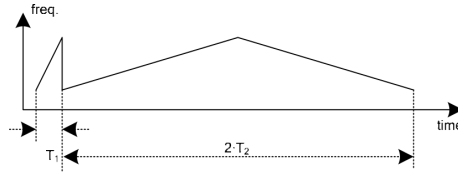


Figure 2.6: Proposed waveform by Hyun [11].

chirps are used like in Figure 2.6. First a short linear sawtooth chirp, followed by a longer linear triangle chirp. Since the Doppler frequency is inversely proportional to the length of modulation, the Doppler shift in short chirps is low. Low enough that the Doppler shift compared to the range frequency is small compared to the

overall range, so using a limited speed the range limits can be determined, see Figure 2.7. In the next chirp all the beat frequencies of the up and down chirp

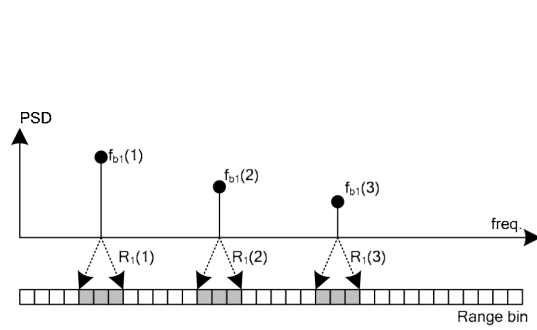


Figure 2.7: The range detection for the first chirp and the power spectral density (PSD) [11].

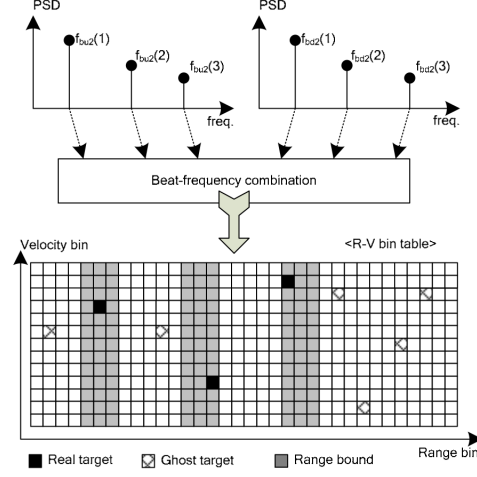


Figure 2.8: Range velocity results using the information from the first and second chirp [11].

are combined into all possible combinations of targets with respective Doppler and range frequencies, as illustrated in Figure 2.8. The combinations which range frequencies outside the limits of the earlier detected target ranges in the short chirp are discarded. This way high detection performance can be achieved with lower complexity than the the method by Rohling, some ghost targets can still occur though.

2.3 Radar Reflection

The radar cross-section (RCS) is a measure for how much energy is reflected from a target. Since the amount of energy reflected determines how well a target can be detected, it is therefore a direct measure of detectability of a target. The target RCS is dependent on its size and material, but also much more complicated features like polarization, incident angle and surface texture [9, 12]

Time varying changes in RCS can occur for targets due to changes in orientation and configuration over time. A paper by Swerling [13] stating four different cases,

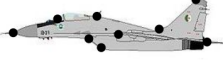
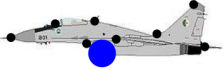
Nature of Scattering	RCS Model	Fluctuation Rate	
		Slow Fluctuation "Scan-to-Scan"	Fast Fluctuation "Pulse-to-Pulse"
Similar amplitudes 	Exponential (Chi-Squared DOF=2) $p(\sigma) = \frac{1}{\bar{\sigma}} \exp\left(-\frac{\sigma}{\bar{\sigma}}\right)$	Swerling I	Swerling II
One scatterer much Larger than others 	(Chi-Squared DOF=4) $p(\sigma) = \frac{4\sigma}{\bar{\sigma}^2} \exp\left(-\frac{2\sigma}{\bar{\sigma}}\right)$	Swerling III	Swerling IV

Figure 2.9: Illustration explaining Swerling targets [19].

now called Swerling targets is a popular model to represent these fluctuations [5]. Figure 2.9 illustrates the different targets. The illustration contains the two different scattering natures, showing a cluster of similar size targets and a large target surrounded by smaller targets. In the RCS model $p(\sigma)$ equals the probability distribution of the measured RCS and $\bar{\sigma}$ the average RCS. In automotive, Swerling targets type 1,2 and 4 have been suggested [14, 15, 16]. A paper from Buller [17] measures the radar cross section of moving vehicles and statistically analyses their reflections and finds them to better fit the Weibull distribution [18]. In the case of “simple” stationary targets, like a pole, Swerling type 4 can be used, or even an ideal non fluctuating target (often referred to as Swerling type 0 and 5 in literature) model can be applied.

2.4 Automotive FM-CW Radar

An early review of automotive radar systems from 1974 [20] does not list Park Distance Control (PDC) as a potential application. It does feature system considerations that also apply to the PDC application. A later paper from 1998 [21] does list it as an application, but sees a couple of problems for the implementation. It does expect market ready products a year later. The first models would appear

already in 1998 though.

There are many papers on the design of millimetre band FM-CW transceivers [22, 23, 24, 25, 26, 27], they all feature a chip design and basic measurements on noise floor and response. Hasch [22] features a good overview of these. None of them however focus on the comparison between ultrasound and radar.

Other papers feature Target detection for automotive [28, 29], modulation waveform design [10] and Direction Of Arrival (DOA) [30] which will be discussed in later sections.

Chapter 3

Signal Processing

3.1 Discrete Time Signals for Radar

Nowadays the IF Signal processing is done digitally, using an analog to digital converter to convert the continuous waveforms to discrete time signals [7]. In Digital Signal Processing (DSP) many factors are to be considered in order to create an optimal system [31].

3.1.1 Matched Filter

In early radar systems, even FM-CW, matched filters were created using electric circuits [32]. For FM-CW however, the matched filter is digitally implemented using a fast fourier transform (FFT) [33]. To avoid a phenomenon known as (spectral) leakage, causing energy of a frequency from one bin to the bins on the side, windowing functions are used [34]. See Figure 3.1 and Figure 3.2 for an illustration of the effects of spectral leakage and a Hamming window. Notice the difference in amplitudes. Notice the lack of tails but also the lower amplitude in the windowed FFT. There are a large number of different windowing functions, Oppenheim gives an overview [36] of the most common windows. Selecting the right window will be part of further research.

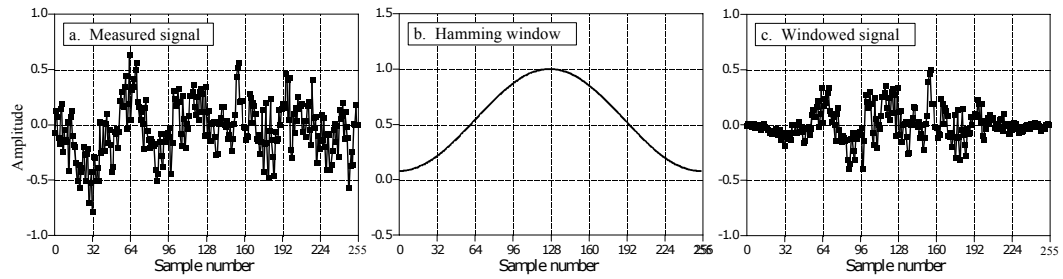


Figure 3.1: Graphs showing the effect of windowing in the time domain [35].

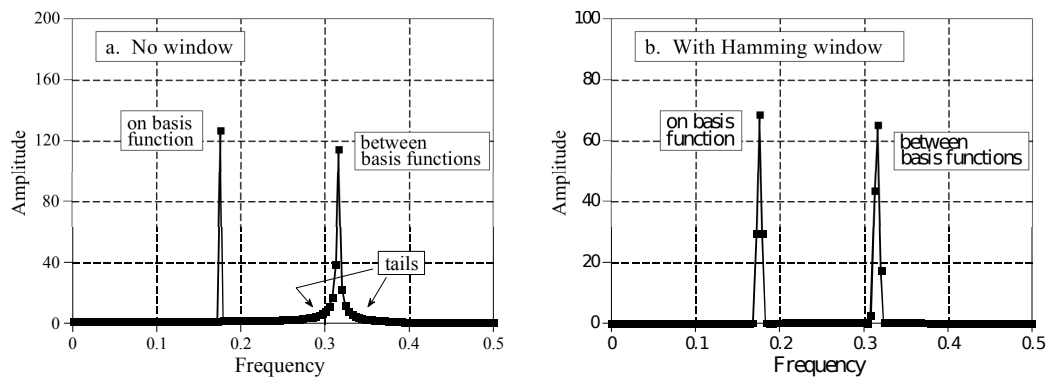


Figure 3.2: Graphs showing FFT of signals with and without a window [35]. Notice the difference in amplitude.

3.2 Automatic Detection

In radar literature, integrators are often called detectors, and automatic detection stating the automatic extraction of targets from the signal from these detectors/integrators [2]. In this report detectors will mean the automatic extraction of targets from a signal, and integrators will indicate the (optional) aggregation of multiple consecutive signals. Automatic detection will be dealt with after integrators but not before looking at criteria often used.

3.2.1 Criteria

Classically the radar signals (optionally after integration) would be observed by a human radar operator that would decide between signal and noise. In automatic detection, the criteria for detection are specified in so-called observers [5]. The observer most used is the Neyman-Pearson observer. Two other observers are the likelihood-ratio receiver and inverse probability receiver. They have been shown however to match the Neyman-Pearson observer under circumstances found in most receivers [5] and are therefore of no further interest. The Neyman-Pearson observer differentiates between a false alarm, noise misunderstood for a signal, and a missed detection, a signal misunderstood for noise. In a Neyman-Pearson observer, the parameters of the detection algorithms are set to match a specified probability of false alarms (false alarm rate).

Another type of observer is a sequential observer, in a series of measurements, it decides whether there is a signal, noise or it cannot decide (ambiguous). When there is a signal it will indicate the target immediately, if undecided it waits for more consecutive measurements to decide based on a measure of uncertainty.

In this section first the difference between coherent and non-coherent integrators is discussed. Next multiple types of integrators that are of interest are discussed. This section finishes with an overview of different detection methods and their advantages and disadvantages.

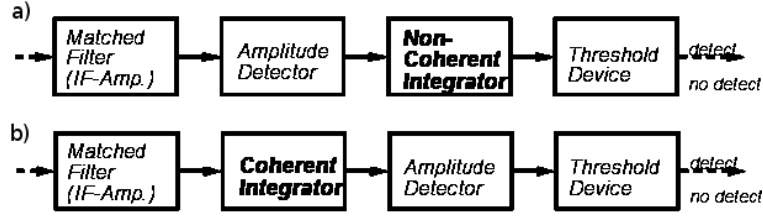


Figure 3.3: Block Diagram of a) coherent integrator and b) non-coherent integrator [37].

3.2.2 Integrators

There are two types of integrators called coherent and non-coherent [37]. The main difference is the loss of phase information in the non-coherent integrator and the location relative to the amplitude detector. A coherent integrator will integrate the signals before any detection is done. The non-coherent integrator afterwards. The difference is illustrated in Figure 3.3 showing a block diagram of the integrator and other common automatic detection blocks. Figure 3.4 illustrates the three integrators used most, explained in the next three subsections.

3.2.2.1 Moving Window Integrator

Moving Window Integrators are a very common integrator in radar systems with digital signal processing. It simply keeps track of the last N measurements by adding any new one and subtracting the last one. It is easy to implement, but memory can be a constrained depending on the size of the digitized signal and the size of the window. It is also susceptible to large interference signals, this is however solvable [5].

3.2.2.2 Batch Integrator

The batch integrator is like a moving window integrator, it is however not moving, so it will wait for N pulses to come in and passes on the summed total. The complexity is very low, and uses less memory than the moving window integrator and has a high angle resolution [2]. The delay between target appearance and detection however is higher.

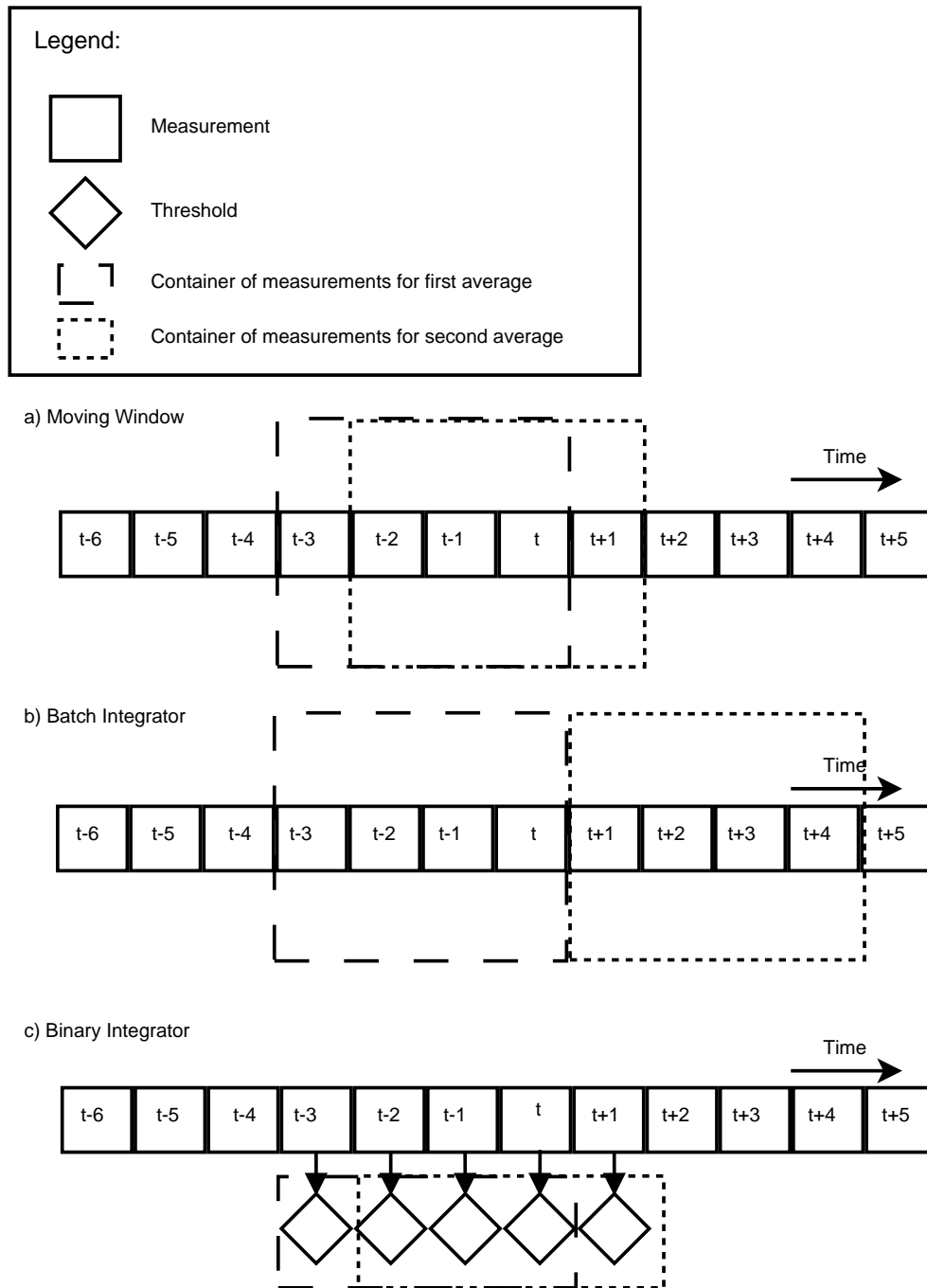


Figure 3.4: Block Diagram of moving window, batch and binary integrator.

3.2.2.3 Binary Integrator

The Binary Integrator was the first integrator developed and is even less complex than the two integrators discussed earlier, but less efficient. It is also known as a double-threshold or m-out-of-n detector. The first threshold is per measurement, the binary outcomes of these thresholds are then summed and a second threshold is applied to determine if there is a target or not. The signal is quantified in two levels however, causing loss in the signal-to-noise ratio [2].

3.2.3 Detectors

In this section detectors of interest are discussed and later an overview including their main advantages and disadvantages is given.

3.2.3.1 Threshold

A fixed threshold is the most basic form of a detector. It will trigger when a value of interest is higher or lower than a certain point. In FM-CW radar the most basic version is to use the amplitude per frequency (Using an FFT and applying a threshold to each bin for instance) as this value of interest. Other values of interest can be the mean, median or variance of integrated samples [2]. Multiple values of interests and their respective thresholds can be combined to improve detection probability or to lower the false alarm probability.

3.2.3.2 CFAR

CFAR is an acronym for Constant False Alarm Rate. It is a form of an adaptive threshold technique commonly found in radar systems. It is based on splitting a signal into range cells. These range cells contain the signal information between a start and end range. In FM-CW radar the bins of an FFT are commonly used as range cells. CFAR determines a threshold for every cell based on the surrounding cells [38]. Figure 3.5 illustrates the use of the surrounding cells, the test cell and the estimation of the noise power.

There are many variants of CFAR, which vary in the method they use to determine the threshold using the surrounding cells [39]. In Table 3.1 an overview is

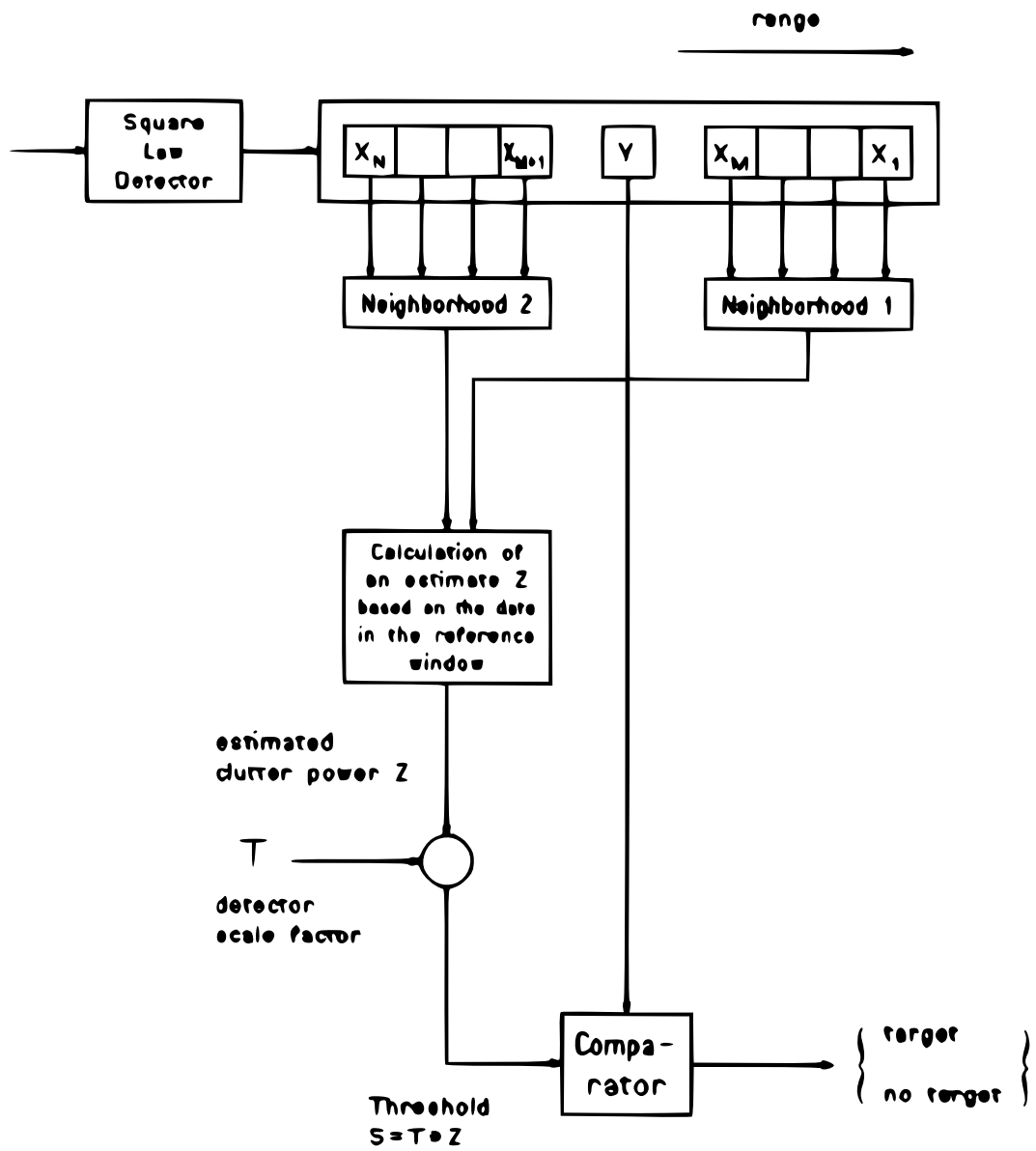


Figure 3.5: Block Diagram of a basic CFAR system [38].

Table 3.1: Table containing CFAR methods and their advantages and disadvantages.

Name	Method	Advantage(s)	Disadvantage(s)
CFAR-CA	Cell Averaging	Simple Implementation	Can cause false detection at clutter edges. Suppresses multiple targets.
SOCA CFAR	Smallest of cell averaging	Combats multiple targets problem of CFAR	High probability of detection at clutter edges.
GOCA CFAR	Greater of cell averaging	Combats false detection of clutter edges	Higher suppression for multiple targets.
S-CFAR	Switching between SOCA, GOCA and CA	Combats both problems	Only combats one problem at a time. Has higher implementation costs.
OS-CFAR[38]	Orderd Statistic	Combats both problems simultaneously	Sorting required of test cells gives higher complexity [40].
And-CFAR Or-CFAR [41]	Combines OS and CA	Better SNR performance	Twice as much processing.

given of the most common methods. The complexity of most algorithms is of

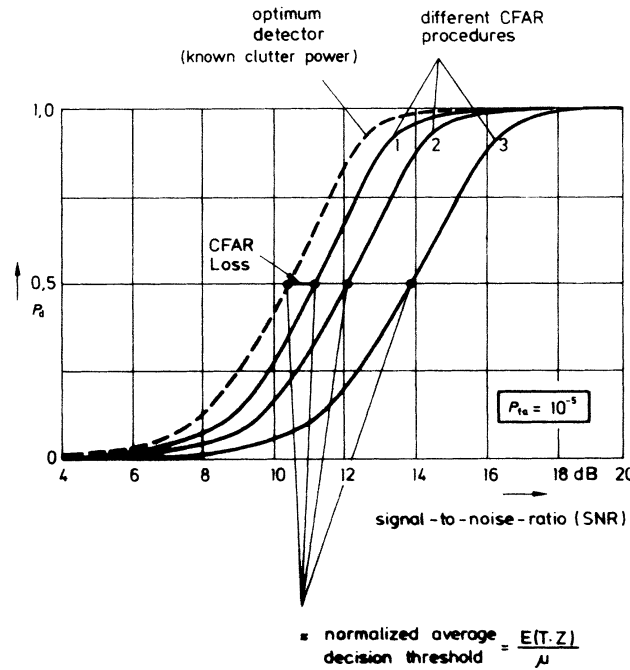


Figure 3.6: Illustration of probability of detection P_d versus SNR [38].

order $O(N)$. In OS-CFAR however the complexity is determined by the sorting algorithm, for which $O(N \log(N))$ can be considered for common algorithms [42]. CFAR algorithms are generally characterized by their probability of detection and respective SNR needed under similar conditions of target type, multiple targets, clutter type etcetera. Comparing an algorithm solely on this performance measure can be deceiving because of different performance in case of different target characteristics. It is however a good measure to compare CFAR algorithms for

very specific situations and a good indicator of its performance [38]. Figure 3.6 illustrates a single target SNR versus detection probability (P_d) of different CFAR procedures.

3.2.3.3 Image Processing Technique

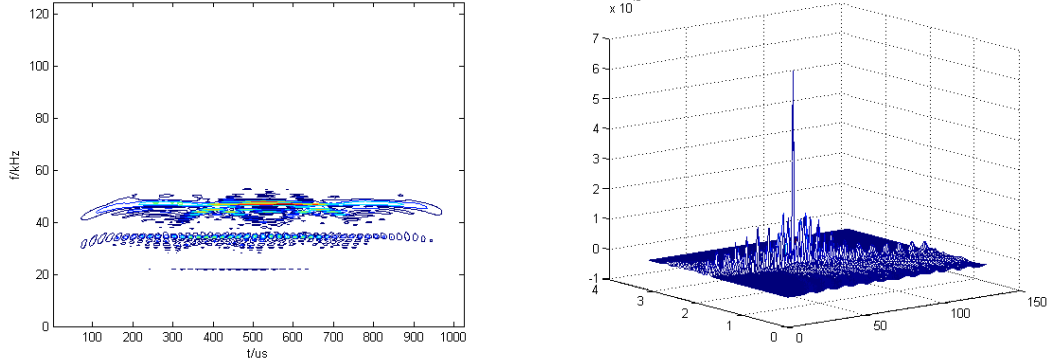


Figure 3.7: WVD transform of an exam-ple signal [43]. Figure 3.8: Hough transform of the WVD [43].

Another method is to use image processing techniques to detect targets in FM-CW radar [43]. The proposed method uses the Wigner-Ville distribution (WVD) as the first step in the analysis which is a form of a spectrogram. In Figure 3.7 a spectrogram using the WVD of an example signal is given of a digitized signal. It shows frequency over time and the colouring indicates the amplitude. Two lines of a large and a small target stand out. Next a Hough Transform is done to detect and locate these lines, which is based on image line detection, see Figure 3.8. Adaptive frequency filtering can then be used to increase the SNR. This method has very high computational complexity though. The WVD transform is of order $O(N^2)$ [44] and the Hough transform algorithm is of complexity $O(N^2 \cdot \theta_{max})$ where θ_{max} is the number of quantization steps [45].

3.2.3.4 Other

Other methods like using state-based systems and knowledge about the signal shape of a target using correlation filters can yield good results [46]. These however

are not suitable for automotive applications due to the large differences between targets. Complexity is also relatively high compared to the CFAR method for example.

3.2.3.5 Overview

In [Table 3.2](#) an overview is given of the interesting detection methods considering automotive FM-CW.

Table 3.2: Overview of detection methods, possible issues and complexity

Method	Possible Issues	Complexity (1= low 5=very high)
Threshold	Needs high number of measurements for good reliability	1
CFAR	CA False detection at clutter edges	2
	SOCA Higher probability of clutter edges false detection	2
	GOCA High multiple targets suppression	2
	S Combats only one problem at a time	2
	OS Higher Complexity	3
Wiener Hough	Very high complexity	5

3.3 Direction of Arrival

Direction of arrival (DOA) is used to indicate at what angle relative to the radar a target is located. To determine the DOA, methods based on the difference in amplitude due to different antenna patterns, and difference in phase due to different lengths of travel of a signal. [Figure 3.9](#) illustrates these theoretical cases including the antenna patterns (beams). For the amplitude comparison the difference in amplitude caused by the different directions of the antenna patterns is used to determine the DOA. In the phase comparison the length of travel of the radio wave differs slightly since one antenna is further away than the other. This causes a phase shift between the two received signals and this can be used to determine the DOA.

In practice using only one of these systems is not possible, so often the complex monopulse system is used where both amplitude and phase are taken into account [\[47\]](#).

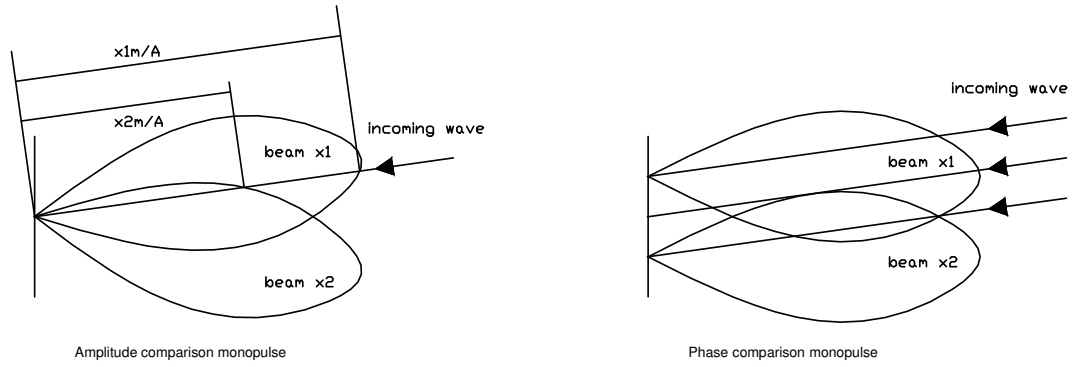


Figure 3.9: Illustration of antenna patterns for theoretical amplitude only comparison and phase only comparison [47].

To solve complex monopulse problems, different algorithms exist, and they differ in performance and complexity [30, 48]. Well known is the sum and difference method which is relatively simple. Another well method is Multiple Signal Classification (MUSIC) [49]. Two well known adaptations that reduce the computational complexity of MUSIC are Root-MUSIC and Beamspace-MUSIC. Another well known system is estimation of signal parameters via rotational invariance techniques (ESPRIT) [50] and adaptations like TLSESPRIT. Figure 3.10 illustrates the differences in performance between these algorithms showing the difference in angle error and SNR for a specific situation. Next to the performance, the complexity is also of interest. The complexity of MUSIC in itself is $O(N^3)$, variants like Beamspace and Root have lower complexity of $O(N^2)$ [51]. The complexity of SUMWE is much lower, and for the amplitude matching sum and difference method the complexity is even lower [52]. Table 3.3 gives an overview of the relative complexity of the algorithms discussed here.

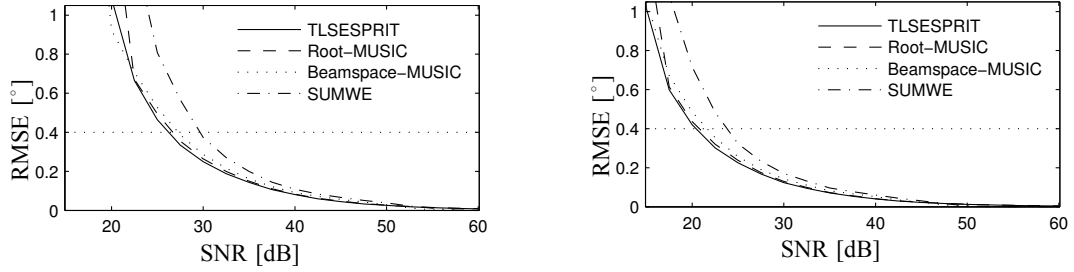


Figure 3.10: Comparison of SNR and angle error for DOA algorithms using two coherent targets. On the left the information from one ramp, or chirp, of a linear modulation period is used. On the right four. [30].

Table 3.3: Overview of relative complexity of common DOA estimators.

Estimator	Relative Complexity
Sum and Difference	Low
SUMWE	Medium
MUSIC	Very High
Root-MUSIC	High
Beamspace-MUSIC	High
ESPRIT	High

Chapter 4

Architecture

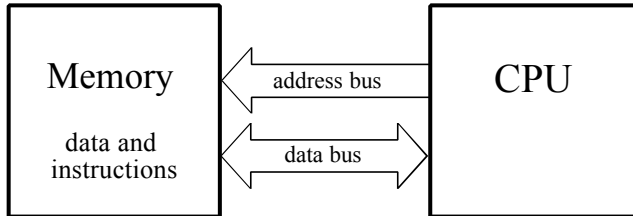
4.1 Digital Architecture

To develop a PDC system, a digital system is needed to do the signal processing. A decision has to be made on the architecture of this system. Different systems are available. This section discusses several options and their advantages and disadvantages.

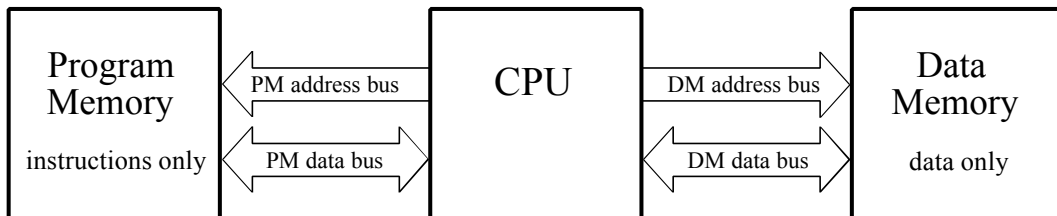
4.1.1 Microprocessor

One main and well known digital system is the microprocessor. It is a processor on a single Integrated Circuit (IC) that features everything necessary for executing programming instructions. It can be combined (on chip) with digital in and out(I/O) communications lines, analog to digital converters (ADC), memory and other peripherals. Three main architectures exist for microprocessors, Von Neumann, Harvard and Super Harvard [53]. The Von Neumann architecture uses a single memory to hold both data and instructions, the Harvard architecture splits these. The splitting of this leads to less pressure on one communication bus. The Super Harvard architecture improves the Harvard structure by adding an instruction cache for faster instruction fetch cycles, and a dedicated I/O controller. [Figure 4.1](#) illustrates the three different architectures.

a. Von Neumann Architecture (*single memory*)



b. Harvard Architecture (*dual memory*)



c. Super Harvard Architecture (*dual memory, instruction cache, I/O controller*)

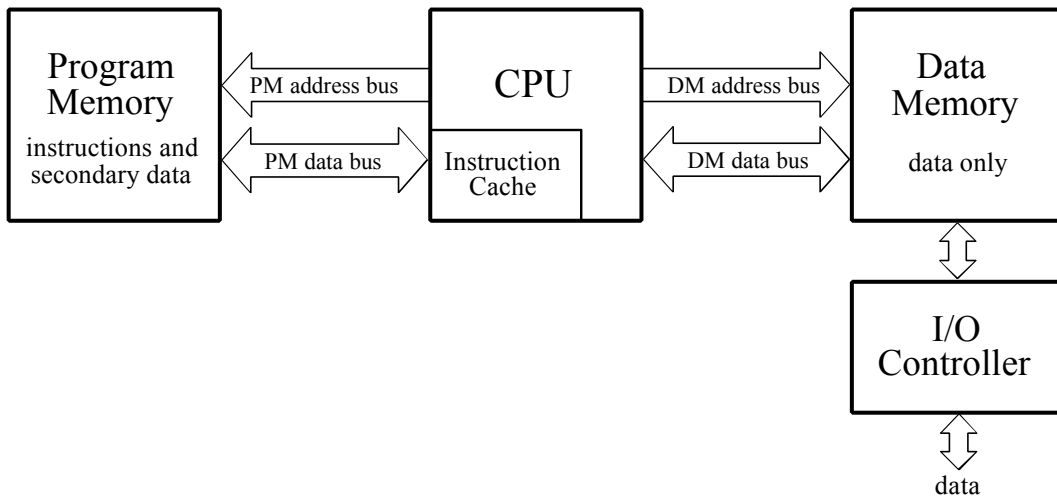


Figure 4.1: Block diagram of Von Neumann, Harvard and Super Harvard architecture [35].

Table 4.1: Comparison of data manipulation and math calculation [35].

	Data Manipulation	Math Calculation
Typical Applications	Word processing, database management, spread sheets, operating systems, etc.	Digital Signal Processing, motion control, scientific and engineering simulations, etc.
Main Operations	Data movement (A \leftrightarrow B) value testing (If A=B then ...)	addition (A+B=C) multiplication (AB=C)

4.1.1.1 General Purpose Microprocessor

General Purpose Microprocessors are those found as a CPU in computer systems. They generally have a wide address bus and data formats, have integrated co-processors and are constructed to support complex high level language functions. Memory and peripherals are found off chip. These CPU's generally have a large silicon area making them costly and with high power consumption.

4.1.1.2 Microcontroller

Microcontrollers (MCU) feature memory and peripherals integrated on the same chip. They are specifically created for embedded system tasks with low demands and therefore feature narrow buses and data formats and simpler addressing modes. They are generally small in silicon area and therefore tend to have low cost and low power consumption.

4.1.1.3 Digital Signal Processor

Computers tend to be good in two areas: Data manipulation and math calculation. Due to trade-offs in hardware it is very hard (read: expensive) to optimize a system for both. Table 4.1 illustrates the differences between these main tasks. The digital signal processor (DSP) optimizes specifically for the math calculation and operations often used in digital signal processing like finite impulse response (FIR) filtering and Fast Fourier Transform(FFT). It is designed to handle common instructions for digital signal processing in parallel. Its architecture generally contains an arithmetic logic unit (ALU) for fast addition and subtraction, a multiplier for fast multiplication and other peripherals to aid in digital signal processing speed. Figure 4.2 illustrates a typical DSP architecture. DSP's feature a fixed or floating point processor, a narrow address bus with specialized addressing modes

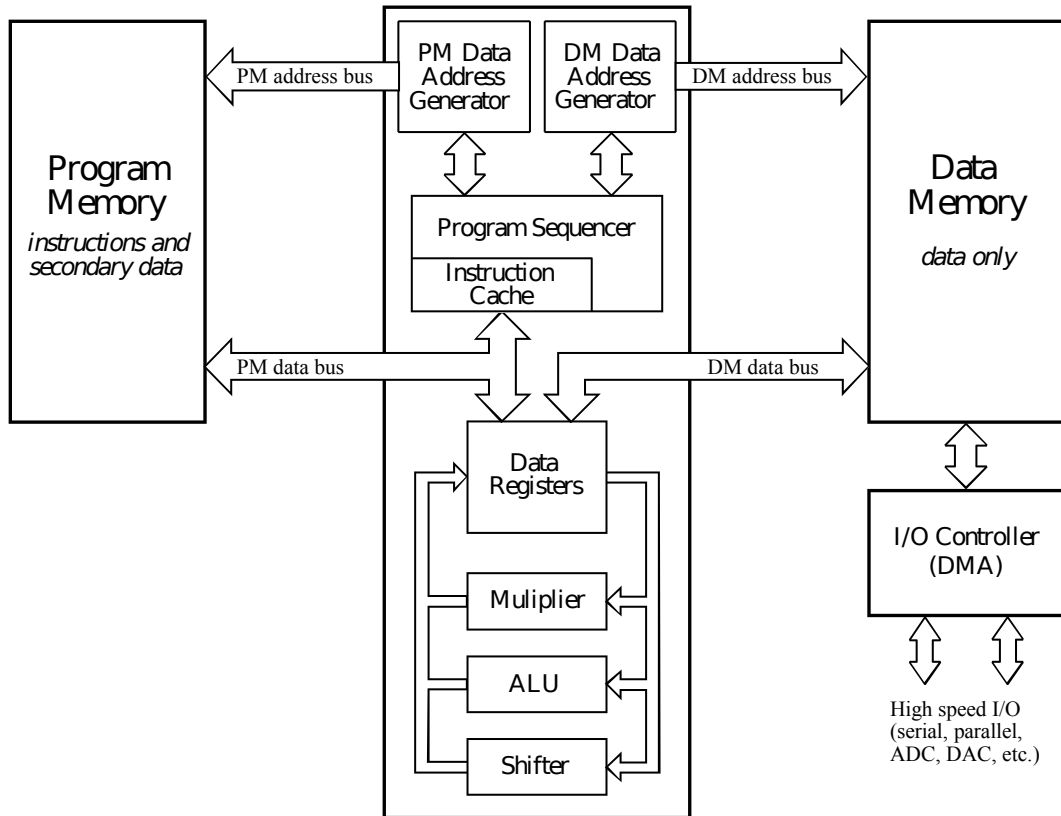


Figure 4.2: An example of a DSP architecture, a simplified diagram of the Analog Devices SHARC DSP[35].

for fast bit-reversing needed for FFT for instance, narrow data formats and specialized peripherals (analog to digital converters (ADC), memory) on chip. Just like MCU's they still have a low silicium area and therefore low cost [54].

4.1.1.4 FFT Processors

A specialized branch of processors is the Fast Fourier Transform (FFT) processor. It is a processor designed for speed optimization in FFT calculations. Using a specialized FFT processor is said to reduce hardware cost by a factor five, and to decrease the processing time by a factor of 20 [55]. These FFT processors are found as a co-processor core in DSP chips to aid in the speed of the FFT. The disadvantages of having a dedicated FFT processor are the lack of flexibility and possible loss of efficiency. The first is due to the tailoring of the FFT processor to a

specific task, and the hardware cannot be changed to suit a different application. The latter is due to the same nature, if the FFT processor is only used for a small fraction of the time it cannot perform other tasks in the remaining time instead. Therefore FFT processors tend to be useful when a very large portion of the processing done is FFT, or the FFT processing time has to be very short.

4.1.2 Field-programmable Gate Array

A Field-programmable gate array (FPGA) contains logic that can be configured in multiple ways. It allows for creating an architecture optimized for a specific application. It can give a high performance compared to processors since all logic is wired in parallel which gives very low “processing” delays. They also can have a lower power consumption, but the main advantage over an processor is their flexibility. Hardware of the FPGA can basically be modified in such a way that is optimal for the application, but it can also be reconfigured later on when changes occur or different requirements have to be met. [56, 57].

In the context of radar signal processing, FPGA’s can be used to test architectures, to get an idea of how much resources are necessary for specific tasks. A paper by Saad [57] illustrates such an architecture, see Figure 4.3. The architecture consists of a state-machine that controls the front end of the radar, an FFT processor, pipeline processing and a MicroBlaze microprocessor. To get an indication of the amount of resources necessary, we reproduce the table from Saad [57] here in Table 4.2, that shows the amount of resources needed for this architecture implemented on an XC2VP30 Virtex-II PRO FPGA. A major disadvantage of FPGAs however is their relative high price compared to processor architectures. Therefore FPGAs are often used in prototyping new architectures and low volume production. They are less useful for high volume production unless high performance and high flexibility is needed.

4.1.3 Other

Complex programmable logic devices (CPLD) are similar to FPGAs in the sense that these two consist of logic blocks that can be configured to suit a specific application. Their difference is that they feature a much lower amount of logic blocks, or “gates”. This makes them much more cost effective, but very limited in their capabilities and are therefore likely not capable of doing the processing needed for radar systems.

4.1.4 Overview

In [Table 4.3](#) an overview of the different options for implementing the digital signal processing is given, together with their advantages and disadvantages.

4.2 Radar Chips Comparison

In [Table 4.4](#) an overview of radar chips is given. Base Frequency and bandwidth are important since the use of frequencies for automotive applications is limited. Bandwidth is also the limiting factor in range resolution. Metrics like on-chip antenna’s, package and technology are given because they affect the complexity and end-price of an overall system. Having to include antenna’s or lodging multiple chips for instance means spending more money on them. Number of transmitters and receivers tells if the system can be used for angular measurement in azimuth and/or elevation.

For the specific application in this report, a single chip radar system is chosen

Table 4.3: Overview of architectures and their main advantages and disadvantages.

Architecture	Advantage(s)	Disadvantage(s)	Cost
General Purpose Microprocessor	High Processing Power Supports High Level instructions	No peripherals	Very High
Microcontroller	On-Chip Peripherals	Low processing power Not optimized for Signal Processing	Low
Digital Signal Processor	On-Chip Peripherals Optimized for Signal Processing	More expensive than MCU	Medium
FFT Processor	Very Fast FFT Processing	Inflexible, possibly inefficient	Low
FPGA	Very Flexible Very High Performance	More expensive than DSP	High

since it requires less development and has lower complexity in design. The choice of chip for doing measurements and testing has fallen on the chip by Omniradar [58]. This decision is made by Sensata due to the low price and high performance they claim to achieve.

The Omniradar chip has a 7GHz bandwidth around the 60GHz ISM band and features one transmitter and two receivers, the latter having an in-phase and quadrature (I/Q) demodulator. It contains radar RF systems in SiGe technology that can be software controlled to allow different configurations, including FM-CW. Omniradar claims a range up to 15m [58].

Table 4.4: Comparison of (single) chip radar systems.

Manufacturer	Base Frequency (GHz)	Bandwith	On chip Antennas	Number of Transmitters	Number of Receivers	Package	Production State	Technology
Omniradar [58]	60	6	yes	1	2	single chip	In production	SiGe
Omniradar [58]	60	6	yes	1	2	single chip	Pre-production	SiGe
Novelic [59]	60	1	no	1	1	single chip	In production	SiGe BiCMOS
Viasat [60]	24	0.25	no	1	1	single chip	In production	?
Infineon(1) [61]	24	2	no	-	-	separate chips	In production	SiGe
Infineon(2) [62]	77	1	no	-	-	Separate chips	In production	SiGe
Success project [63]	122	?	yes	?	?	single chip	Pre-production	
Silicon Radar [64]	120	7	yes	1	1	single chip	In production	SiGe BiCMOS
Google Project Soli [65]	60	?	no	1	2	single chip	In production	?
NXP [66]	77	1	no	2	3	seperate chips	In production	?
RFBeam [67]	24	0.13	yes	1	2	(big) module	In production	?
Novelda xethru [68]	6	2.5	no	1	2	single chip	In production	CMOS
Thomas Zwick [69]	122	1	yes	1	1	single chip	Only Theoretical	SiGe
innosent [70]	25	0.25	no	1	1	Module	In production	SiGe
Analog Devices [71]	25	0.25	no	1	4	separate chips	In production	CMOS
Giamello [72]	25 & 77	?	?	?	?	chipset	In Research	BiCMOS
Imec [73]	79	?	yes	-	-	Single Chip	IP Block Design	CMOS
NXP [74]	77	2	no	3	4	Single Chip	Pre-production	RFCMOS
ROACH [75]	77	0.5	yes	1	4	single chip	Pre-production	RFCMOS
Hitachi [76]	77					single chip	In Research	GaAs
Microwave Sensors [77]	24	0.25	no	1	?	?	Prototype	?

Chapter 5

Parking Sensor Norms and Standards

Apart from an ISO norm (ISO 17386) there is a norm from the Department of Transportation (RIN 2127-AK43) and a specification (2.4.7-U-01e-2014_Gen2) by a consortium of car builders (BMW, Daimler, Porsche, Audi and VW) that are used worldwide to define measuring methodology. All three of them specify grids to place objects in. In illustration [Figure 5.1](#) the measuring grid for ISO 17386 is shown, in [Figure 5.2](#) the grid by the consortium is shown and in [Figure 5.3](#) the grid by the Department of Transportation is shown.

The grid size and resolution and also the objects specified differ for all three specifications. The specification by the consortium is by far the most demanding, having the largest grid (3.5 by 7m) with a high resolution (10cm) and relatively small objects (10mm and larger). All three specifications specify between cells in which objects have to be detected, cells in which objects can be detected, and cells in which objects should not be detected. These cells are not to be confused with the radar range cells. The cells here are locations at which the objects are set to test their detection. The ISO norm specifies a coverage area as a measurement, being the ratio between the number of cells and the number of cells in which objects are detected. It also defines “detection holes” which are defined by the biggest area in which objects are not detected. ISO specifies the minimum coverage area of 88% up to 1m. The norm does not define this after 1m, but coverage area and

detection hole are metrics that can be applied to tests with our radar system. The consortium specifications state an accuracy of 1cm or less for the communicated distance.

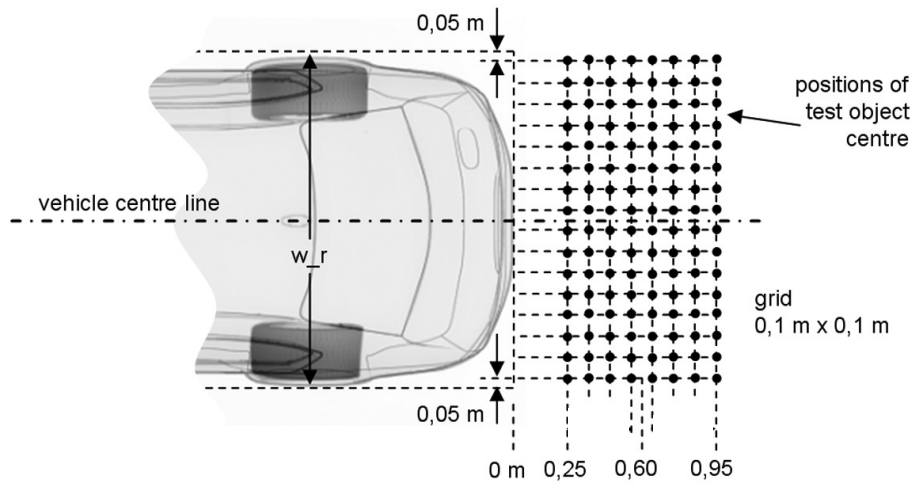


Figure 5.1: ISO 17386 measurement grid.

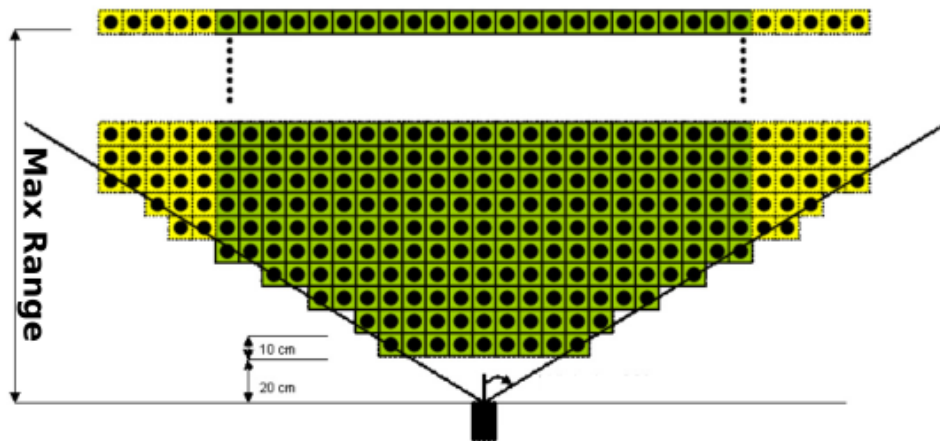


Figure 5.2: Measurement grid from consortium specifications.

5.1 Target Speed

The maximum speed at which measurements should work is defined by the ISO norm as 1m/s. The consortium specifications however set a speed for up to 44m/s for “PLV” mode (Park Lücken Vermessung, meaning looking for available parking space. In PDC(park distance) control mode however this speed is lowered to 17m/s and in ultra near range mode even to 4m/s. For the parking application a maximum speed of 4m/s is the most realistic.

5.2 Detection Time

The ISO norm states that signalling to the user should be done within 500ms of appearance of a target in the covered area.

Chapter 6

Conclusions

In this chapter the research questions and research method for the future research are proposed.

6.1 Research Questions

The main research question is: How can a radar park distance control system be implemented most cost effectively to match current ultrasound systems.

To answer this question it is divided into several sub-question:

1. What metrics are useful for comparing an ultrasound and radar PDC system?
2. Can the ultrasound specifications be met by radar?
3. How can these specifications be met?
 - (a) Which detector(s) meet(s) these specification?
 - (b) Which architecture is best fit for the detector(s)?

The first of these questions is answered in [section 6.2: Research Method](#).

6.2 Research Method

The future research will consist mainly of testing different methods for target detection, range and direction of arrival estimation. The method for this is to use

the previously mentioned radar made by Omnicor to record data for analysis. For repeatability and checking a grid similar to that of the consortium will be used. Furthermore, recordings of the raw I and Q signals for different modulation types and lengths will be made for different positions on the grid for a multitude of targets and target combinations.

Afterwards the data will be processed, to find the combination of window type, automatic detector, DOA and range estimator that deliver the performance equal to that of current ultrasound systems. Next the architecture to best fit this combination. To compare the different combinations a set of metrics is proposed.

6.2.1 Metrics for comparison

1. Signal-to-noise ratio is an important metric to select the right window type because it is connected with the probability of detection as shown before.
2. The coverage ratio as the ratio of grid cells in which a target is detected versus those where it is not, as by the ISO 17386 norm.
3. The largest blind spot, as by the ISO 17386 norm.
4. The accuracy in the range of the target, defined as the ratio between the error and the actual range.
5. The accuracy of the DOA estimator as an error to the actual angle.
6. The complexity of different detection, range and DOA estimators since higher complexity generally equals higher cost.

References

Note: Any websites referenced were visited last on the first of February 2016.

- [1] T. Geiger, “Jetzt kommt der nachfolger des regenbogen-porsche,” 2015. <http://www.welt.de/motor/modelle/article138730127/Jetzt-kommt-der-Nachfolger-des-Regenbogen-Porsche.html>. 1
- [2] M. I. Skolnik, “Radar handbook,” 1970. ISBN:0-07-057913-X. 1, 3, 4, 12, 13, 15
- [3] H. Rohling, M.-M. Meinecke, M. Klotz, and R. Mende, “Experiences with an experimental car controlled by a 77 ghz radar sensor,” in *International Radar Symposium, IRS98, München*, 1998. 1
- [4] D. Jones, “Navy electricity and electronics training series,” 1998. 3
- [5] M. I. Skolnik, “Introduction to radar,” *Radar Handbook*, vol. 2, 1962. ISBN: 0-07-057909-1. 4, 5, 8, 12, 13
- [6] A. G. Stove, “Linear fmcw radar techniques,” in *IEE Proceedings F (Radar and Signal Processing)*, vol. 139, pp. 343–350, IET, 1992. 4
- [7] G. M. Brooker, “Understanding millimetre wave fmcw radars,” in *1st international Conference on Sensing Technology*, pp. 152–157, 2005. 4, 10
- [8] M. Jalilvand, “Microwave fmcw radar,” 5
- [9] W. Wiesbeck, “Radar system engineering,” in *IHE*, 2007. 5, 7

-
- [10] H. Rohling and M.-M. Meinecke, “Waveform design principles for automotive radar systems,” in *Radar, 2001 CIE International Conference on, Proceedings*, pp. 1–4, IEEE, 2001. [6](#), [9](#)
 - [11] E. Hyun, W. Oh, and J.-H. Lee, “Multi-target detection algorithm for fmcw radar,” in *Radar Conference (RADAR), 2012 IEEE*, pp. 0338–0341, IEEE, 2012. [6](#), [7](#)
 - [12] B. R. Mahafza, *Radar systems analysis and design using MATLAB*. CRC press, 2002. [7](#)
 - [13] P. Swerling, “Probability of detection for fluctuating targets,” *Information Theory, IRE Transactions on*, vol. 6, no. 2, pp. 269–308, 1960. [7](#)
 - [14] D. Kok and J. S. Fu, “Signal processing for automotive radar,” in *Radar Conference, 2005 IEEE International*, pp. 842–846, IEEE, 2005. [8](#)
 - [15] T. O. Grosch, “Radar sensors for automotive collision warning and avoidance,” in *SPIE’s 1995 Symposium on OE/Aerospace Sensing and Dual Use Photonics*, pp. 239–247, International Society for Optics and Photonics, 1995. [8](#)
 - [16] A. Stove, “80 ghz automotive radar,” in *Automotive Electronics, 1991., Eighth International Conference on*, pp. 145–149, IET, 1991. [8](#)
 - [17] W. Buller, B. Wilson, L. Van Nieuwstadt, and J. Ebling, “Statistical modelling of measured automotive radar reflections,” in *Instrumentation and Measurement Technology Conference (I2MTC), 2013 IEEE International*, pp. 349–352, IEEE, 2013. [8](#)
 - [18] W. Weibull, “Wide applicability,” *Journal of applied mechanics*, vol. 103, 1951. [8](#)
 - [19] R. M. ODonnell, “Radar systems engineering lecture 6 detection of signals in noise,” [8](#)
 - [20] D. M. Grimes and T. O. Jones, “Automotive radar: A brief review,” *Proceedings of the IEEE*, vol. 62, no. 6, pp. 804–822, 1974. [8](#)

-
- [21] J. Wenger, “Automotive mm-wave radar: Status and trends in system design and technology,” in *Automotive Radar and Navigation Techniques (Ref. No. 1998/230)*, *IEE Colloquium on*, pp. 1–1, IET, 1998. 8
- [22] J. Hasch, E. Topak, R. Schnabel, T. Zwick, R. Weigel, and C. Waldschmidt, “Millimeter-wave technology for automotive radar sensors in the 77 ghz frequency band,” *Microwave Theory and Techniques, IEEE Transactions on*, vol. 60, no. 3, pp. 845–860, 2012. 9
- [23] B.-H. Ku, O. Inac, M. Chang, and G. M. Rebeiz, “75–85 ghz flip-chip phased array rfc with simultaneous 8-transmit and 8-receive paths for automotive radar applications,” in *Radio Frequency Integrated Circuits Symposium (RFIC), 2013 IEEE*, pp. 371–374, IEEE, 2013. 9
- [24] H. Forstner, H. Knapp, H. Jager, E. Kolmhofer, J. Platz, F. Starzer, M. Tremml, A. Schinko, G. Birschkus, J. Bock, *et al.*, “A 77ghz 4-channel automotive radar transceiver in sige,” in *Radio Frequency Integrated Circuits Symposium, 2008. RFIC 2008. IEEE*, pp. 233–236, IEEE, 2008. 9
- [25] D. Saunders, S. Bingham, G. Menon, D. Crockett, J. Tor, R. Mende, M. Behrens, N. Jain, A. Alexanian, *et al.*, “A single-chip 24 ghz sige bicmos transceiver for fmcw automotive radars,” in *Radio Frequency Integrated Circuits Symposium, 2009. RFIC 2009. IEEE*, pp. 459–462, IEEE, 2009. 9
- [26] R. Reuter, H. Li, Y. Yin, A. Ghazinour, D. Jahn, D. Morgan, J. Feige, P. Welch, S. Braithwaite, B. Knappenberger, *et al.*, “Fully integrated sige-bicmos receiver (rx) and transmitter (tx) chips for 76.5 ghz fmcw automotive radar systems including demonstrator board design,” in *Microwave Symposium, 2007. IEEE/MTT-S International*, pp. 1307–1310, IEEE, 2007. 9
- [27] M. Camiade, D. Domnesque, Z. Ouarch, and A. Sion, “Fully mmic-based front end for fmcw automotive radar at 77ghz,” 2000. 9
- [28] E. Hyun, W. Oh, and J.-H. Lee, “Two-step moving target detection algorithm for automotive 77 ghz fmcw radar,” in *Vehicular Technology Conference Fall (VTC 2010-Fall), 2010 IEEE 72nd*, pp. 1–5, IEEE, 2010. 9

-
- [29] V. Winkler, “Range doppler detection for automotive fmcw radars,” in *Microwave Conference, 2007. European*, pp. 1445–1448, IEEE, 2007. 9
- [30] M. Schoor and B. Yang, “High-resolution angle estimation for an automotive fmcw radar sensor,” in *Proc. of Intern. Radar Symposium (IRS), Cologne, Germany*, 2007. 9, 20, 21
- [31] S. J. Orfanidis, *Introduction to signal processing*. Prentice-Hall, Inc., 1995. 10
- [32] M. Withers, “Matched filter for frequency-modulated continuous-wave radar systems,” in *Proceedings of the Institution of Electrical Engineers*, vol. 113, pp. 405–412, IET, 1966. 10
- [33] B. J. Lipa and D. E. Barrick, “Fmcw signal processing,” *FMCW signal processing report for Mirage Systems*, 1980. 10
- [34] A. Girgis, F. M. Ham, *et al.*, “A quantitative study of pitfalls in the fft,” *Aerospace and Electronic Systems, IEEE Transactions on*, no. 4, pp. 434–439, 1980. 10
- [35] S. W. Smith *et al.*, “The scientist and engineer’s guide to digital signal processing,” 1997. 11, 23, 24, 25
- [36] A. V. Oppenheim, R. W. Schaffer, J. R. Buck, *et al.*, *Discrete-time signal processing*, vol. 2. Prentice-hall Englewood Cliffs, 1989. 10
- [37] C. Wolff, “Pulse integration,” 2015. <http://www.radartutorial.eu/10.processing/sp50.en.html>. 13
- [38] H. Rohling, “Radar cfar thresholding in clutter and multiple target situations,” *Aerospace and Electronic Systems, IEEE Transactions on*, no. 4, pp. 608–621, 1983. 15, 16, 17, 18
- [39] M. A. Richards, *Fundamentals of radar signal processing*. Tata McGraw-Hill Education, 2005. ISBN:978-0-07-060737-8. 15
- [40] E. Hyun and J.-H. Lee, “A new os-cfar detector design,” in *Computers, Networks, Systems and Industrial Engineering (CNSI), 2011 First ACIS/JNU International Conference on*, pp. 133–136, IEEE, 2011. 17

-
- [41] L. Zhao, W. Liu, X. Wu, and J. S. Fu, “A novel approach for cfar processors design,” in *Radar Conference, 2001. Proceedings of the 2001 IEEE*, pp. 284–288, IEEE, 2001. [17](#)
 - [42] D. Knuth, “The art of computer programming 1: Fundamental algorithms 2: Seminumerical algorithms 3: Sorting and searching,” 1968. [17](#)
 - [43] W. Xue and X.-W. Sun, “Multiple targets detection method based on binary hough transform and adaptive time-frequency filtering,” *Progress In Electromagnetics Research*, vol. 74, pp. 309–317, 2007. [18](#)
 - [44] R. N. Bracewell, “The fast hartley transform,” *Proceedings of the IEEE*, vol. 72, no. 8, pp. 1010–1018, 1984. [18](#)
 - [45] A. N. Choudhary and R. Ponnusamy, “Implementation and evaluation of hough transform algorithms on a shared-memory multiprocessor,” *Journal of Parallel and Distributed Computing*, vol. 12, no. 2, pp. 178–188, 1991. [18](#)
 - [46] A. Carr, L. Cuthbert, and A. Olver, “Digital signal processing for target detection in fmcw radar,” in *IEE Proceedings F: Communications Radar and Signal Processing*, vol. 128, pp. 331–336, 1981. [18](#)
 - [47] W. Kederer and J. Detlefsen, “Direction of arrival (doa) determination based on monopulse concepts,” in *Microwave Conference, 2000 Asia-Pacific*, pp. 120–123, IEEE, 2000. [19](#), [20](#)
 - [48] P. Wenig, M. Schoor, O. Günther, B. Yang, and R. Weigel, “System design of a 77 ghz automotive radar sensor with superresolution doa estimation,” in *Signals, Systems and Electronics, 2007. ISSSE’07. International Symposium on*, pp. 537–540, IEEE, 2007. [20](#)
 - [49] R. O. Schmidt, “Multiple emitter location and signal parameter estimation,” *Antennas and Propagation, IEEE Transactions on*, vol. 34, no. 3, pp. 276–280, 1986. [20](#)
 - [50] R. Roy, A. Paulraj, and T. Kailath, “Estimation of signal parameters via rotational invariance techniques-esprit,” in *30th Annual Technical Symposium*, pp. 94–101, International Society for Optics and Photonics, 1986. [20](#)

- [51] G. Xu, S. D. Silverstein, R. H. Roy, and T. Kailath, “Beamspace esprit,” *Signal Processing, IEEE Transactions on*, vol. 42, no. 2, pp. 349–356, 1994. 20
- [52] J. Xin and A. Sano, “Computationally efficient subspace-based method for direction-of-arrival estimation without eigendecomposition,” *Signal Processing, IEEE Transactions on*, vol. 52, no. 4, pp. 876–893, 2004. 20
- [53] B. Paillard, “An introduction to digital signal processors,” *Sec. 6.4. 2. Génie électrique et informatique R eport, Université de Sherbrooke, April 2004*, 2002. 22
- [54] E. J. Tan and W. B. Heinzelman, “Dsp architectures: past, present and futures,” *ACM SIGARCH Computer Architecture News*, vol. 31, no. 3, pp. 6–19, 2003. 25
- [55] G. D. Bergland, “Fast fourier transform hardware implementations—an overview,” *Audio and Electroacoustics, IEEE Transactions on*, vol. 17, no. 2, pp. 104–108, 1969. 25
- [56] R. Kenny, “Fpga signal processing for radar/sonar applications,” *RF Design.*, 2007. 26
- [57] J. Saad, A. Baghdadi, and F. Bodereau, “Fpga-based radar signal processing for automotive driver assistance system,” in *Rapid System Prototyping, 2009. RSP’09. IEEE/IFIP International Symposium on*, pp. 196–199, IEEE, 2009. 26, 27
- [58] Omniradar, “Omniradar products,” 2015. <http://www.omniradar.com/products/>. 29, 30
- [59] N. Microsystems, “Millimeter-wave integrated radar front end - technical brief,” 2015. <http://www.novellic.com/index.php/solutions-ips/radar-sensor-ic-tech-brief>. 30
- [60] ViaSat, “Single chip 24 ghz radar transceiver,” Unknown. <https://www.viasat.com/technologies/single-chip-24-ghz-radar-transceiver>. 30

-
- [61] Infineon, “mmwave-mmhc (transceivers 24-86 ghz),” 2013. <http://www.infineon.com/cms/en/product/rf-and-wireless-control/mm-wave-mmhc/channel.html?channel=db3a304339d29c450139d8bdb700579d>. 30
- [62] Infineon, “Radar-in-package sensor,” 2009. <http://www.infineon.com/cms/en/product/sensor/radar-in-package-sensor/channel.html?channel=db3a30431ddc9372011e213568da414b>. 30
- [63] S. Project, “Welcome to the success-project,” 2015. <http://www.success-project.eu/>. 30
- [64] S. Radar, “Overview of transceivers,” 2014. http://www.siliconradar.com/transceiver_e.html. 30
- [65] Google, “About project soli,” 2015. <https://www.google.com/atap/project-soli/>. 30
- [66] NXP, “Mr2001: Multi-channel 77 ghz radar transceiver chipset,” 2015. http://www.nxp.com/products/rf/millimeter-wave-solutions/radar-technology/multi-channel-77-ghz-radar-transceiver-chipset:MR2001?tab=Documentation_Tab&pspll=1&SelectedAsset=Documentation&ProdMetaId=PID/DC/MR2001&fromPSP=true&assetLockedForNavigation=true&componentId=2&leftNavCode=1&pageSize=25&Documentation=Documentation/00610Ksd1nd%2560%2560Data%2520Sheets&fpssp=1&linkline=Data%2520Sheets. 30
- [67] RFbeam, “K-mc4 radar transceiver,” 2015. <http://www.rfbeam.ch/products/k-mc4-transceiver/>. 30
- [68] X. by NOvelda, “Inspiration kit,” 2014. <https://xethru.com/inspiration-kit.html>. 30
- [69] S. Scherr, B. Gottel, S. Ayhan, A. Bhutani, M. Pauli, W. Winkler, J. C. Scheytt, and T. Zwick, “Miniaturized 122 ghz ism band fmcw radar with mi-

- crometer accuracy,” in *Radar Conference (EuRAD), 2015 European*, pp. 277–280, IEEE, 2015. 30
- [70] Innosent, “Leading radar systems and frontends,” unknown. <http://www.innosent.de/en/home/>. 30
- [71] A. Devices, “Adf5904 datasheet and product info,” 2015. <http://www.analog.com/en/products/rf-microwave/integrated-transceivers-transmitters-receivers/microwave-mmwave-tx-rx/adf5904.html>. 30
- [72] V. Giammello, E. Ragonese, and G. Palmisano, “A 24/77-ghz sige bicmos transmitter chipset for automotive radar,” *Microwave and Optical Technology Letters*, vol. 55, no. 4, pp. 782–786, 2013. 30
- [73] Imec, “Single-chip 79 ghz radar,” ? <http://www2.imec.be/content/user/File/Leaflets/79G-radar-leaflet.pdf>. 30
- [74] NXP, “Nxp radar technology accelerates adas adoption,” 2016. <http://media.nxp.com/phoenix.zhtml?c=254228&p=irol-newsArticle&ID=2125903>. 30
- [75] M. Li, R. J. Evans, E. Skafidas, and B. Moran, “Radar-on-a-chip (roach),” in *Radar Conference, 2010 IEEE*, pp. 1224–1228, IEEE, 2010. 30
- [76] T. Nagasaku, K. Kogo, H. Shinoda, H. Kondoh, Y. Muto, A. Yamamoto, and T. Yoshikawa, “77ghz low-cost single-chip radar sensor for automotive ground speed detection,” in *Compound Semiconductor Integrated Circuits Symposium, 2008. CSIC’08. IEEE*, pp. 1–4, IEEE, 2008. 30
- [77] M. Zander, A. Volkswagen, *et al.*, “A multifunctional automotive short range radar system,” in *German Radar Symposium, GRS2000, Berlin*, 2000. 30

Appendix B

System Design

B.1 Introduction

This chapter contains two sections. In the first section different options for design choices are considered. In the second the chosen options are combined to create a proposed design for a radar based park-distance control system.

B.2 Design Considerations

To determine the system design for a radar PDC system several considerations have to be made with respect to distribution, modulation and processing.

B.2.1 Distribution

In a radar PDC system, there will be multiple systems sensors. The digitisation and processing can therefore be locally located at the sensor, centralized at some sort of central processing unit or anywhere in between these two. The fusion of data from different sensors cannot be done locally however. The three different distributions considered are illustrated in [Figure B.1](#). In [Table B.1](#) three different options are considered.

1. A system where the raw analog signals from the different sensors are distributed towards a central digitisation and processing unit.
2. A system where the analog signal is digitized and then carried towards the central processing unit for processing.

-
3. A system where all the processing and detection is done locally, and only the fusion between the sensors is done at a central processing unit.

Table B.1: Table showing different options and the effects on cabling and the distribution of computing power.

	Central digitization(1)	Local digitization(2)	Local Processing(3)
Cabling	8 cables carrying differential signals	twisted pair ethernet	Low bandwidth connection
Computing power	None locally, all central	None locally, all central	Local and central

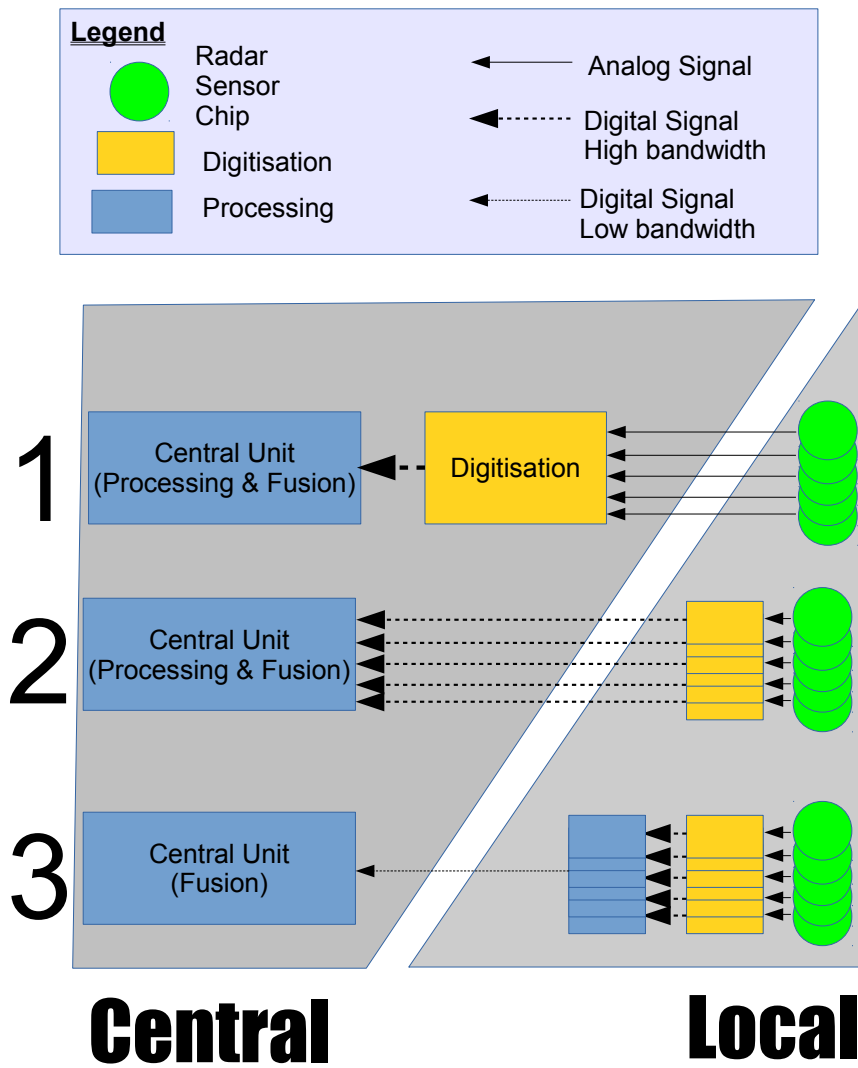


Figure B.1: Different options for distribution.

Data Transport

Choosing between local and central digitization and processing has an effect on the way to transport data and with it the cabling. When using central digitization four pairs of wires, totalling eight have to be wired to the central processing units carrying the differential analog IQ signals for both receivers. This weighs heavy on the cost, weight and space requirements that are very tight on modern cars [32]. Furthermore, the addition of noise and signal leads to SNR loss meaning lower detection performance.

Another option is to digitize the signal at the sensor, and use a digital bus like TTEthernet. This means that only two wires link the sensors to the central unit. These digital wires can also be used for communication in two directions besides the data for instance for enabling or disabling sensors and diagnostics. The method of digitisation determines the speed necessary for transferring this digital data, see [subsection B.2.3: Digitisation](#). Disadvantage of local digitisation is the need for a local A/D-converter and possibly more logic to deal with the digital bus used for data transfer to the central unit.

To reduce the load on the cabling even more, besides digitisation processing and detection of objects can also be done locally. Doing this only the information about objects (location, optionally size) reducing the load on the communication bus to a very low level. Sending information about 20 objects every second, using 2 bytes for location and 1 more for size this takes only 60bytes per second.

B.2.2 Modulation

In the experimental setup an external chip was used to generate the modulated signal. Omniradar however has an internal PLL and VCO that can also be used. In the RIC60B version of this chip, this modulator is underdeveloped however causing problems in linearity with a severe reduction in SNR. The next version of the RIC60B however will contain a proper modulator on board, which saves the trouble of having to add more logic for the modulation. As for the modulation type and length, from [chapter 5: Experiments: single Object](#) we deduce that a sweeptime of 25ms is long enough, and the use of only a triangular up-sweep is sufficient.

B.2.3 Digitisation

Digitisation is done using an A/D converter. The signals from the Omniradar chip are differential and the chip uses I and Q demodulation. That means that for the two receivers on the chip four differential A/D converter channels are needed. The two main specifications for A/D converters are samplerate and resolution, see also [section 2.6: Digitization](#).

Using a modulation time 25ms, the maximum beat frequency of interest is 5.6kHz. Using the Nyquist frequency theorem, the samplerate should be at least 11.2kHz. To increase the SNR a higher samplerate is better, but a samplerate of 1Mhz as used in the experiments is excessive.

In the experiments a resolution of 16 bits is used. The different plots in [subsection 5.2.2: Precision](#) show that 10 bits or more are sufficient amount of quantization steps.

B.2.4 Processing

The FFT is the most computationally intensive part of the processing of the data. Per sensor two complex FFT's have to be done. The time it takes to compute an FFT depends on the amount of datapoints. Using the minimum sweeptime of 25ms and samplerate of 100kHz there will be 2500 datapoints.

Different options for calculating the FFT are given in [Research Topics Report](#). As the most cost-effective solution the microprocessor solution is explored first. On a rather simple architecture known as the ARM cortex-M3 a 1024 point FFT takes 98803 cycles [33]. At 32MHz cpu speed, a common speed on commercially available cores, this means that it takes 3ms. The complexity of an FFT is $0.5 \cdot N \cdot 2 \log N$, using this complexity an FFT of 2500 datapoints takes approximately 7ms. Calculating two FFT's per sensor, having for instance 5 sensors on a car means that it takes 70ms for all the FFT's to calculate. Dedicated FFT processors have a much shorter delay in calculating the FFT for use in realtime systems, but these much cost more.

Timing

The ISO Specifications from [section 1.5: Specifications](#) say that the driver has to be informed within 500ms after an object appears within detection range. This means that measurements have to be taken at 500ms minus the times it takes for measuring, digitizing, transferring the data, processing and signalling. Sensata has set the time for signalling to 100ms. From the previous section it is shown that it takes 70ms to calculate the FFT's. As a safe estimate the processing after FFT's is estimated as another 70ms. Using time-triggered ethernet as suggested in [\[32\]](#) the latency is $372\mu\text{s}$. This latency does not incorporate additional latencies that might be caused by a higher level protocol such as IP and TCP. The measurement takes at least 50ms as given a sweep of 50ms. This means that measurements have to be taken approximately every 200ms.

B.3 Recommended Design

From the distribution options, the proposed design uses option 2 using minimal logic to transfer the digital signal and control the radar chip. This because the cost of having six more wires and the reduction of SNR caused by noise do not weigh up to the cost of adding digitization and ethernet logic to the local units. It also allows for easy diagnostics and added safety features. The proposed system design is illustrated in [Figure B.2](#). As seen in [subsection B.2.4: Processing](#) a microcontroller with an ARM cortex-M3 or more powerful is sufficient for calculating the FFT's and doing detection and fusing targets from multiple sensors. The exact architecture of the Cortex-M3 is proprietary unfortunately, but architecture with similar or better performance will also work in this setup.

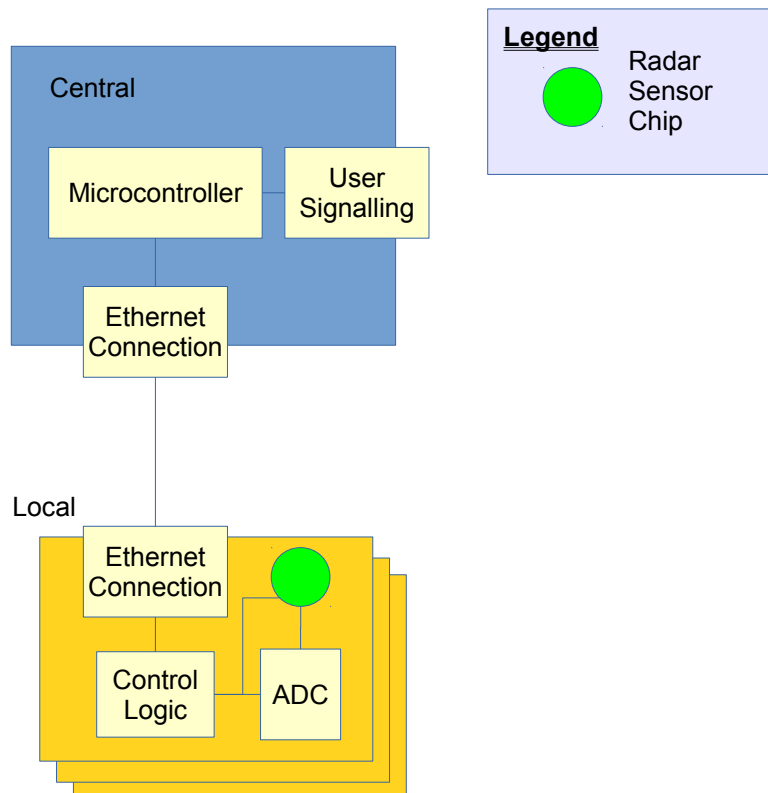


Figure B.2: Proposed system design.

Appendix C

MATLAB Code

The MATLAB code is attached in a zip file named *matlab.zip*.

References

Note: Any websites referenced were visited last on the first of May 2016.

- [1] M. I. Skolnik, “Radar handbook,” 1970. ISBN:0-07-057913-X. [1](#), [13](#), [16](#), [17](#), [19](#), [22](#), [23](#)
- [2] D. Jones, “Navy electricity and electronics training series,” 1998. [1](#)
- [3] M. I. Skolnik, “Introduction to radar,” *Radar Handbook*, vol. 2, 1962. ISBN: 0-07-057909-1. [2](#), [3](#), [4](#)
- [4] A. G. Stove, “Linear fmcw radar techniques,” in *IEE Proceedings F (Radar and Signal Processing)*, vol. 139, pp. 343–350, IET, 1992. [2](#)
- [5] G. M. Brooker, “Understanding millimetre wave fmcw radars,” in *1st international Conference on Sensing Technology*, pp. 152–157, 2005. [3](#)
- [6] M. Jalilvand, “Microwave fmcw radar,” [4](#)
- [7] Omniradar, “Omniradar ric60 datasheet,” 2016. Datasheet attached in appendix. [7](#), [14](#), [23](#), [30](#)
- [8] C. Canali, G. De Cicco, B. Morten, M. Prudenziati, and A. Taroni, “A temperature compensated ultrasonic sensor operating in air for distance and proximity measurements,” *Industrial Electronics, IEEE Transactions on*, no. 4, pp. 336–341, 1982. [8](#), [9](#)
- [9] I. T. Union, “Attenuation by atmospheric gasses,” 2012. ITU-R, P.676-6. [16](#)
- [10] G. R. Curry, *Radar essentials*. The Institution of Engineering and Technology, 2012. [16](#)

- [11] J. Ryde, *The attenuation and radar echoes produced at centimetre wavelengths by various meteorological phenomena*. Physical Society, 1946. [17](#)
- [12] E. Bogatin, *Signal integrity: simplified*. Prentice Hall Professional, 2004. [17](#)
- [13] D. K. Ghodgaonkar, V. V. Varadan, and V. K. Varadan, “A free-space method for measurement of dielectric constants and loss tangents at microwave frequencies,” *Instrumentation and Measurement, IEEE Transactions on*, vol. 38, no. 3, pp. 789–793, 1989. [18](#)
- [14] W. Wiesbeck, “Radar system engineering,” in *IHE*, 2007. [18](#)
- [15] P. Swerling, “Probability of detection for fluctuating targets,” *Information Theory, IRE Transactions on*, vol. 6, no. 2, pp. 269–308, 1960. [19](#)
- [16] W. Kederer and J. Detlefsen, “Direction of arrival (doa) determination based on monopulse concepts,” in *Microwave Conference, 2000 Asia-Pacific*, pp. 120–123, IEEE, 2000. [21](#)
- [17] J. W. Cooley, P. A. Lewis, and P. D. Welch, “The fast fourier transform and its applications,” *Education, IEEE Transactions on*, vol. 12, no. 1, pp. 27–34, 1969. [24](#)
- [18] J. W. Cooley and J. W. Tukey, “An algorithm for the machine calculation of complex fourier series,” *Mathematics of computation*, vol. 19, no. 90, pp. 297–301, 1965. [24](#)
- [19] C. Ding and K. Kennedy, “The memory of bandwidth bottleneck and its amelioration by a compiler,” in *Parallel and Distributed Processing Symposium, 2000. IPDPS 2000. Proceedings. 14th International*, pp. 181–189, IEEE, 2000. [24](#)
- [20] R. C. Agarwal, F. G. Gustavson, and M. Zubair, “An efficient parallel algorithm for the 3-d fft nas parallel benchmark,” in *Scalable High-Performance Computing Conference, 1994., Proceedings of the*, pp. 129–133, IEEE, 1994. [24](#)

- [21] A. Girgis, F. M. Ham, *et al.*, “A quantitative study of pitfalls in the fft,” *Aerospace and Electronic Systems, IEEE Transactions on*, no. 4, pp. 434–439, 1980. 25
- [22] F. J. Harris, “On the use of windows for harmonic analysis with the discrete fourier transform,” *Proceedings of the IEEE*, vol. 66, no. 1, pp. 51–83, 1978. 25, 47
- [23] A. V. Oppenheim, R. W. Schaffer, J. R. Buck, *et al.*, *Discrete-time signal processing*, vol. 2. Prentice-hall Englewood Cliffs, 1989. 26
- [24] S. Watts, “Cell-averaging cfar gain in spatially correlated k-distributed clutter,” in *Radar, Sonar and Navigation, IEE Proceedings-*, vol. 143, pp. 321–327, IET, 1996. 27
- [25] H. Rohling, “Radar cfar thresholding in clutter and multiple target situations,” *Aerospace and Electronic Systems, IEEE Transactions on*, no. 4, pp. 608–621, 1983. 27, 63
- [26] E. Hyun and J.-H. Lee, “A new os-cfar detector design,” in *Computers, Networks, Systems and Industrial Engineering (CNSI), 2011 First ACIS/JNU International Conference on*, pp. 133–136, IEEE, 2011. 27
- [27] L. Zhao, W. Liu, X. Wu, and J. S. Fu, “A novel approach for cfar processors design,” in *Radar Conference, 2001. Proceedings of the 2001 IEEE*, pp. 284–288, IEEE, 2001. 27
- [28] A. Devices, “Eval ad9913 evaluation board,” 2008. <http://www.analog.com/en/design-center/evaluation-hardware-and-software/evaluation-boards-kits/eval-ad9913.html>. 29
- [29] A. DAusilio, “Arduino: A low-cost multipurpose lab equipment,” *Behavior research methods*, vol. 44, no. 2, pp. 305–313, 2012. 29
- [30] M. E. Herniter, “Programming in matlab,” *cell*, vol. 400, p. 58, 2003. 30
- [31] N. Instruments, “Device specifications ni6366,” 2015. <http://www.ni.com/manuals>. 30

- [32] L. L. Bello, “The case for ethernet in automotive communications,” *ACM SIGBED Review*, vol. 8, no. 4, pp. 7–15, 2011. [130](#), [132](#)
- [33] I. Mellen, “Complex 16 bit radix 4 fft and inverse fft for cortex-m3,” 2008. <https://github.com/gabonator/DS203/blob/master/Source/HwLayer/ArmM3/bios/FFTCM3.s>. [131](#)